2010

Performance evaluation and finite element verification of an ultra-high performance concrete pi-girder bridge

Owen Bryant Berg
Iowa State University

Performance evaluation and finite element verification of an ultra-high performance concrete pi-girder bridge

by

Owen Berg

A thesis submitted to the graduate faculty
in partial fulfillment of the requirements for the degree of
MASTER OF SCIENCE

Major: Civil Engineering (Structural Engineering)

Program of Study Committee:
Jon M. Rouse, Major Professor
Terry J. Wipf
Kejin Wang

Iowa State University
Ames, Iowa
2010

TABLE OF CONTENTS

LIST OF TABLES

LIST OF FIGURES

ACKNOWLEDGEMENTS

Most importantly, I would like to thank my family and my fiancée Ashley. I would especially like to thank my mother for her love and support during my time at Iowa State. Without her, I would have most likely starved to death during my junior year. Secondly, I would like to thank my Major Professor Dr. Jon (a.k.a. Matt) Rouse for his support and guidance throughout my graduate studies. Without Dr. Rouse's numerous comments to my thesis and lunch meetings at the local Mexican restaurant, my thesis never would have been completed. One could not ask for a more helpful or caring "boss/friend".

I was also able to work with Dr. Terry Wipf during my graduate studies at Iowa State. I was lucky to have someone with such a vast knowledge of bridge testing and behavior helping to coordinate my research. His numerous contributions to my thesis and submitted journal articles, along with his patience and guidance are much appreciated. I had the pleasure of working with Dr. Fouad Fanous for the finite element verification portion of my thesis. Iowa State is lucky to have someone who cares about student's knowledge as much as Dr. Fanous. I would like to thank Dr. Brent Phares, and Dean Beirwagen for their contributions and suggestions to my research. I would also like to thank Dr. Kejin Wang for being on my graduate committee. It was a pleasure to work with and learn from people who are so well regarded in their fields.

My field and laboratory testing was supervised by the "famed gymnast" and structural laboratory manager Doug Wood. I would like to thank Doug for helping coordinate field testing and setting up numerous tests in the structures laboratory. Without Doug, Dr. Rouse and I would probably be frozen in a creek in Buchanan County. In regards to field testing, I also wanted to thank Jake Bigelow, Owen Steffens, and Andrew Barone for their help.

I was able to make three very good friends during my graduate studies at Iowa State. Casey Faber, Thomas Lewin, and Mitchell Pohlkamp all provided numerous jokes, guidance, and sarcastic remarks during the writing of my thesis. Graduate school was a lot easier with great friends.

Outside the walls of Town Engineering Building, I was blessed to live with Blake Rubino for five short years. I wanted to thank Blake for being a terrible roommate and an excellent best friend. Living with you always kept life “interesting”.

Finally, I would like to thank the Federal Highway Administration, Buchanan County, Iowa Highway Research Board, and Iowa Department of Transportation for sponsoring this research.

ABSTRACT

The Jakway Park Bridge in Buchanan County, Iowa is the first bridge constructed with a new prestesssed girder system composed of precast Ultra-High Performance Concrete (UHPC). These girders employ an integral deck to facilitate construction and are referred to as pi-girders for the resemblance of their cross-section to the Greek letter, "π". The evolution of the girder geometry, simplifying assumptions, and finite element analysis techniques used in design of the bridge are examined, and the results of laboratory and live load testing are presented to quantify behavior. The effectiveness of the finite element analysis, structural performance of the bridge, including live load distribution, is evaluated to provide guidance for future designs employing these girders.

1 GENERAL

1.1 Introduction

Recently, there has been increased interest and research in using Ultra-High Performance Concrete (UHPC) in bridges in North America. By using UHPC, departments of transportation hope to gain significant advantages in the mechanical properties and durability of concrete. Tradeoffs of using UHPC include increased cost of materials, increased batch time for mixes, modification of forms due to increased shrinkage, and long setting and curing times tie up precast beds (Bierwagen and Abu-Hawash 2005).

The Jakway Park Bridge in Buchanan County, Iowa is the first bridge constructed with a second generation prestresssed girder system composed of precast UHPC. The girders have a unique cross section named for their resemblance to the Greek letter "π", and hereafter will be referred to as the UHPC pi-girders. The girders, which include an integral deck, introduce complex geometry and materials that posed challenges to designers. The project and bridge design was conceived and completed by the Office of Bridges and Structures at the Iowa Department of Transportation (Iowa DOT).

The cross sectional dimensions of the second generation UHPC pi-girders were based on an optimized section that was the result of an analytical study conducted at the Massachusetts Institute of Technology (MIT) (Park 2003) (Soh 2002). In 2008, the Iowa DOT and the Federal Highway Administration (FHWA) took the initiative to build a UHPC pi-girder demonstration bridge in Iowa. Funding for the project was awarded to the Iowa DOT through the Federal Highway Administration (FHWA) Innovative Bridge Research and Construction Program (IBRC). However, testing of the first generation pi-section raised concerns over lateral load distribution and the possibility of crack formation in the thin deck under American Association of State and Highway Transportation Officials (AASHTO) service loads (Graybeal 2009a).

This thesis documents the evolution of the pi-section, design assumptions and approach, and analytical techniques used in design. The results of laboratory testing, construction monitoring, and live load field testing are presented to quantify the local and global behavior of the Jakway Park Bridge to provide guidance to future designs that employ UHPC pi-girders.

1.2 Objectives and Scope

The primary objectives of this investigation were to quantify the local and global behavior of the bridge, and to provide guidance for future designs employing UHPC pi-girders. Through construction monitoring and live load testing, conservatism of the design approach was quantified and specific parameters, such as lateral live load distribution factors, dynamic amplification factors, and maximum span length, were determined.

To complete the overall objectives, the project included the following tasks:

- Documentation of bridge design process
- Construction strain monitoring
- Completion of two live load field tests considering both static and dynamic loads.
- Completion of laboratory tests of UHPC cylinder and beam specimens cast from material used in the pi-girders.
- Verification of analytical approach used in design by comparison of field tests to predicted analytical results.

1.3 Background

1.3.1 UHPC Material

UHPC exhibits significant advantages in mechanical properties when compared to normal strength concrete. A typical UHPC mix contains sand, cement, crushed quartz, silica fume, superplasticizer, water, and fibers. In general, UHPC has compressive strengths of 28 ksi

(193 MPa) and a tensile strength of 1.5 ksi (10.3 MPa). The UHPC used for this project was provided by LaFarge, a worldwide construction materials supplier. The Lafarge mix used was Ductal®, and the general constituent material and mix proportions are available and can be found in (Graybeal 2009b).

In general, the material selections of UHPC are based on an optimization of particles to ensure maximum density, mechanical homogeneity, and "spacing packing" of the mix. Optimization of the granular mixture can be achieved through the use of packing models. Larrard and Sedran (1994), found that the Solid Suspension Model (SSM) packing model proved a valuable tool in optimizing high packing densities for cementitious materials. Mechanical homogeneity was improved through the removal of coarse aggregates, and improved mechanical properties of the paste. Mechanical homogeneity is desirable as it allows for a more uniform stress distribution, therefore reducing stress concentrations on individual particles. To ensure spacing packing, as opposed to apollonian packing, a wide distribution of particle sizes is selected such that each particle is surrounded by more than one layer of the next smallest particle size, see Figure 1.1 (Vernet 2004). Spacing packing creates a more disperse and uniform transmission of stress by eliminating the stress concentrations at the particle interfaces (Vernet 2004). Richard and Cheyrezy (1995), found that maintaining a minimum ratio between the mean diameters of two consecutive granular class sizes of thirteen, i.e. the diameter of sand particles should be thirteen times larger than the diameter of cement particles, provides the desired spacing packing. The combination of maximizing density, ensuring mechanical homogeneity, and spacing packing allows UHPC to achieve large compressive stresses, often in the range of 28 ksi (193 MPa).

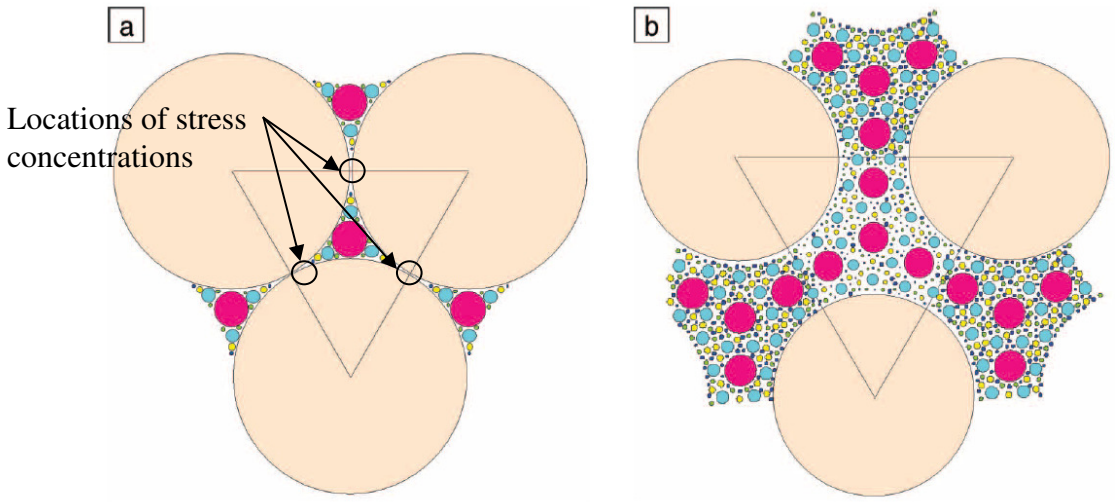

Figure 1.1-Packing Diagrams a) Appollonian Packing b) Spacing Packing-(Vernet 2004)

[The following sections provide a more detailed description of the individual components in UHPC]

Sand

The sand particles in UHPC provide the role of minimizing the maximum paste thickness (MPT). Larrard and Sedran (1994) showed that a critical parameter to mix design is MPT. MPT is the mean distance between two coarse aggregates. As MPT increases, the compressive strength of UHPC was found to decrease (de Larrard and Sedran 1994). This provides evidence that the aggregate has a positive confining effect on the paste. As the MPT is directly proportional to the diameter of the aggregate, an aggregate with a minimal diameter, e.g. monosize sand, should be selected (de Larrard and Sedran 1994). Sand with mean particle diameter of 250μm should be selected to maintain a diameter factor of thirteen, as previously discussed, between granular classes (Richard and Cheyrezy 1995). Sand is also a readily available low cost material.

One problem generated by the use of smaller particles and spacing packing is an increase in global shrinkage. In a normal concrete, the large aggregates (sand and gravel) are the majority components in terms of volume, and form a rigid skeleton of continuous particles.

This skeleton restrains a major portion of the paste shrinkage. With UHPC, the aggregates do not form a rigid skeleton, but rather a set of inclusions contained in a continuous matrix. Each inclusion is free to move relative to the surrounding inclusions. Paste shrinkage is blocked locally around the particles, but global shrinkage is not restrained. This property of UHPC requires special consideration in regards to formwork. (Richard and Cheyrezy 1995)

Cement

Regular Portland cement can be used for UHPC. It is recommended that cement with low shrinkage be used due to the high cement content of UHPC (Vande Voort, Suleiman and Sritharan 2008). The best cement in terms of rheological properties and mechanical performance is high-silica modulus cement (Aitcin, et al. 1991). Fifty percent of the cement in UHPC will remain unhydrated after the initial hydration occurs (Vernet 2004). This anhydrous material allows UHPC to be self-healing. As microcracks occur and water is allowed to migrate into the material, hydration begins again thus sealing the microcracks.

Crushed Quartz

The crushed quartz is in the same granular size class as cement. As not all of the cement is hydrated, a portion of it can be replaced by crushed quartz. Work completed by Ma and Schneider showed that up to 30 percent of the volume of cement could be replaced by crushed quartz with no reduction in compressive strength. Along with reducing the cement content, crushed quartz also improves the rheological properties of UHPC (Vande Voort, Suleiman and Sritharan 2008). This could be due to a filling effect since the crushed quartz particles are slightly smaller than the cement particles (Vande Voort, Suleiman and Sritharan 2008).

Silica Fume

The modifying effects of silica fume in concrete are attributed to its pozzolanic reaction with calcium hydroxide to form calcium silicate hydrate, a secondary hydrate. Silica fume also has a filler effect in the voids around various particles in the mix, thus increasing the density of the mix. Along with providing improvements in strength, silica fume also improves the

rheological properties of the mix due to the perfect sphericity of the particles. (Richard and Cheyrezy 1995)

Fibers

Steel fibers in UHPC provide increased ductility and tensile capacity. General dimensions of the steel fibers are as follows: diameter of 0.008 in. (0.2 mm), length of 0.5 in. (12.7 mm), and a minimum tensile strength of 377 ksi (2600 MPa). The addition of small steel fibers at a ratio of 2-2.5 percent per volume increases the ductility of UHPC (Richard and Cheyrezy 1995). The steel fibers act as reinforcing to the UHPC increasing the tensile capacity of UHPC. As microcracking initiates, the fibers carry tensile forces across the cracks analogous to mild steel reinforcing in normal reinforced concrete. In (Graybeal 2006a) quality control tests showed that the average yield strength of fibers was 458 ksi with an ultimate capacity of 474 ksi. These tests demonstrated that these fibers have little reserve capacity beyond yield (Graybeal 2006a).

1.3.2 First Generation Pi-Section

The original pi-section was designed at the Massachusetts Institute of Technology (MIT) and tested by the Federal Highway Administration (FHWA). The cross sectional dimensions of the prototype UHPC pi-girder were determined through analytical work completed at MIT (Park 2003) (Soh 2002). The analytical work consisted of one, two, and three-dimensional analysis of the prototype girder subjected to the loadings prescribed in the 2002 AASHTO LRFD Bridge Design Specification. This pi-section was optimized to exploit the superior tensile, shear, and compressive properties of UHPC while minimizing cross sectional area. To reduce erection time, the pi-section included an integrated deck. Figure 1.2 provides the cross-section of the first generation pi-section.

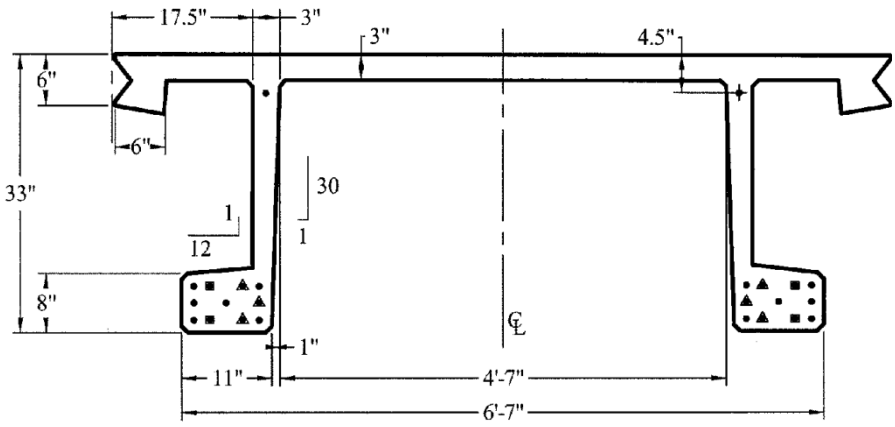

Figure 1.2-First Generation Pi-Section

The first generation pi-section contained 24 prestressing strands, and was designed to span 70 to 120 ft (21.3-36.6 m). The prestressing consisted of 0.5" diameter, 270 ksi (1860 MPa) low relaxation strands. The strands were all stressed to 29.2 kips (130 kN). The section did not contain any mild steel reinforcing. The section has an area of 609 in^2 (0.392 m^2), a strong axis moment of inertia of 89,060 in^4 (37.07x10^9 mm^4), and a self-weight of 675 lb/ft (978 kg/m) of section.

Testing of the first generation pi-section was conducted at the FHWA Turner-Fairbank Highway Research Center Structures Laboratory. Seven tests were performed on four pi-girders to evaluate primary flexure, primary shear, and transverse flexure of the section. The testing consisted of two main parts, the first being the construction and testing of a two girder 70 ft. (21.3 m) span bridge, followed by laboratory testing of an additional two girders. For a more detailed analysis of the test procedures and results, see (Graybeal 2009a).

The testing of the first generation section validated the global shear strength and flexural strength of the section, but revealed concerns about the transverse deck stiffness, cracking behavior at service loads, and the lateral live load distribution between adjacent girders. (Graybeal 2009a)

The average flexural strength of the section was slightly less than the flexural loading

requirement of the 2007 AASHTO LRFD Bridge Design Specification for a span of 70 ft (21.3 m). However, the flexural strength of the section could easily be improved by increasing the prestressing force. (Graybeal 2009a)

The minimum shear capacity of the section was 75 percent greater than the demand required by the 2007 AASHTO LRFD Bridge Design Specification for a span of 70 ft (21.3 m). Therefore, no modification to the shear strength of the section was required. (Graybeal 2009a)

The transverse flexural response of the first generation pi-girder was insufficient to carry the full live load plus impact factor required by the 2007 AASHTO LRFD Bridge Design Specification. Results from the transverse flexural testing revealed that first cracking of the deck would occur at 24 kips (106 kN) of total applied load, which is roughly 55% less than the AASHTO required loading. When steel straps were placed near midspan to limit bulb spreading, the cracking load of the deck marginally increased to 26 kips (116 kN). From these results, it is reasonable to assume that the midspan diaphragms had little effect on the elastic strength of the section. Modifications to the section would be necessary to improve the transverse flexural response of the section. (Graybeal 2009a)

The prototype girder exhibited a limited ability to distribute live loads between adjacent webs and girders. Test results showed distribution factors of 0.85 and 0.95 between adjacent girders. From these results, it is reasonable to assume that a distribution factor of 1.0 should be used for design. However, the test bridge only contained two girders, and a minimum of three girders would be required for a two-lane bridge. (Graybeal 2009a)

1.3.3 Second Generation Pi-Section

A second generation pi-section was developed by addressing the concerns identified during testing of the first generation section (Keierleber, et al. 2008). To help address these concerns the Iowa DOT requested the Bridge Engineering Center (BEC) at Iowa State

University (ISU) to perform an analytical study to evaluate the effects of a proposed set of modifications. Several alternative design configurations such as adding transverse and longitudinal ribs to increase the stiffness of the bridge deck were considered (Keierleber, et al. 2008).

The 3-D finite element model (FEM) used for the analytical study of the second generation section was created with the commercial software, ANSYS. The model was generated by using the ANSYS parametric design language (APDL). APDL was utilized to minimize the required inputs and to expedite the generation of the model when changing one or more key geometric variables, or the mesh size of the model. The model was limited to elastic analysis since no cracking of the UHPC was to be allowed for service level loads (Keierleber, et al. 2008). Thus, all stresses and strains predicted by the model were checked to be within the elastic range of the UHPC. Figure 1.2 illustrates the single girder model geometry while the elastic material properties used for the UHPC are given in Table 1.1.

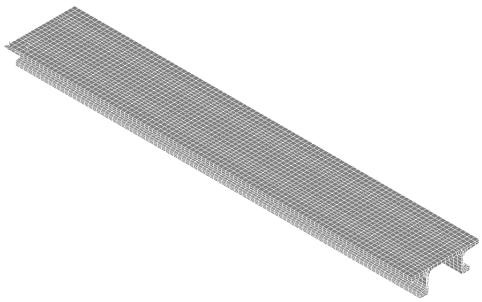

Figure 1.3-Single Girder Finite Element Model

Table 1.1-Finite Element Model Elastic Material Properties

Property	Value
Modulus of Elasticity	7,600 ksi (52,400 MPa)
Poisson's Ratio	0.18

Modeling the support conditions was given careful consideration. As a baseline, simply supported end conditions were simulated by restraining the nodes at the ends of the girders on the bottom of the bulbs that would be in contact with bearing pads. On one end, these

nodes were restrained in all three dimensions while on the other end these nodes were restrained in the vertical and transverse directions only. The effects of concrete end diaphragms that encased the ends of the girder were considered as well for comparison to the simply supported conditions. To model the effects of these end diaphragms all the nodes within six inches of the girder ends were restrained. On one end, the nodes on the bottom of the bulbs were restrained in all three dimensions while the remaining nodes on this end were restrained against vertical and transverse translation. On the opposing end, the corresponding nodes were restrained only in the vertical and transverse directions. These diaphragms had the effect of providing some degree of global rotational restraint at the ends of the girders.

To simplify modeling, the longitudinal prestressing tendons in the girder were incorporated into the model as uniformly distributed pressures on the bulbs at the ends of the girder. The mild steel reinforcement present in the bottom of the deck was not included in the model because the decision to add the reinforcement was made after the analytical work was completed. This decision was made despite analytical results that predicted no tensile stresses would exceed the allowable tensile strength of the UPHC at these locations.

The results of the analytical study were used by the Iowa DOT bridge office along with collaboration among the BEC, LaFarge, and FHWA to establish a second generation pi-section. Figure 1.4 shows the second generation pi-section.

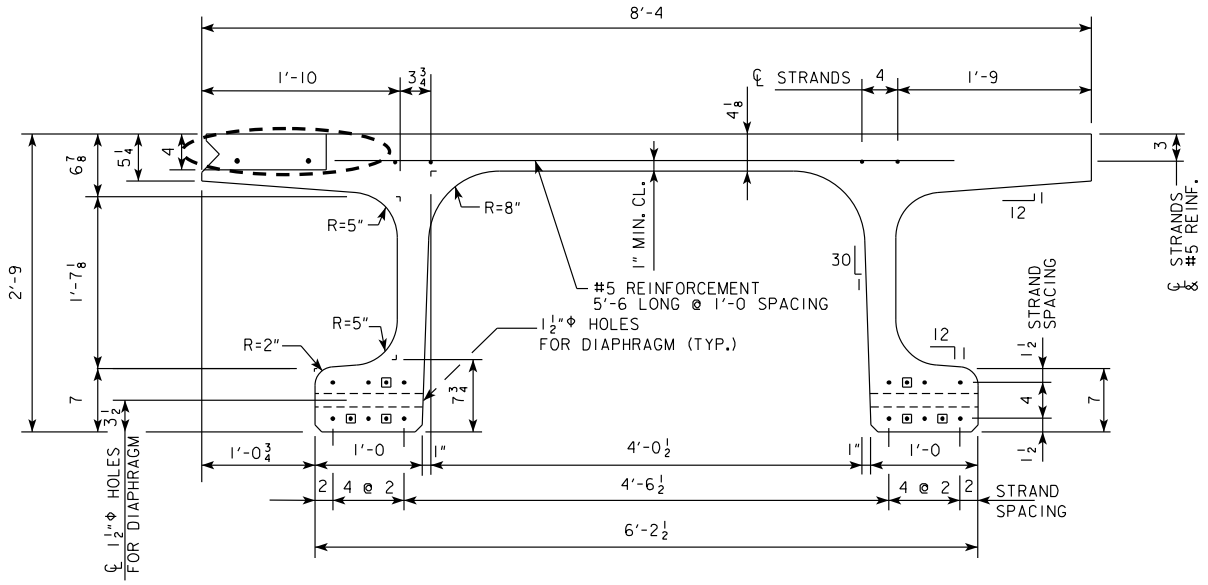

Figure 1.4-Second Generation Pi-Section-(Keierleber, et al. 2008)

To address the concerns with lateral live load distribution characteristics, larger radii were used at the web-deck interface, and the deck thickness was increased from 3 in. to 4-1/8 in. (7.6 cm to 10.5 cm). The decision to thicken the deck to the 4-1/8 in. (10.5 cm) was based on the FEM analysis by limiting the predicted service tensile stresses below 840 psi (5.8 MPa), as shown in Table 2.1. The larger radii also decreased stress concentrations at the web-deck interface and improved material flow during placement of the UHPC. The transverse strength and stiffness of the deck were enhanced by increasing the thickness of the deck and by reducing the web spacing from 4 ft 9 in. to 4 ft 2 ½ in. (144.8 cm to 128.3 cm). Note that the decreased web spacing also provided a more uniform spacing of the bulbs in a multi-girder bridge configuration. These alterations were also intended to improve the lateral live load distribution characteristics. Placement of ribs on the underside of the deck was considered as another option to increase the transverse strength and stiffness of the deck while keeping the deck thickness at 3 in. (7.62 cm). However, to lower fabrication costs by reusing existing formwork, it was decided to use a deck of constant thickness of 4-1/8 in. (10.5 cm) with #5 bars spaced at 12 in. (15.9 mm diameter bars spaced at 30.5 cm) placed near the bottom of the deck (Keierleber, et al. 2008). The thickness of the webs was also increased from 3 in. to 3-3/4 in. (7.6 cm to 9.5 cm) to improve material flow during casting. Each pi-girder has a cross-sectional area of 860.8 in^2 (0.555 m^2), a moment of inertia of

105,730 in^4 ($44x10^9$ mm^4), a self-weight of 932 lb/ft (1,390 kg/m) and a neutral axis depth of 10.5 in. (26.7 cm) from the top of the girder. A comparison of first and second pi-section properties is shown in Table 1.2.

Table 1.2-Comparison of 1st and 2nd Generation Pi-Girder Properties

Section	Area (in^2)	MOI (in^4)	Self-Weight (lb/ft of section)
First Generation	609	89,060	657
Second Generation	861	105,730	932
Percent Increase (%)	41	19	42

2 BRIDGE DESIGN

2.1 Introduction

The design of the Jakway Park Bridge was completed by the Office of Bridges and Structures at the Iowa DOT. The following sections describe the design of Jakway Park Bridge and provide a detailed description of the UHPC centerspan.

2.2 Preliminary Design

Because no domestic design specifications for UHPC bridges exist, the Iowa DOT requested that the Bridge Engineering Center (BEC) at Iowa State University (ISU) perform a finite element analysis of the pi-girder centerspan of the bridge. The design of the bridge was based on the finite element analysis results, a review of international guide specifications and research reports (Japan Society of Civil Engineers 2006) (Gowripalan and Gilberg 2000) (Graybeal 2006a) (Graybeal 2006b) (Ulm 2004) and collaboration among the Iowa DOT, the BEC, LaFarge, and the FHWA.

Several key assumptions were made during girder design. The UHPC tensile stresses were limited to the cracking threshold. This restriction was in response to test results of the first generation section showing that deck failure occurred due to longitudinal underside deck cracking (Graybeal 2009a). In addition, it was intended that the durability of the bridge would be improved if the tensile stresses were limited so as to avoid cracking. Because of lack of experience, lack of standard specifications, and the test results of the first generation section, it was assumed that the lateral live load distribution factor was 1.0 (i.e., each girder was designed to resist the entire design vehicle independently). The pi-girder centerspan was assumed to be simply supported.

The material properties and allowable design properties of the UHPC were based on experience with the Wapello County, IA bridge project (the first road bridge in the United States of America to use UHPC), FHWA testing, and manufacturer recommendations (Keierleber, et al. 2008). For design, compressive stresses were limited to 21,500 psi, due to

concerns about using ready-mix trucks for girder fabrication. The pertinent properties are shown in Table 2.1.

Table 2.1-Design Values for Material Prop. of UHPC

Property	Value	
Modulus of elasticity at release	5,800 ksi	(39,990 MPa)
Modulus of elasticity final	7,800 ksi	(53,780 MPa)
Design compressive strength at release	12,500 psi	(86 MPa)
Design compressive strength final	21,500 psi	(148 MPa)
Tensile strength	1,200 psi	(8.3 MPa)
Allowable compressive release stresses 60% of 12.5 ksi	7,500 psi	(51.7 MPa)
Allowable compressive stress at service 60% of 21.5 ksi	12,900 psi	(89 MPa)
Allowable tensile stress at service 70% of 1.2 ksi	840 psi	(5.8 MPa)

The type, size, and location (TS&L) requirements at the proposed bridge site required a total bridge length of approximately 120 ft (36.6 m). Because the test results for the first generation section only verified the behavior at a span length of 70 ft (21.3 m) (Graybeal 2009a), it was necessary that the bridge have multiple spans. Due to budget constraints, only the center span was constructed with the UHPC pi-section.

2.3 Analysis of UHPC Pi-Girder Centerspan

To analyze the UHPC pi-girder span a finite element model of the three-girder centerspan was generated. The model was created by combining three individual girders to create a model composed of over 25,000 solid elements. APDL language was again used so that critical parameters could be quickly modified. The model was used by adjusting the span length, prestressing force, support conditions, connections between individual girders, number of diaphragms, the spacing of diaphragms, and mesh size to provide estimates of stresses and strains for design. The finite element model of the centerspan is shown in Figure 2.1.

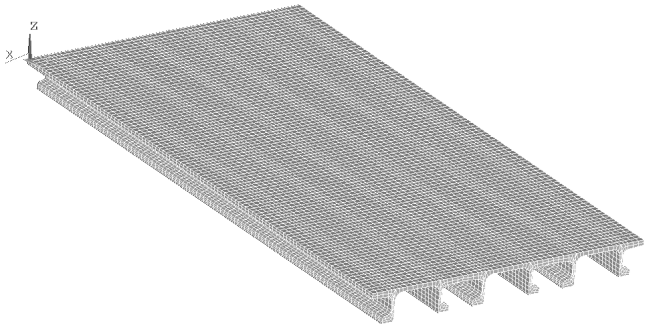

Figure 2.1-Centerspan Finite Element Model

The individual girder geometry was established by experimental and analytical work done at the Iowa Department of Transportation, Iowa State University, LaFarge, and the Federal Highway Administration (Keierleber, et al. 2008). Once the initial geometry of the girders was established (Section 1.3.3), the FEM of the entire bridge was used by modifying the previously listed parameters to provide estimates of stresses and strains for design.

To simulate the girder-to-girder connection detail in the FEM (see Figure 2.10), adjacent girder nodes were coupled in all directions at every 18 in. (45.7 cm.) corresponding to tie bar placement along the length of the girders. To prevent relative transverse displacements of the girders, all of the nodes along the girder-to-girder interface were coupled in the transverse direction. The HSS diaphragm members were modeled as steel three dimensional axial force truss members connecting the bulbs of the girders transversely at the quarterspans and midspan of the pi-girders. The modeling of support conditions and prestressing for the single girder model is discussed in Section 1.3.3.

2.4 Final Design Description

The subject bridge is located on a low volume road in Buchanan Co., Iowa, as shown in Figure 2.2, Figure 2.3, and Figure 2.4. The bridge is 25 ft (7.62 m) in width, 115 ft 4 in. (35.15 m) in length, and consists of three spans. An elevation photograph of the bridge can be seen in Figure 2.5. The center span of the bridge consists of three UHPC pi-girders each with a span length of 50 ft-0 in. (15.24 m). A cross section view of the center span is

presented in Figure 2.6. The end spans are 18 in. (45.72 cm) thick, normal strength reinforced concrete slabs with spans of 31 ft.-8 in. (9.65 m). An elevation view of the end spans is shown in Figure 2.7. An asphalt wearing surface was placed on the bridge in Spring of 2009.

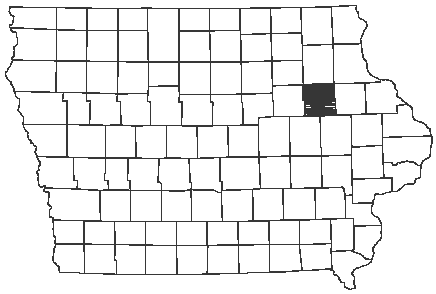

Figure 2.2-Location of Buchanan County in Iowa

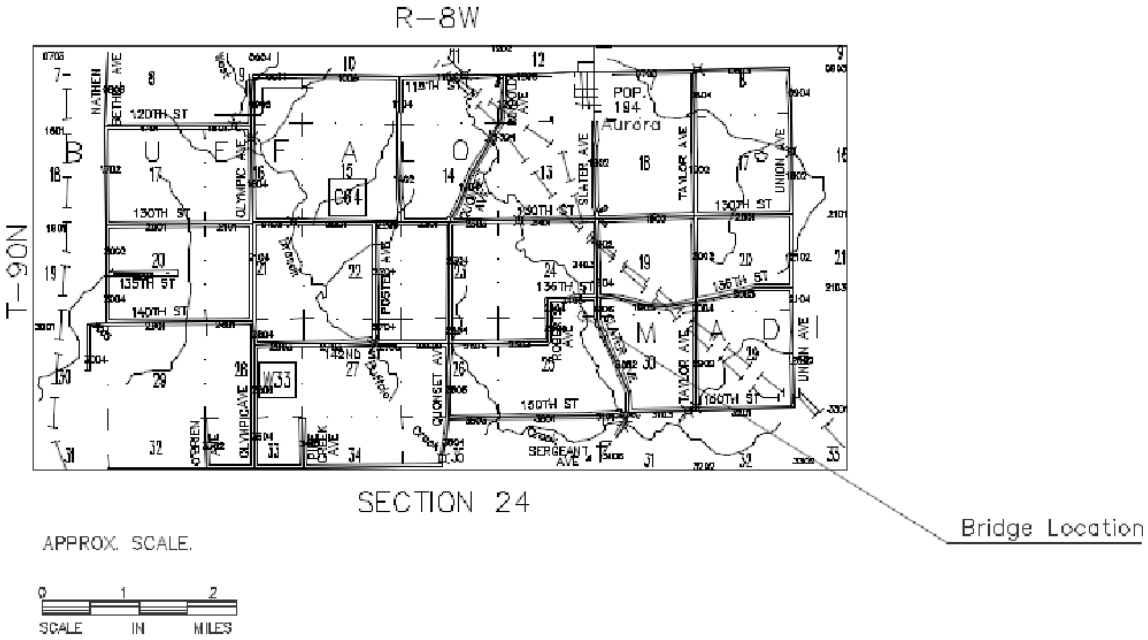

Figure 2.3-Bridge Location in Buchanan County

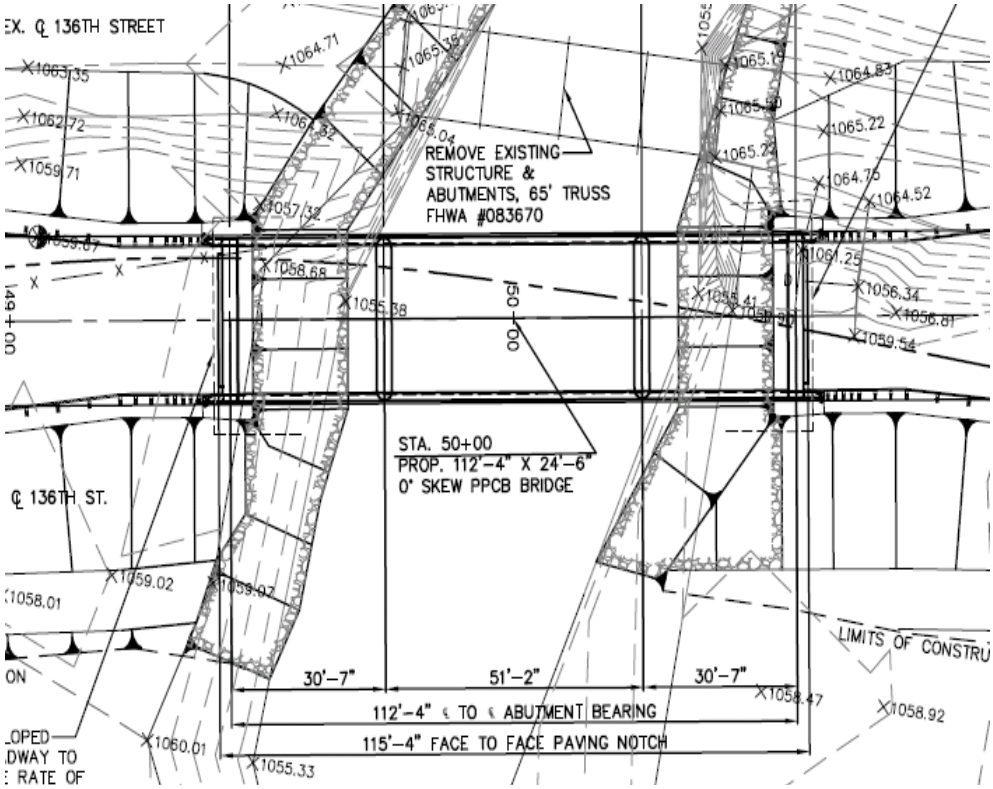

Figure 2.4-Situation Plan of Buchanan County Pi Girder Bridge-(Keierleber, et al. 2008)

Figure 2.5-Elevation Photograph of Pi-Girder Bridge

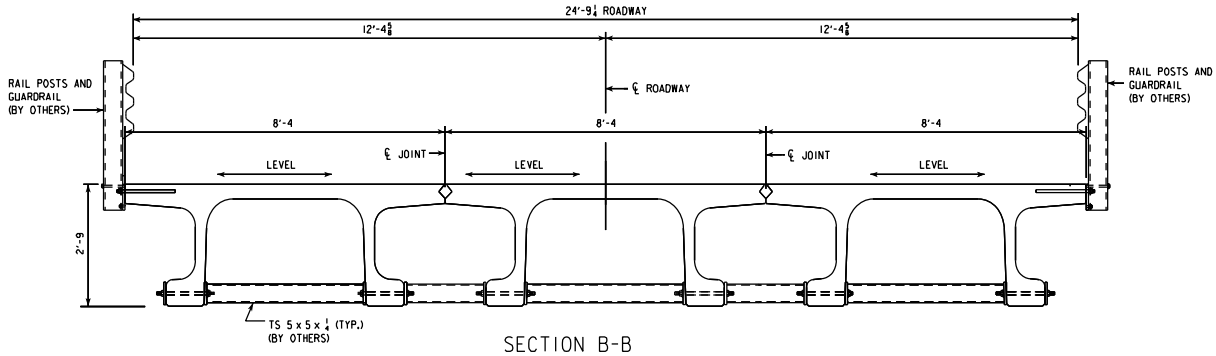

Figure 2.6-Cross-Section of Center Span-(Keierleber, et al. 2008)

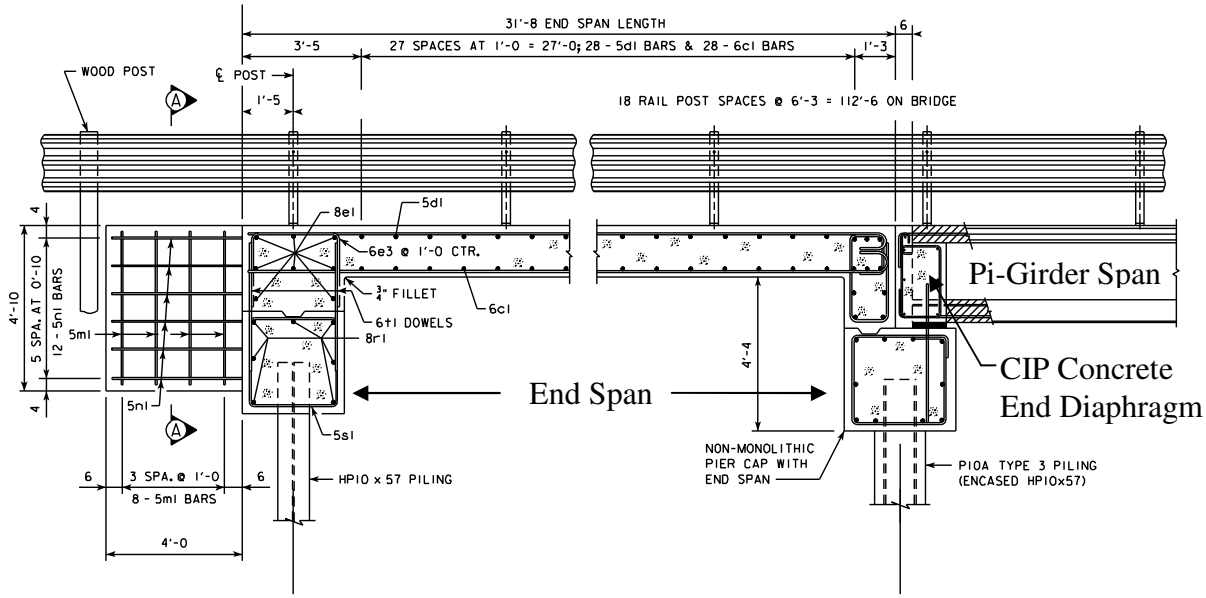

Figure 2.7-Elevation View of End Spans and Pier-(Keierleber, et al. 2008)

For the pi-girder span, steel tube diaphragms were placed at quarterspan and midspan. Although these diaphragms were primarily installed to improve the lateral live load distribution (Keierleber, et al. 2008), previous tests results on the first generation section suggested that these diaphragms would significantly increase the ultimate strength of the section (Graybeal 2009a). The steel diaphragms are shown in Figure 2.6, Figure 2.8, and Figure 2.9. The girder ends were seated on neoprene bearing pads and were encased in cast-in-place concrete diaphragms as shown in Figure 2.7. A bond breaker was placed between the pi-girder span and endspan.

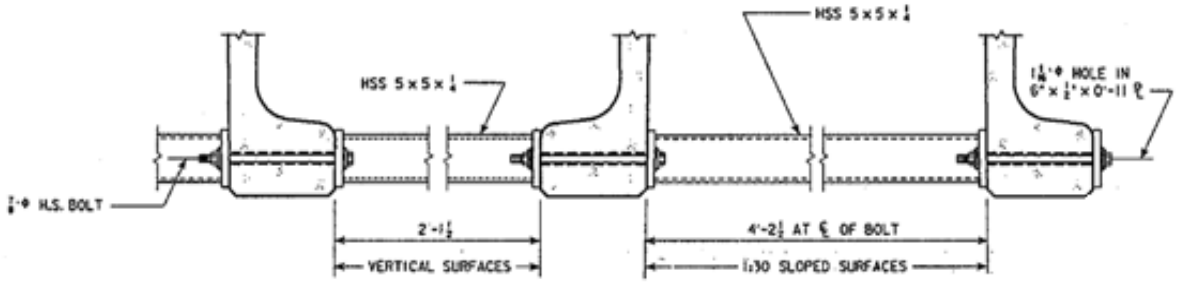

Figure 2.8-Construction Details of HSS Diaphragms

a. Diaphragm in a girder **b. Diaphragm between adjacent girders**

Figure 2.9-Steel Tube Diaphragm Placement Photographs

A cast-in-place shear key was used to connect adjacent girders at the deck level. In addition, #8 bars (25 mm diameter bars) were placed in grout pockets on the top of the deck every 18 in. (45.7 cm.). The location of the grout pockets is shown in Figure 1.4 with a dashed oval, while Figure 2.10 and Figure 2.11 provide the construction details and pictures for the connection.

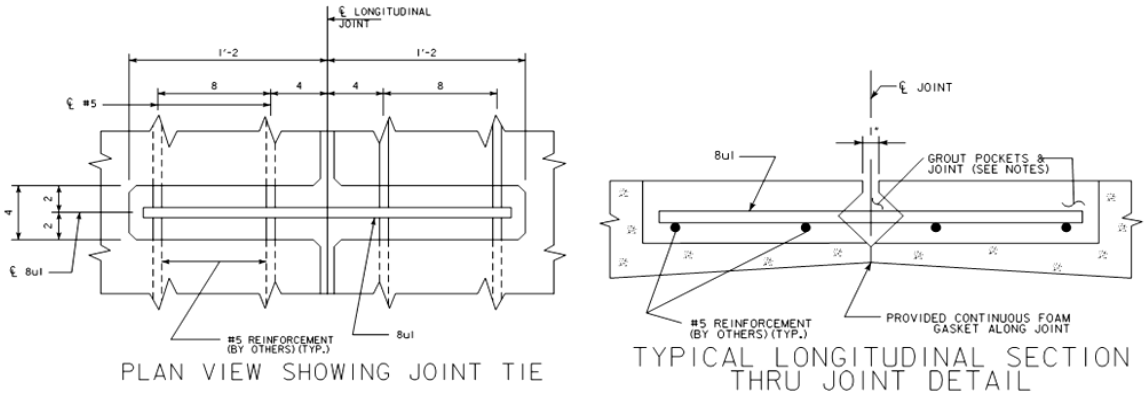

Figure 2.10-Pi-Girder Longitudinal Joint Connection Detail

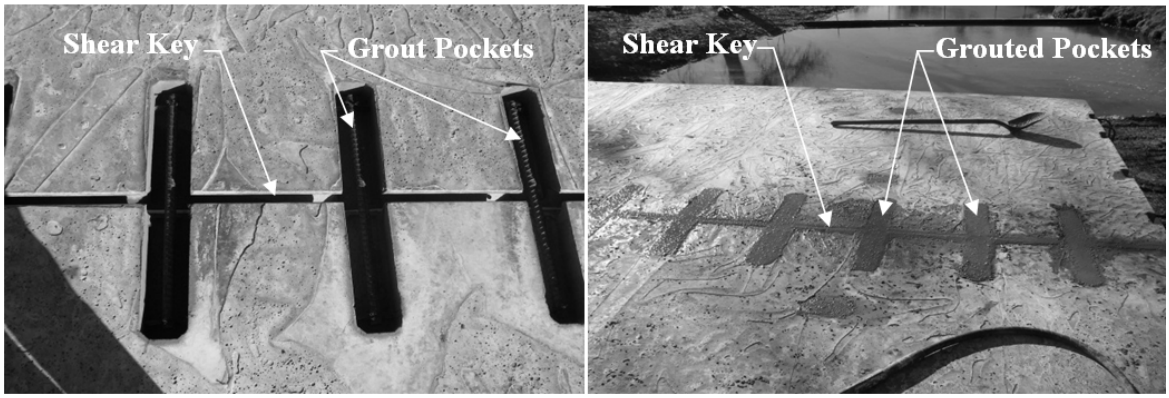

Figure 2.11-Longitudinal Joint Connection Photographs

Longitudinal reinforcement details for the pi-girders are shown in Figure 1.4. Twenty-two 0.6 in diameter, low-relaxation prestressing strands provided the flexural reinforcement. Eighteen strands were placed in the bottom of the bulbs, nine in each bulb, and tensioned to a total force of 766 kips (3407 kN). The four strands located in the deck were prestressed to a total initial force of 170 kips (756 kN). Along with Figure 1.4, Figure 2.12 and Figure 2.13 display the layout of the longitudinal prestressing strands.

Figure 2.12-Pi-Girder Longitudinal Prestressing

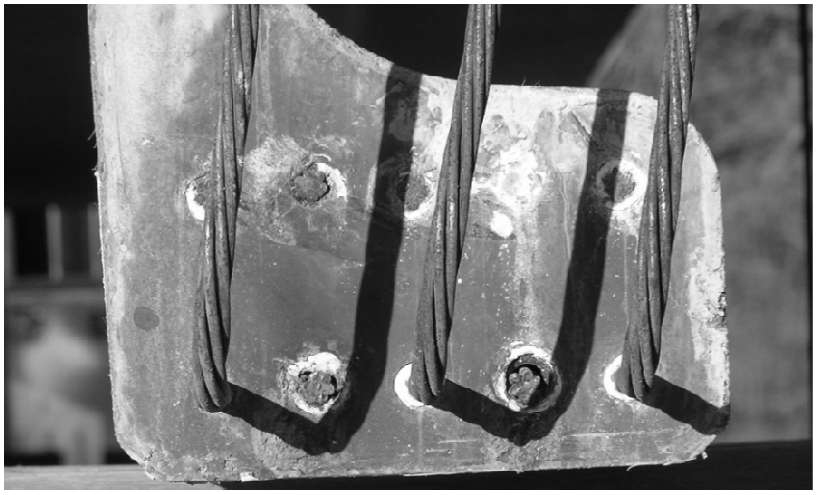

Figure 2.13-Bottom Bulb Longitudinal Prestressing

Transverse flexural reinforcement consisted of mild #5 (15.9 mm) bars placed in the bottom of the deck at 1 ft. on center shown in Figure 1.4. The transverse flexural strength of the UHPC alone was estimated to be larger than the design forces, but the #5 bars (15.9 mm) were added to provide reinforcing to the section if the UHPC in the deck were to experience inelastic deformation.

The pi-girders contained no mild steel shear reinforcing. The steel fibers in the UHPC increase the tensile strength of the concrete, therefore enhancing the concretes ability to resist inclined web shear cracking and flexure-shear cracking. The shear strength of the UHPC alone was estimated to be larger than the design shear forces.

3 CONSTRUCTION

3.1 Introduction

Construction of the Jakway Park Bridge was conducted throughout the fall of 2008. The total construction time of the bridge was 52 days and the bridge was opened to traffic on November 26, 2008. The following sections describe the construction monitoring conducted on the UHPC centerspan.

3.2 Strain Monitoring

In October of 2008, the BEC, the Iowa DOT, and Buchanan Co. developed an experimental test plan for monitoring strains during critical portions of the construction of the Jakway Park Bridge. The test plan focused on monitoring strains in the webs induced by placement of the steel HSS diaphragm members during construction. A total of 16 transducers, 12 at midspan and 4 at the three-eighths span, were placed on the bridge. The twelve strain transducers placed at midspan were placed vertically on the upper and lower portions of each side of the webs; the layout is shown in Figure 3.1. The layout of the transducers at three-eighths span is shown in Figure 3.2.

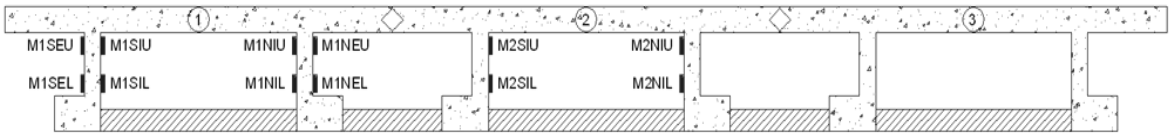

Figure 3.1-Layout of Vertical Web Transducers at Midspan

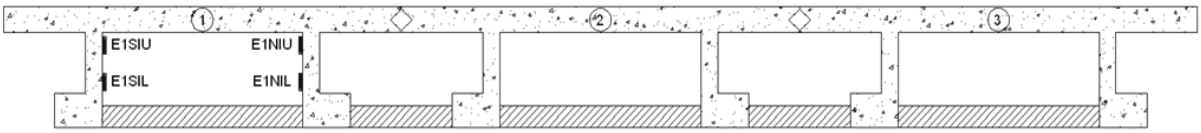

Figure 3.2-Layout of Vertical Web Transducers at 3/8 Span

During installation of the diaphragms, it was observed that some of the HSS members needed to be modified to fit between the webs. Modifications included lubrication of the members

as well as shaving off portions of the base plates. Even with adjustments to the members, the diaphragm installation was sometimes difficult. The installation process often resulted in members being forced into place. Possible explanations for the tight fit of diaphragm members include; shrinkage of the section, deformation of the webs under prestressing and self-weight, and tolerances of HSS members were not strict enough.

3.3 Midspan Construction Strain

The construction strains measured in the vertical transducers at midspan ranged from -65 to 65 με. After all of the diaphragm members had been installed, the maximum residual tensile strain in the webs was roughly 45 με recorded at M1SIU. Forty-five με is significant as the maximum live load strain measured in the webs during live load testing was 45 με recorded along path 3, see Table 5.6. Figure 3.3 displays the measured construction strains at midspan.

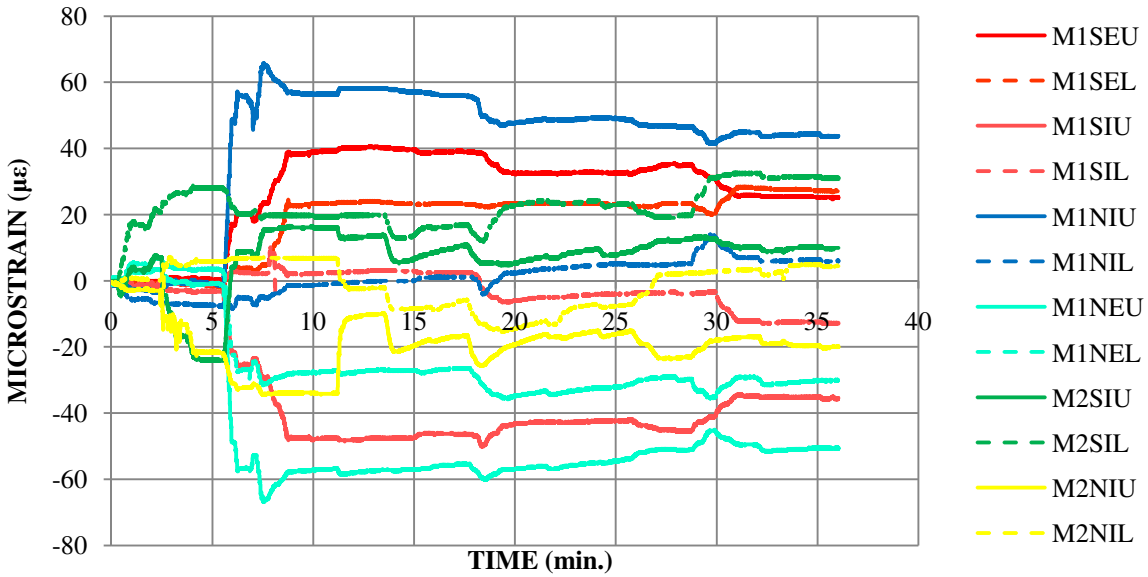

Figure 3.3-Construction Vertical Web Strain Measured at Midspan

3.4 Three-Eighths Span Construction Strain

The construction strains measured in the vertical transducers at three-eighths span ranged from -50 to 65 με. After all of the diaphragm members had been installed, the maximum residual tensile strain in the webs was roughly 40 με recorded at E1NIU. Figure 3.4 displays the construction strains measured at three-eighths span.

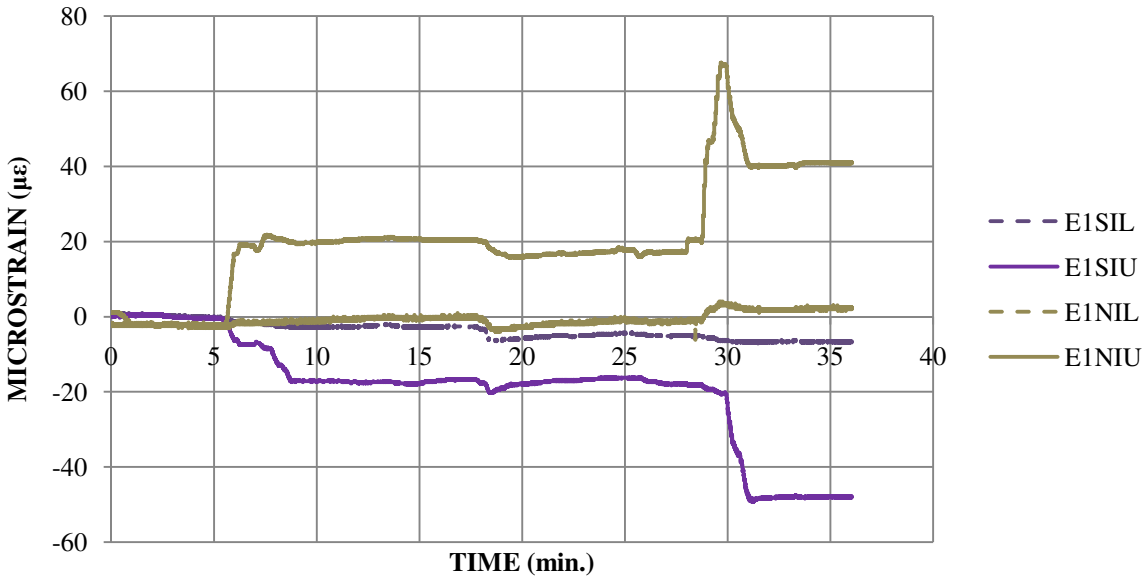

Figure 3.4-Construction Vertical Web Strain Measured at 3/8 Span

4 LABORATORY TESTING

4.1 Introduction

Laboratory testing involved concrete material tests for compressive and flexural strength. Specimens cast at the La Farge plant in Winnipeg, Canada were sent to Iowa State University for testing. The test samples were cast alongside the girder in September of 2008 and tested in May 2009 and October 2009.

4.2 Compressive Strength Test Procedure

Sixteen three-inch diameter cylinders were tested in compression in accordance with ASTM C39. The ends of the cylinders were precut by La Farge ensuring that each end was smooth and free of defects. Sulfur compound was originally used to test the compressive strength of the UHPC specimens. After several trials, it was observed that cracking of the sulfur cap induced lateral spreading of the top of the specimen. The forces created by the lateral spreading lowered the compressive strength of the UHPC cylinders. One specimen was tested with metal caps that included neoprene pads. During testing, it was observed that the specimen was forcing the neoprene out of the caps, and that the neoprene provided confinement to the top of the specimens. The compressive stress measured for the test with the metal caps was 37.1 ksi. As the neoprene was severely damaged during the test, it was decided that the best method to test the specimens would be without any type of cap.

4.3 Compressive Strength Test Results

Compressive strength results for the three-inch concrete cylinders taken are presented in Table 4.1. From the compressive tests with no caps, the compressive strengths ranged from 24,075 psi to 29,675 psi, and had an average value of 28,000 psi at 250 days. This value is 30% larger than the value used for design of 21,500 psi shown in Table 2.1. As previously

mentioned, compressive stresses were limited to 21,500 psi due to concerns about using ready-mix trucks for girder fabrication.

Table 4.1-Compression Test Results

GIRDER	SAMPLES	AVERAGE (ksi)	STD. DEV (ksi)
1	5	29.0	1.26
2	6	26.8	1.77
3	5	28.3	1.36
BRIDGE	***16***	***28.0***	***1.69***

4.4 Flexural Strength Test Procedure

Eighteen beams, six from each girder, were tested in order to determine the modulus of rupture of UHPC, which may be used as an estimate of tensile strength. The beams tested had cross sectional dimensions of 1.56 in. x 1.56 in. (40 mm x 40 mm) and a length of 6.3 in. (160 cm). A three-point load test with a span length of 4.5 in. (115 mm) was used to establish the modulus of rupture.

4.5 Flexural Strength Test Results

To estimate the tensile strength f_{ct}, the tensile strength obtained from small-scale flexural testing $f_{ct,flexure}$ must be corrected for scale effects (Graybeal 2006a). Chanvillard and Rigaud, 2003 provide Equation 5.1 to correct $f_{ct,flexure}$ obtained from small-scale testing; the coefficient α depends on the concrete formulation, and varies between 1 and 2 depending on the concrete's brittleness. Chanvillard and Rigaud, 2003 determined that the ratio of $f_{ct,flexure}$ *to* f_{ct} to be 1.76 for beams with cross sectional dimensions of 1.57 in. x 1.57 in. and a span length of 6.30 in. (40 mm x 40 mm x 160 cm). A corresponding α value of 2.5 was determined to maintain this ratio. The corrected tensile strengths ranged from 1,640 psi to 2,415 psi, and had an average of 1,855 psi. This value is 55% larger than the value of 1,200 psi seen in Table 2.1 used for design. The flexural strength test results are presented in Table 4.2.

$$f_{ct} = f_{ct,flexure} \frac{\alpha * \left(\frac{h}{h_o}\right)^{0.7}}{1 + \alpha * \left(\frac{h}{h_o}\right)^{0.7}} \quad (4.1)$$

Where f_{ct} is the direct tensile strength, $f_{ct,flexure}$ is the flexural tensile strength, α is a coefficient that depends on concrete formulation and varies depending on the concrete's brittleness, h is the depth of the specimen, and h_o is a reference depth of 4 in. (100 mm).

Table 4.2-Modulus of Rupture Test Results

GIRDER	SAMPLES	AVERAGE (psi)	CORRECTED AVE. (psi)
GIRDER 1	6	3,250	1,850
GIRDER 2	6	3,200	1,800
GIRDER 3	6	3,400	1,900
BRIDGE	***18***	***3,300***	***1,850***

5 FIELD TESTING

5.1 Introduction

Field testing of the Buchanan Co. UHPC Bridge took place in both November 2008 and September 2009. The tests were conducted roughly a year apart to allow for changes in the behavior of the bridge throughout the first year of operation. Through the use of field testing, this investigation was able to quantify the response of the bridge under service level loads and subsequently quantify the conservatism present in design. The following sections describe the instrumentation and methodology as well as the test results from the static and dynamic loading of the bridge for the 2008 and 2009 live load tests. To allow for comparison, the field test results will be presented with the corresponding finite element model predictions for strain or deflection. The FEM was used as a predictive tool to obtain estimates of the strains and deflections that were measured in the field. Because the model had not been modified since its use during design, the FEM results presented were available prior to construction and field testing. Unless otherwise noted, the FEM node best corresponding to the location of the strain transducer or displacement transducer was used to report the FEM predictions of strain or displacement.

The strains measured during testing and shown in the following sections are live load (LL) strains. Since the initial strains in the pi-girders were not monitored, the total strains for the bridge were not measured directly. However, initial strains, dead load strains, could be computed with the finite element model. The total strains reported in the following sections were determined by the addition of the measured live load test strains and the analytically computed dead load strains. The estimated total strains are critical to verify the assumption that the tensile strains of the bridge are below the estimated cracking threshold. For reference, the cracking strain for UHPC is conservatively estimated to be +150 to +160 με. Note that for the results presented in the following sections, positive strains are tensile and negative strains are compressive. Downward deflections are negative and upward deflections are positive.

5.2 Field Test Methodology and Instrumentation

Cooperatively, the BEC, the Iowa DOT, and Buchanan Co. developed an experimental test plan for evaluating the structural behavior of the Jakway Park Bridge. In general, the test consisted of monitoring both strains and deflections at locations deemed critical to quantify bridge behavior while a known, tandem-axle dump truck crossed the bridge. The test plan called for two tests approximately a year apart as to quantify changes in bridge behavior. In addition, the second test would consist of both dynamic and static loads.

For the first test in 2008, thirty-two surface mounted strain transducers and six displacement transducers were attached to the bridge to quantify its response under a known static live load. The strain transducers were located at the pi-girder midspan, quarterspan, and near the eastern end. Twenty-six of the thirty-two strain transducers were located at midspan. The six displacement transducers were installed at midspan to monitor maximum vertical deflections. The layout of the 2008 strain transducers and displacement transducers at midspan as well as the naming key can be seen in Figure 5.1 and Table 5.1 respectively. The quarterspan instrumentation consisted of three strain transducers located on bottom of the three southernmost bulbs oriented longitudinally. The instrumentation near the eastern pier consisted of three longitudinal strain transducers, two of which were located on the bottom of the southernmost bulbs oriented longitudinally with the remaining transducer located on the top of the deck over the northern bulb on girder 1 also oriented longitudinally.

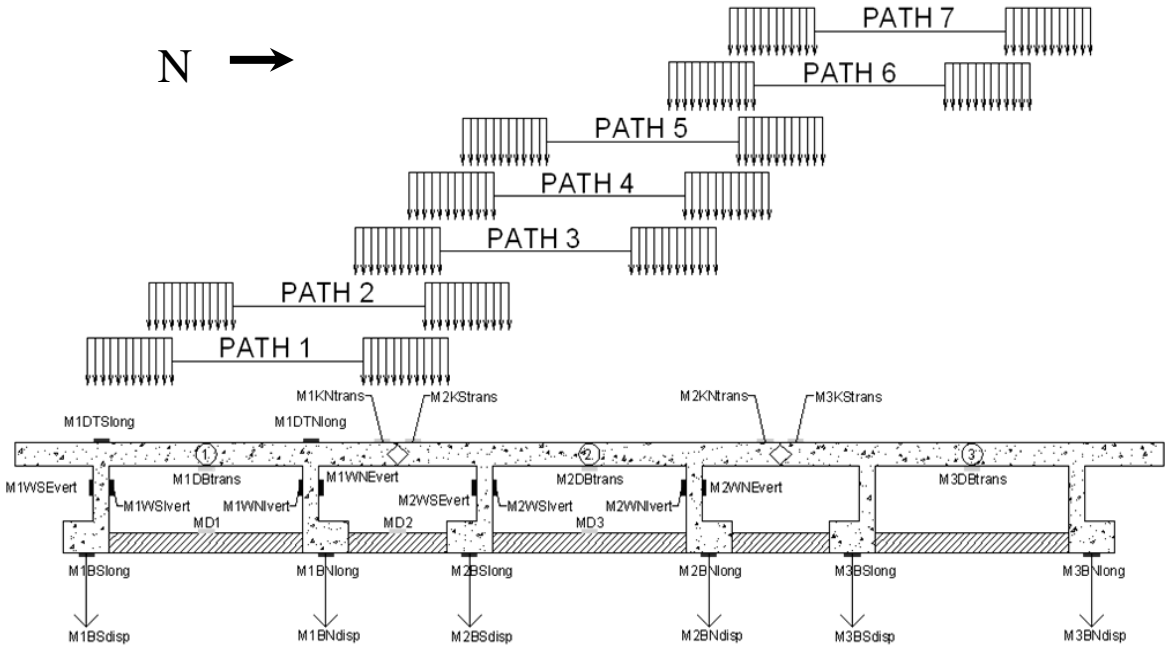

Figure 5.1-Schematic Layout of 2008 Transducers and Loading Paths at Midspan

Table 5.1-Transducer Nomenclature

SPAN LOCATION		GIRDER #	LOCATION ON X-SECTION		ORIENTATION	
M	MIDSPAN	1	BS	BULB SOUTH	long	LONGITUDINAL
Q	1/4 SPAN	2	BN	BULB NORTH	trans	TRANSVERSE
E	3/8 SPAN	3	WSE	WEB SOUTH EXTERIOR	vert	VERTICAL
P	NEAR EAST PIER		WSI	WEB SOUTH INTERIOR	disp	DISPLACEMENT
			WNE	WEB NORTH EXTERIOR		
			WNI	WEB NORTH INTERIOR		
			DTS	DECK TOP SOUTH		
			DTN	DECK TOP NORTH		
			DB	DECK BOTTOM		
			KS	SOUTH SHEAR KEY		
			KN	NORTH SHEAR KEY		

EXAMPLE-M1BSlong=Midspan on girder 1 at the South Bulb orientated longitudinally

The 2009 live load test conducted in September 2009 consisted of the same transducer layout as the 2008 test with the addition and relocation of several transducers. Displacement

transducers were not used, as it was verified from the first test that the strain transducers could provide similar information in terms of distribution factors. Strain transducers located on the top of the deck for the 2008 test were relocated underneath due to placement of an asphalt wearing surface on the deck. Three additional transducers were placed on the quarterspan diaphragm to monitor forces in these members. The layout of the 2009 strain transducers at midspan can be seen in Figure 5.2.

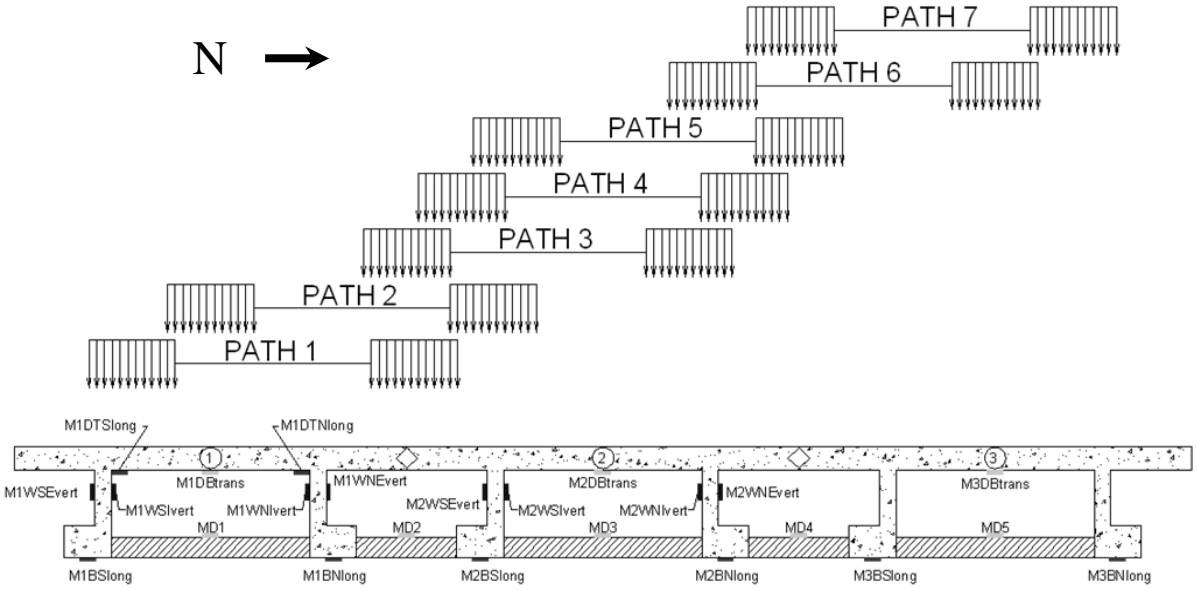

Figure 5.2-Schematic Layout of 2009 Transducers and Loading Paths at Midspan

The both tests were conducted by driving a three-axle truck slowly across the bridge along 7 specified load paths. Each load path was traversed twice to ensure precision of the data. Note that paths 2 and 6 are along the center of each respective lane and are useful in computing live load distribution factors. The layout of all load paths for the 2008 and 2009 tests can be seen in Figure 5.1 and Figure 5.2. The live load consisted of a fully loaded three-axle dump truck similar to an AASHTO WB-40 standard truck. The fully loaded weight of the truck used in the 2008 field testing was 60,680 lbs compared with the 2009 truck weight of 60,600 lbs. The weight of each rear axle was roughly 22.5 kips for each test, which is slightly less than the design 2008 Interim AASHTO tandem of 25 kips/axle. The

configuration of the test truck along with the axle weights for both the 2008 and 2009 test can be seen in Figure 5.3.

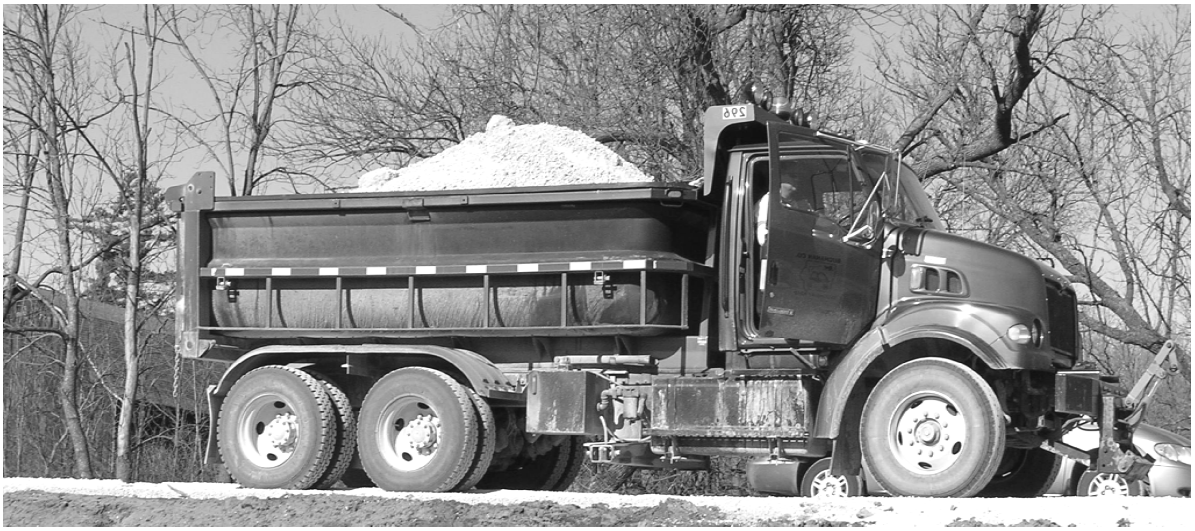

a. 2008 & 2009 Test Truck

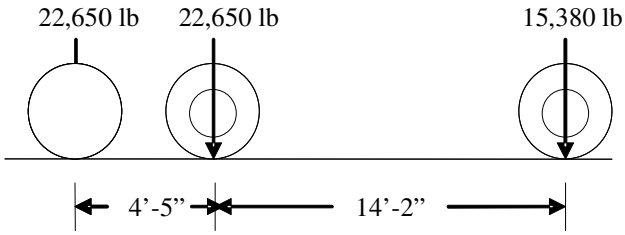

b. 2008 load values

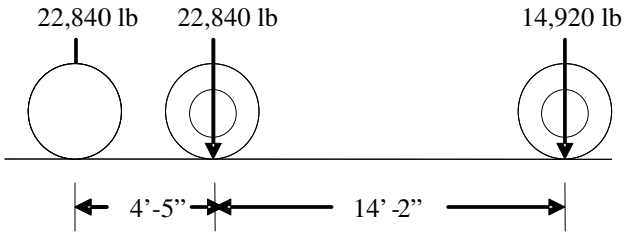

c. 2009 load values

Figure 5.3-Test Truck Configuration and Loading

5.3 2008 Static Live Load Test

The seven transverse load paths shown in Figure 5.1 were used for the static load test conducted 2008. In total, 28 passes were made during the test, 14 with the midspan diaphragm bolts tight and 14 with the midspan diaphragm bolts loose. The initial 14 passes were to quantify the bridge behavior under normal service conditions. These initial passes could then be compared to the passes made with the diaphragm bolts loose to examine the effect of the HSS diaphragm members on the bridge.

5.3.1 Longitudinal Live Load Strain Measured at Midspan

Longitudinal strain transducers located at midspan measured the flexural response and were used to quantify the actual load fractions and distribution factors. In general, the maximum longitudinal live load strain was recorded when the truck's forward rear axle position was roughly at midspan of the pi-girder portion of the bridge. Live load strains of +107 and +101 με were the largest strains recorded by the transducers located on the bottom of the bulbs and occurred at the outermost bulbs when loaded along paths 1 and 7. The maximum bulb live loads strains are shown in Table 5.2. A representative sample of the data can be seen in Figure 5.4. The vertical black bars indicate the beginning and end of the pi-girder span. Once the truck reached the end span, the strain reversed in sign indicating some degree of continuity between the end span and pi-girder span. Analytical modeling showed compressive total strains on the bottom bulbs at all sections for all loading conditions indicating that the prestressing forces maintained the bulbs in compression even when the live load is applied. The maximum estimated total strain was -115 με, indicating that cracking of the bulbs is unlikely under service level conditions.

Using these measured strains and conservatively assuming a UHPC tensile strength of 8.27 MPa (1.2 ksi), a maximum span length was computed based on limiting tensile stresses to the cracking threshold. Allowing for a 5 cm (2 in.) asphalt overlay, and an impact factor of 1.33, the girder span could be increased to roughly 20 m (65 ft) for Interim 2008 AASHTO LRFD

specified loads. As a comparison, Graybeal (Graybeal 2009b) estimates a maximum span length of 87 ft for Service III and Strength I level loads for the same section with increased prestressing force.

Table 5.2-Maximum LL Longitudinal Strains at Midspan

	Path Number						
	1	2	3	4	5	6	7
Strain (με)	107	80	69	71	71	74	101
Location	M1BSlong	M1BSlong	M2BSlong	M2BSlong	M2BSlong	M3BNlong	M3BNlong

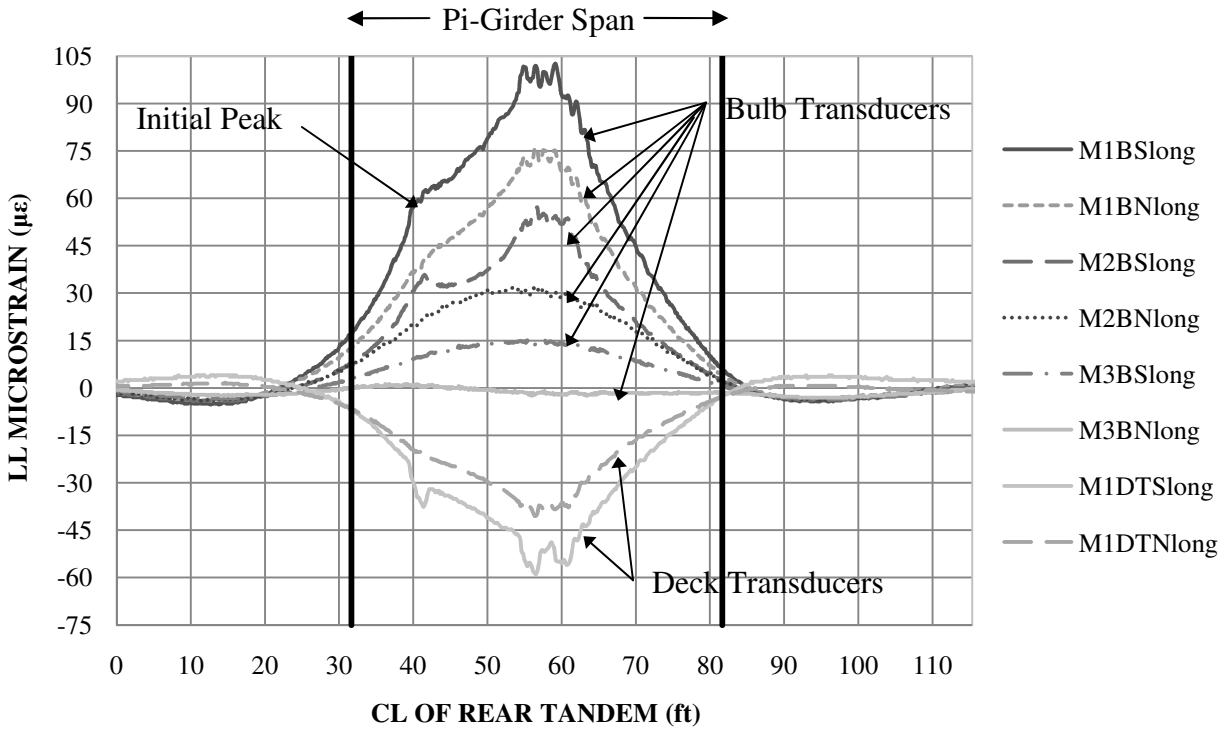

Figure 5.4-Representative Sample of LL Longitudinal Strain at Midspan along Path 1

Two longitudinal strain transducers were located on the top of the deck to further quantify the flexural response and to locate the neutral axis. Strain transducers located on the top of the deck recorded live load strains ranging from -65 to +5με. The maximum measured live load tensile strain occurred on the southernmost transducer while the truck moved along path 7. The top deck transducers registered tensile strains while the truck was located on the end spans again indicating some degree of continuity. The maximum total strain in the top of the

deck was estimated to be -4 με, indicating that transverse cracking of the deck is unlikely under service level conditions. Figure 5.4 shows a representative sample of the data.

A trend present in a majority of the longitudinal strain data was the presence of an initial spike in the strain caused by the front axle passing directly over the transducers. The spike occurs in Figure 5.4 when the centerline of the rear tandem axle is roughly 40 ft beyond the beginning of the bridge.

From the top deck strains and the bottom bulb strains, the location of the neutral axis was determined to be 11.6 in. from the top of the girder. For comparison, the location of the neutral axis, as shown on the construction documents was 10.5 in. from the top of the girder, and was calculated by the finite element model to be 10.43 in. (neglecting steel reinforcement), from the top of the girder. As the section is 33 in. deep, the difference in neutral axis depth between test results and analytical calculations is less than 5%.

5.3.2 Longitudinal Live Load Strain at Midspan Predicted by FEM

The strain predicted by the FEM at midspan varies greatly depending on which node on the bottom of bulb is being considered. The possible nodes for consideration are shown in Figure 5.5. Variations of up to 25 με were observed between the three nodes on the bottom of the bulbs at midspan. Figure 5.6 displays the strain variation between nodes along the centerline of the bridge for path 4. Strain transducer placement in the field was not always along the centerline of the bulb due to limitations on ladder placement and individual worker capabilities. Therefore, to account for deviations of transducer location from the bulb centerline, the maximum strain reading of the three nodes located on the bottom of the bulbs will be reported in this section as the FEM prediction.

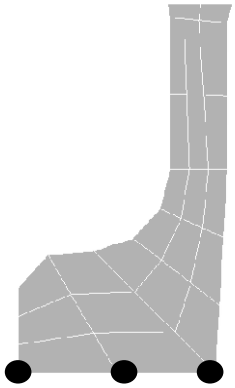

Figure 5.5-Location of FEM Nodes on the Bottom of the Bulbs

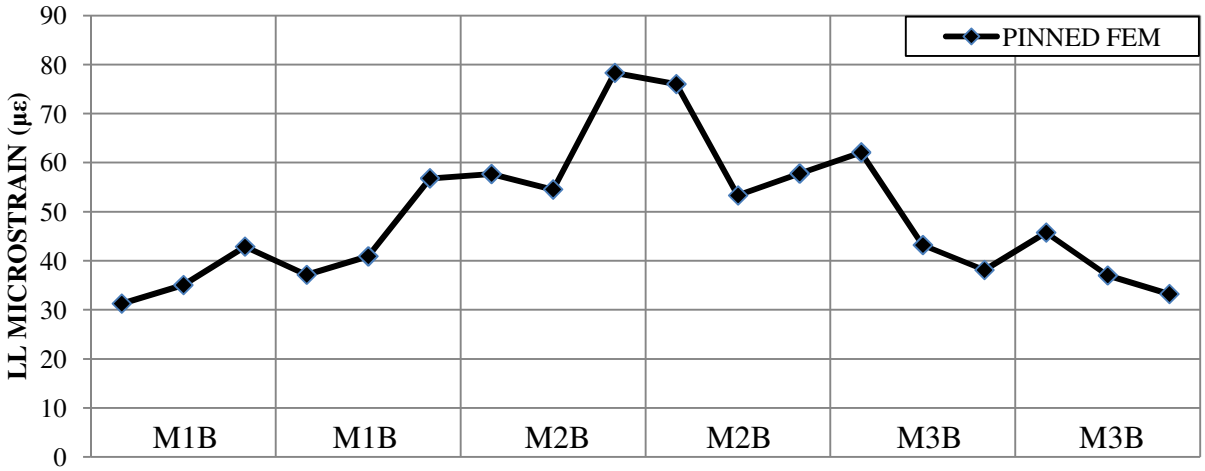

Figure 5.6-Localized LL Longitudinal Strain Variation between Nodes at Midspan

The longitudinal live load strains at the bottom of the girder bulbs were predicted using the previously described simply supported end conditions and end conditions including concrete end diaphragms. The predictions for load paths 1 through 4 are shown in Figure 5.7a-d. Paths 5-7 are not shown due to their close similarity to paths 1-3.

Note: The legend presented in the graph of path 1 is applicable to all of the graphs in the set. For the FEM support conditions excluding the concrete end diaphragms, the legend is labeled SS (i.e. simply supported) FEM. For the FEM support conditions including the effects of the concrete end diaphragms, the legend is labeled PR (i.e. partially restrained) FEM. This note is applicable to all sets of FEM graphs in this thesis.

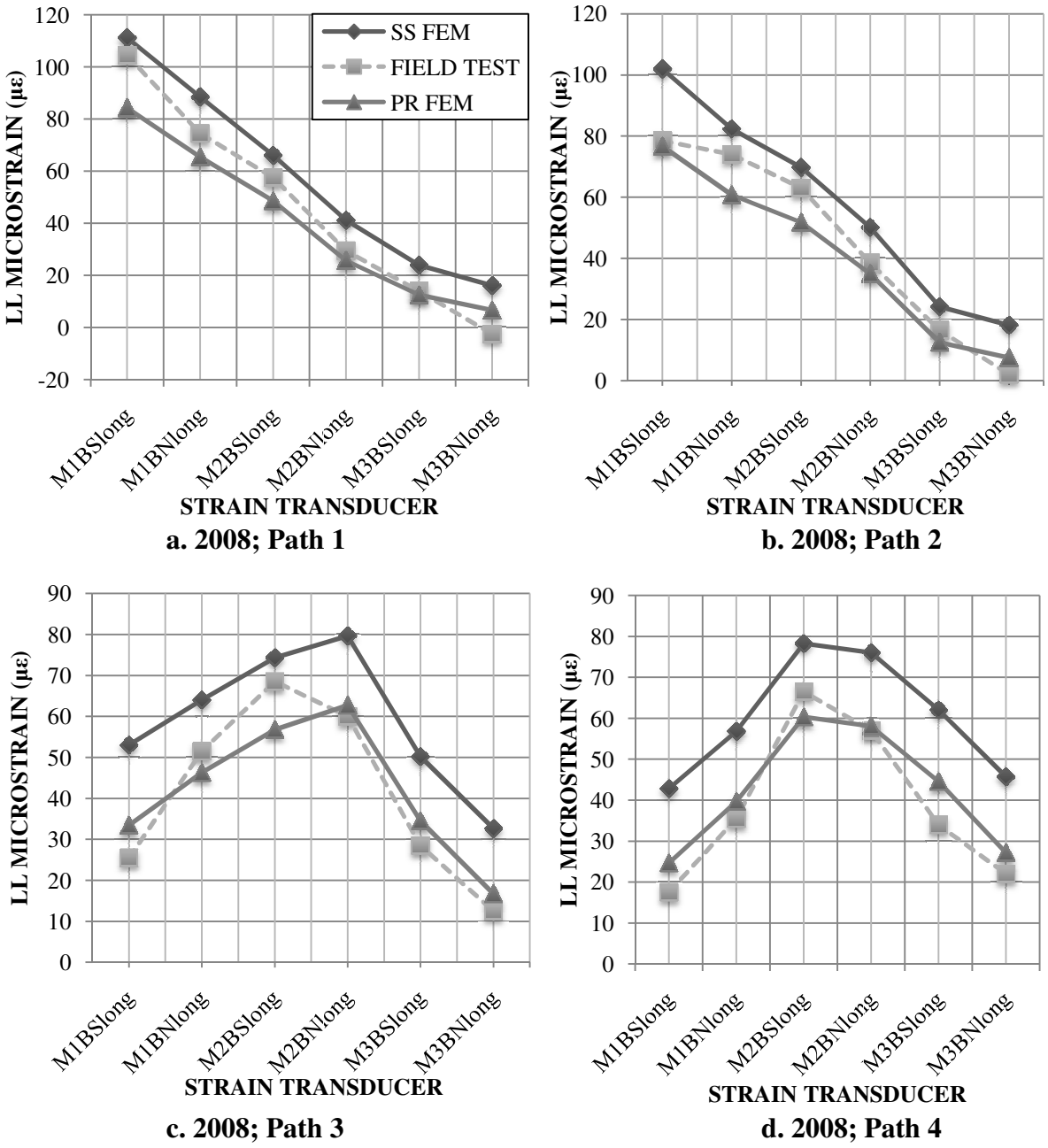

Figure 5.7-FEM LL Longitudinal Bulb Strain at Midspan Paths 1-4

The results of the field testing indicated that, as expected, the supports for the pi-girder span provided some degree of rotational constraint. In other words, the actual support conditions lay somewhere between simply supported and partially restrained. In general, the FEM model was highly effective at predicting live load strains. At worst, the measured field test

strain lay outside of the bounded predictions by only 11 με at M3BS along path 4. Minor discrepancies between predicted and measured strains are likely attributable to the shear key connection between the girders in the model being stiffer than the actual connection in the field. To better reflect the actual distribution of loads among girders, this connection could be modeled with an elastic spring.

The longitudinal deck strains at midspan were also predicted with the FEM. Since only two transducers were orientated longitudinally on the top of the deck, only two data points were available for comparison. The strains were predicted using both a simply supported and partially restrained end condition. The predictions for load paths 1 through 4 are shown in Figure 5.8a-d. Paths 5-7 are not shown due to their similarity to paths 1-3.

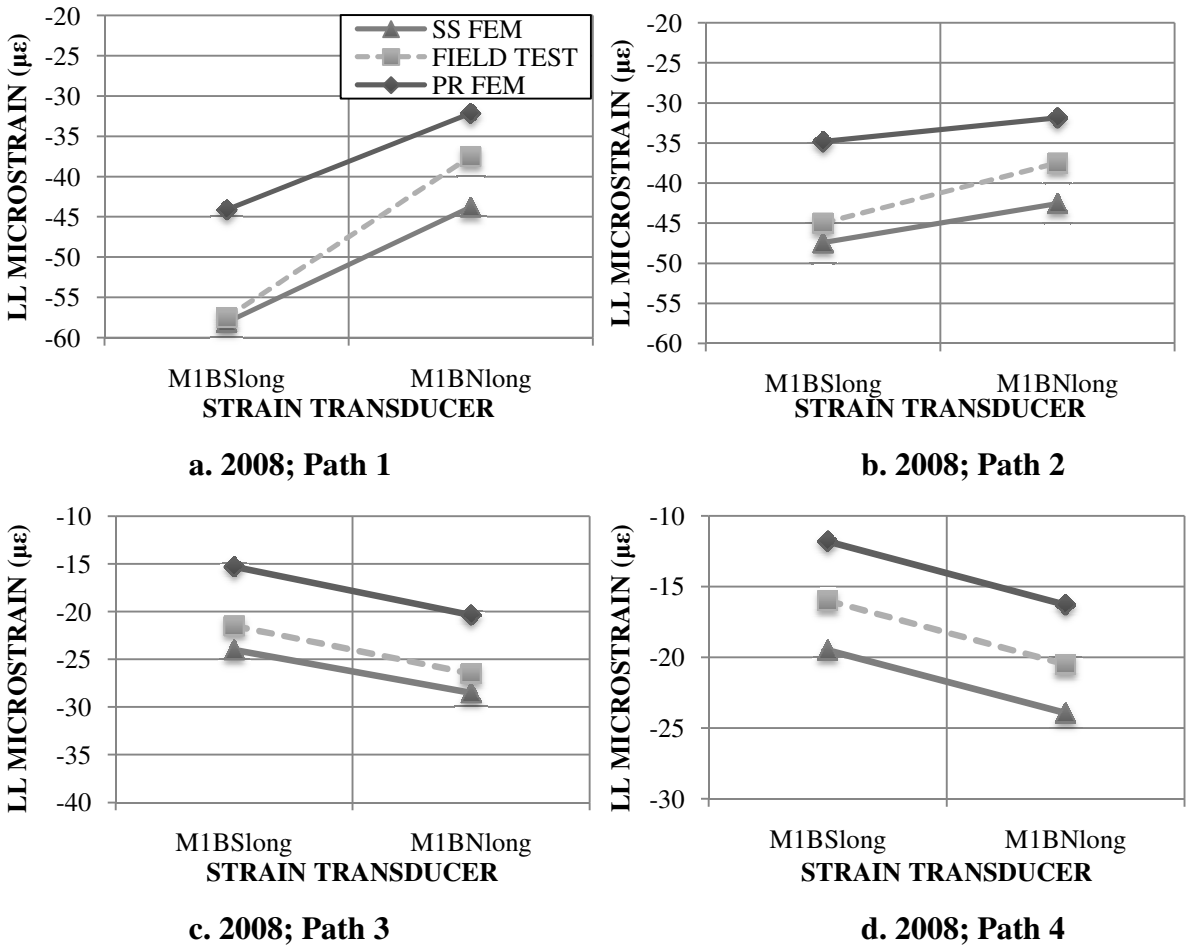

Figure 5.8-FEM LL Longitudinal Deck Strain at Midspan Paths 1-4

The FEM predictions bounded the field test results for all load paths. The predictions were generally within 10 με of the field test results. However, as only two data points on girder 1 were available, conclusions made regarding the accuracy of the model to predict longitudinal top deck strains are difficult to make.

5.3.3 Live Load Deflections Measured at Midspan

The deflection data generally replicated the trends observed in the strain data. Again, the maximum deflection was generally recorded when the truck's forward rear axle position was approximately at midspan of the pi-girders. The largest deflection of -0.13 in. (-3.3 mm) occurred at the exterior bulbs during testing of load paths 1 and 7. Positive (i.e. upward) deflection of the bridge occurred as the truck entered the end span. As before, this indicates some degree of unintended continuity between spans. A representative sample of the data can be seen in Figure 5.9. The maximum live load deflections can be found in Table 5.3.

Table 5.3-Maximum LL Deflections at Midspan

	Path Number						
	1	2	3	4	5	6	7
Deflection	-0.13	-0.10	-0.08	-0.07	-0.07	-0.09	-0.13
Location	M1BSdisp	M1BSdisp	M2BSdisp	M2BSdisp	M2BSdisp	M3BNdisp	M3BNdisp

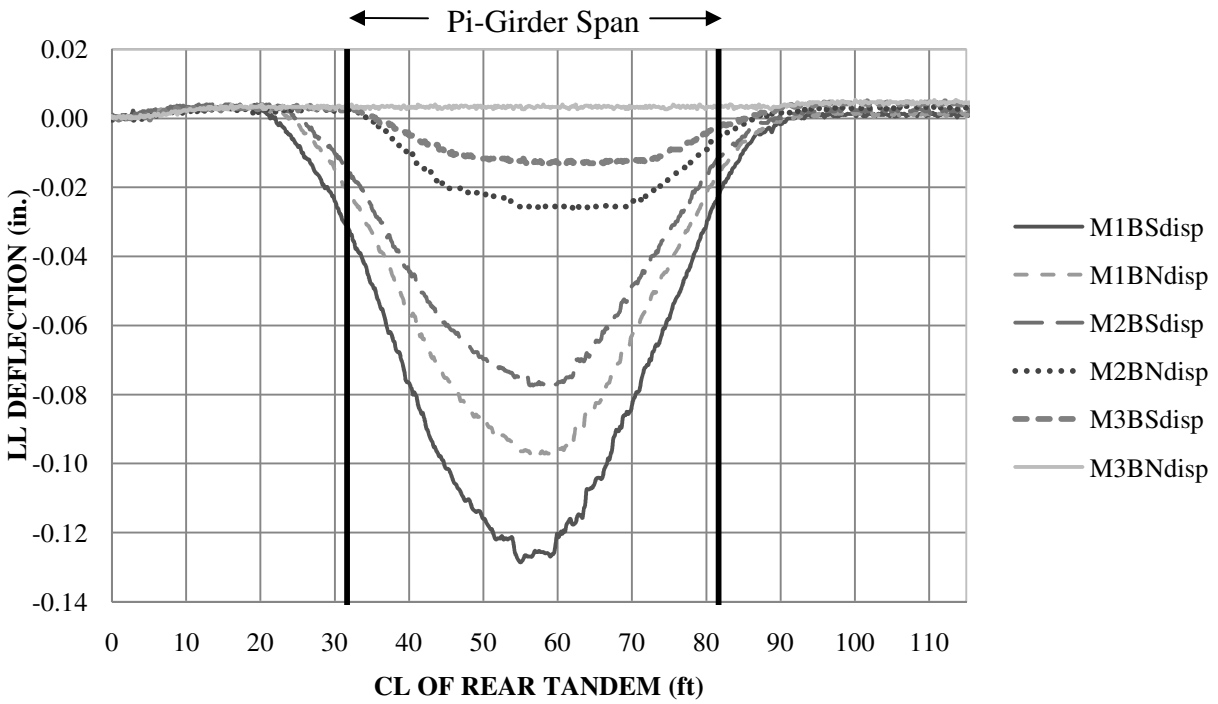

Figure 5.9-Representative Sample of LL Deflection at Midspan along Path 1

5.3.4 Live Load Deflections at Midspan Predicted by FEM

The deflections predicted by the FEM at midspan vary a minimal amount depending on which node on the bottom of bulb is being considered. Figure 5.10 displays the deflection variation along the centerline of the bridge along path 4. Variations between deflection predictions for the same bulb were less than 0.001 in. Therefore, deflections reported in this section will be based on the node corresponding to the centerline of the bulb.

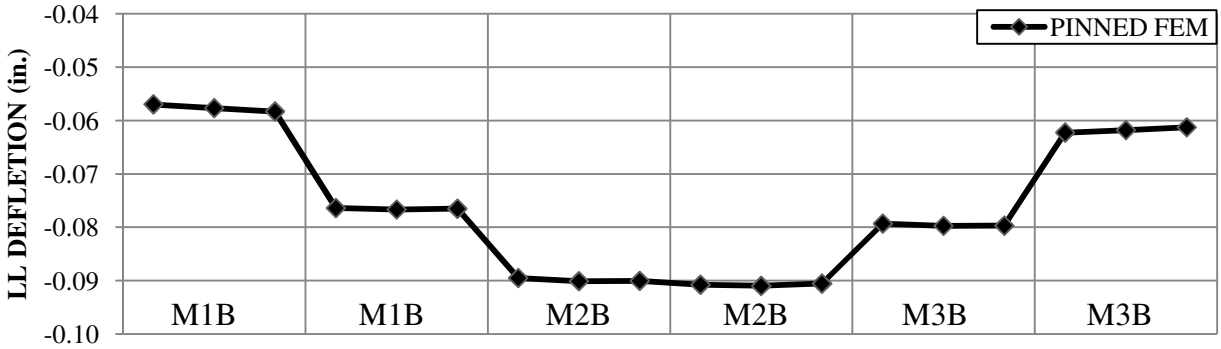

Figure 5.10-Localized LL Deflection Variation between Nodes at Midspan

As with the longitudinal strains measured at midspan, the deflections measured at midspan almost always fell between those predicted with the simply supported and partially restrained boundary conditions of the FEM model for all paths. Similarly, the measured deflections indicate that the bridge distributes the loads somewhat less effectively than predicted by the FEM. This is evident on paths 1, 2, 6, and 7 where sharp decreases in measured strain occur on bulbs on the opposite side of the bridge. Figure 5.11a-d shows the results from paths 1 through 4 at midspan. The results for paths 5-7 are not shown, as they are very similar to the results from paths 1-3.

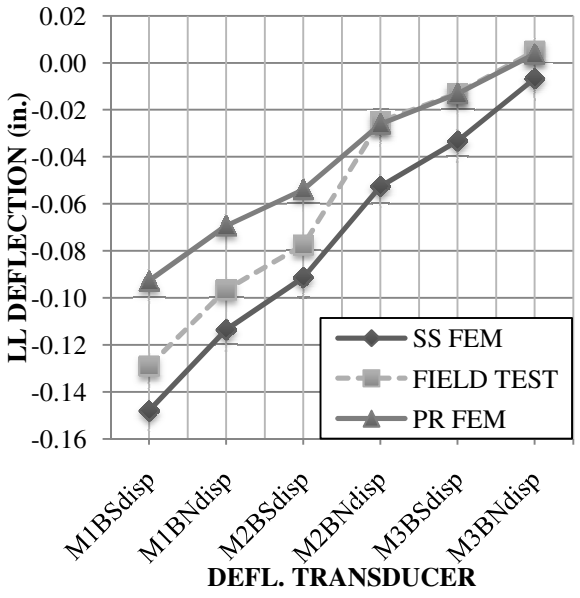

a. 2008; Path 1

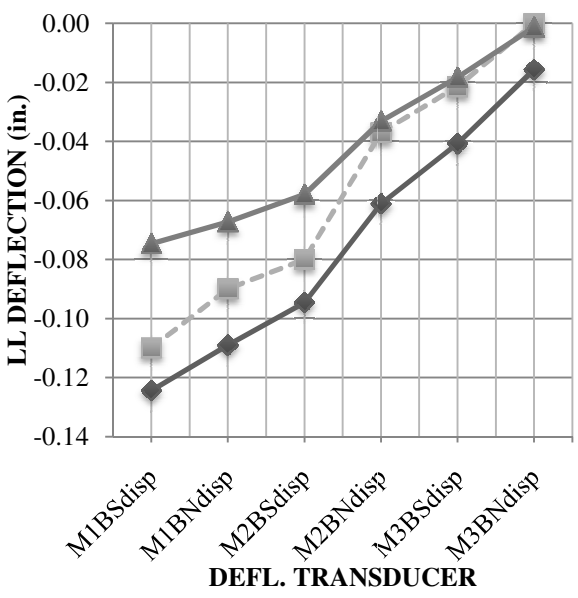

b. 2008; Path 2

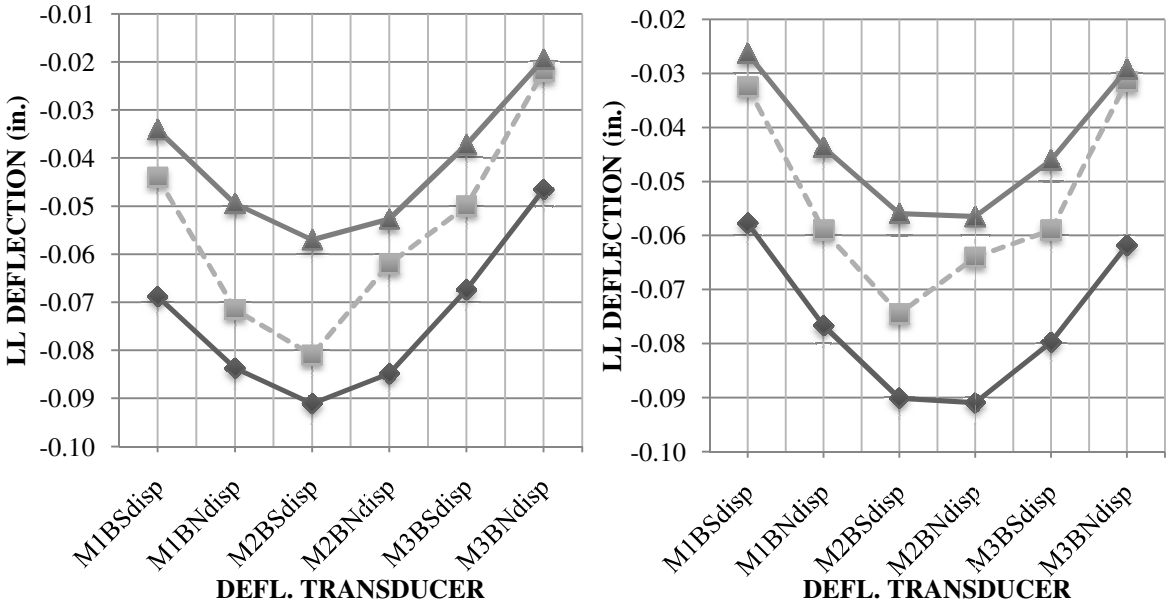

c. 2008; Path 3 **d. 2008; Path 4**

Figure 5.11-FEM LL Deflection at Midspan Paths 1-4

5.3.5 Longitudinal Live Load Bulb Strain Measured at Quarterspan

Longitudinal strain transducers were placed on the three southernmost bulbs at the eastern quarterspan to quantify flexural response, and to compare the trends at quarterspan to those at midspan. In general, the maximum longitudinal live load strain was recorded when the truck's rear axle position was roughly at the quarterspan of the pi-girder portion of the bridge or 45 ft from the beginning of the first end span. Seventy-five με was the largest strain recorded by the transducers located on the bottom of the bulbs at quarterspan, and occurred at the southernmost bulb when loaded along path 1. The maximum quarterspan bulb live loads strains are shown in Table 5.4. Once again, the strain reversal when the truck reached the end span indicates some degree of continuity between the end span and pi-girder span. A representative sample of the data can be seen in Figure 5.12. Similar to the longitudinal strains at midspan, the total strain in the bottom of the bulbs was estimated based on the initial strains predicted by the FEM. The nearest the bulbs at quarterspan approached total strain tensile values was -175 με. This indicates that cracking of the bulbs at quarterspan under service level loads is unlikely.

Table 5.4-Maximum LL Longitudinal Strains at Quarterspan

	Path Number						
	1	2	3	4	5	6	7
Strain (με)	75	56	49	49	48	24	18
Location	Q1BSlong	Q1BSlong	Q2BNlong	Q2BNlong	Q2BNlong	Q2BNlong	Q2BNlong

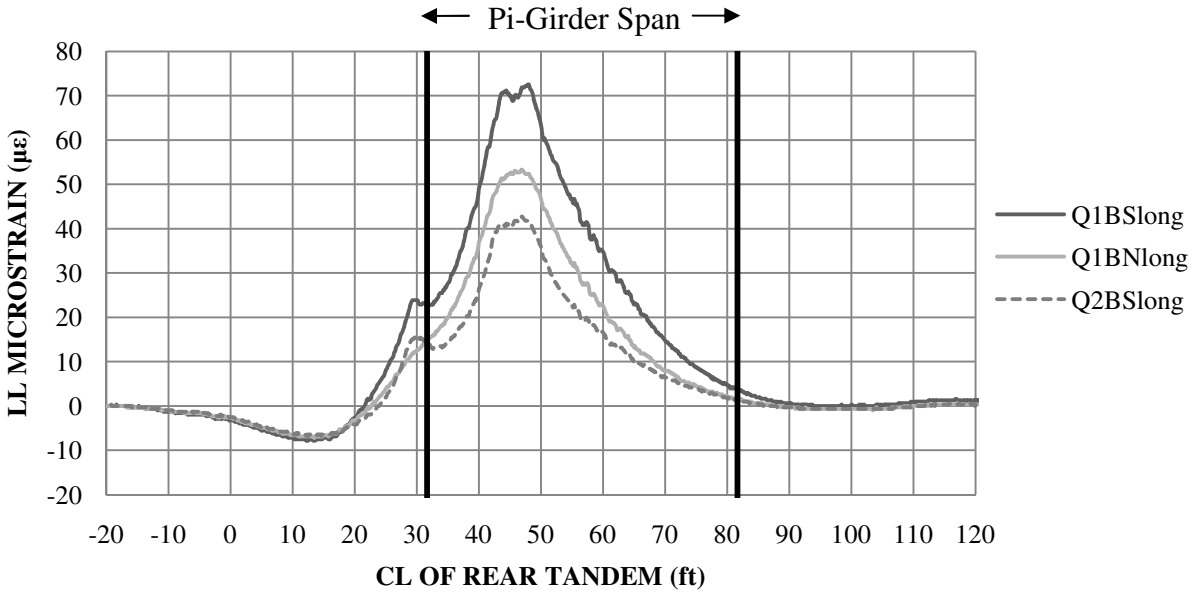

Figure 5.12-Representative Sample of LL Longitudinal Strain at Quarterspan along Path 1

5.3.6 Live Load Longitudinal Live Load Bulb Strain at Quarterspan Predicted by FEM

The FEM predictions for a pinned end condition for the quarterspan bulb strain were very similar to the field test strains. Ten με, recorded along path 7, was the largest difference between the FEM predictions and the field test results when the field test results were not bounded by the predictions. As the truck transitioned from paths 5 through 7 there is a pronounced decrease in the strains measured from the field test compared to the FEM predictions. This effect is likely due to the model distributing the loads more effectively than was observed in the field. Ignoring paths 4 through 7 and only considering paths 1 through 3 when the majority of the wheel loads were on girders 1 and 2, the FEM was able to bound all

of the field test results. The predictions for load paths 1 through 7 are shown in Figure 5.13a-g.

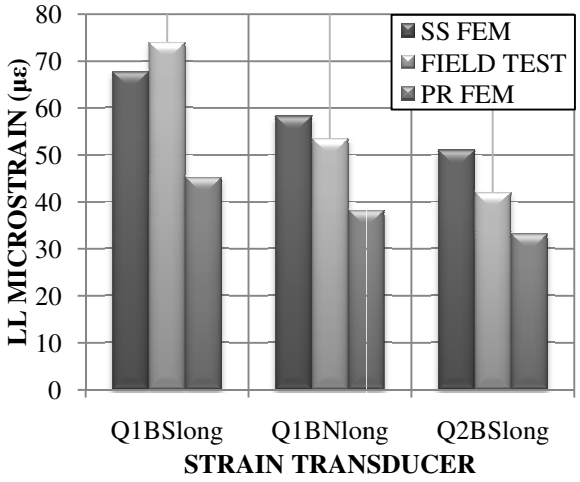

a. 2008; Path 1

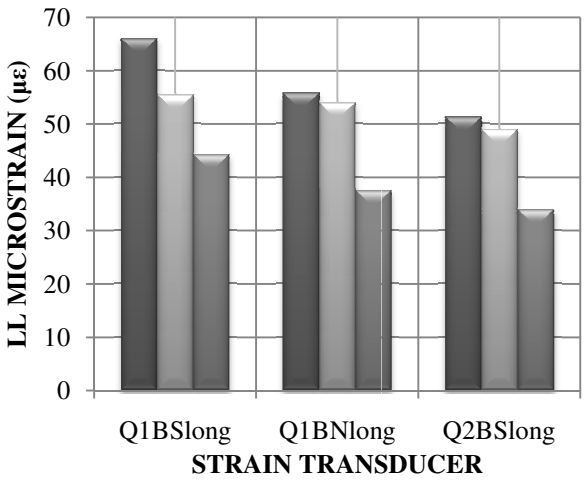

b. 2008; Path 2

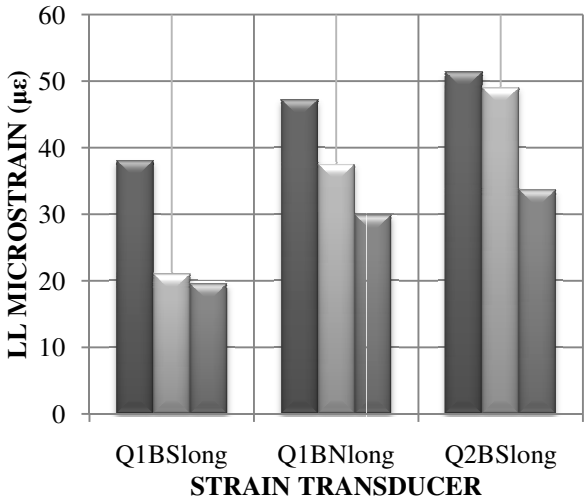

c. 2008; Path 3

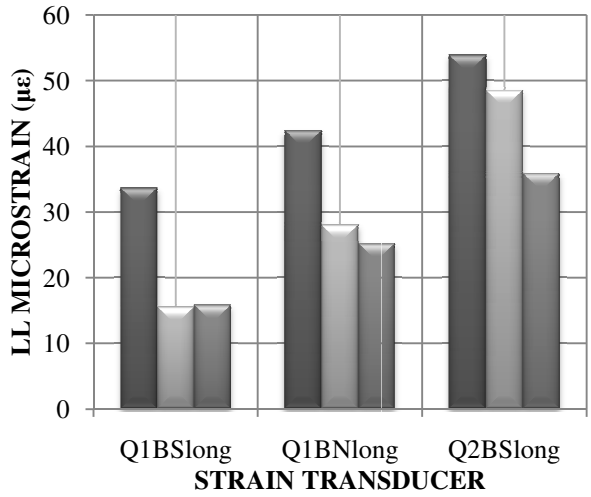

d. 2008; Path 4

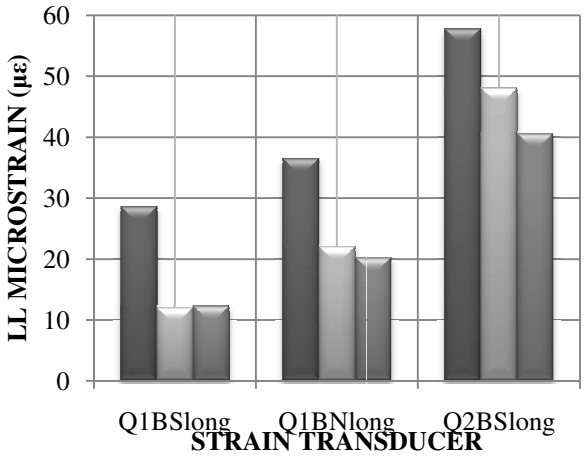

e. 2008; Path 5

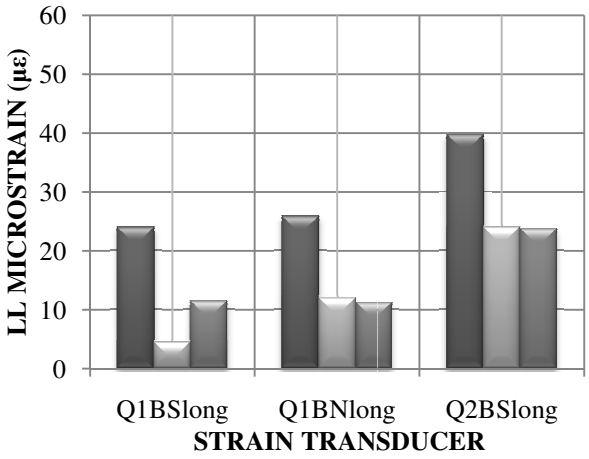

f. 2008; Path 6

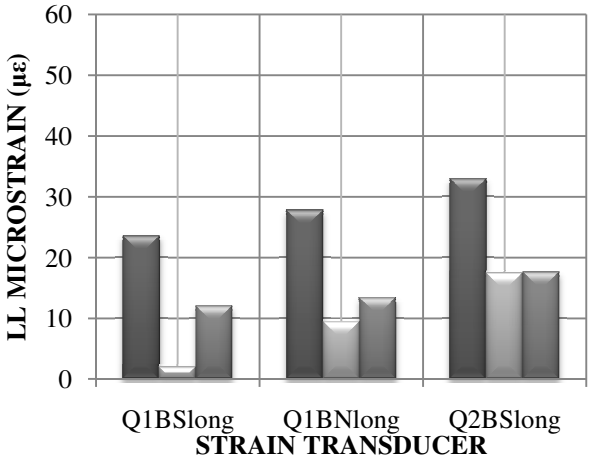

g. 2008; Path 7

Figure 5.13-FEM LL Longitudinal Bulb Strain at Quarterspan Paths 1-7

5.3.7 Live Load Transverse Bottom Deck Strain Measured at Midspan

To examine the response of the deck in the transverse direction, seven strain transducers, four on the top and three on the bottom, were placed transversely on the deck at midspan. As expected, the maximum transverse strains on the bottom of the deck were recorded on paths 2 and 6 when one of the wheel loads was near the centerline of a girder. Again, the maximum strain was recorded when the truck's forward rear axle position was approximately at midspan of the pi-girders. The maximum measured tensile strain occurred at the center of the southernmost girder with a magnitude of 55 με along path 2. The maximum total strain

was estimated to be roughly 70 με. This maximum value is less than half of the predicted cracking strain of UHPC. Therefore, cracking in the longitudinal direction on the bottom of the deck is unlikely to occur under service level loads. The maximum live load tensile transverse deck strains can be seen in Table 5.5. A representative sample of the data can be seen in Figure 5.14.

Table 5.5-Maximum LL Transverse Tensile Deck Strain at Midspan

	Path Number						
	1	2	3	4	5	6	7
Strain (με)	21	55	23	23	30	43	9
Location	M1DBtrans	M1DBtrans	M2DBtrans	M2DBtrans	M2DBtrans	M3DBtrans	M3DBtrans

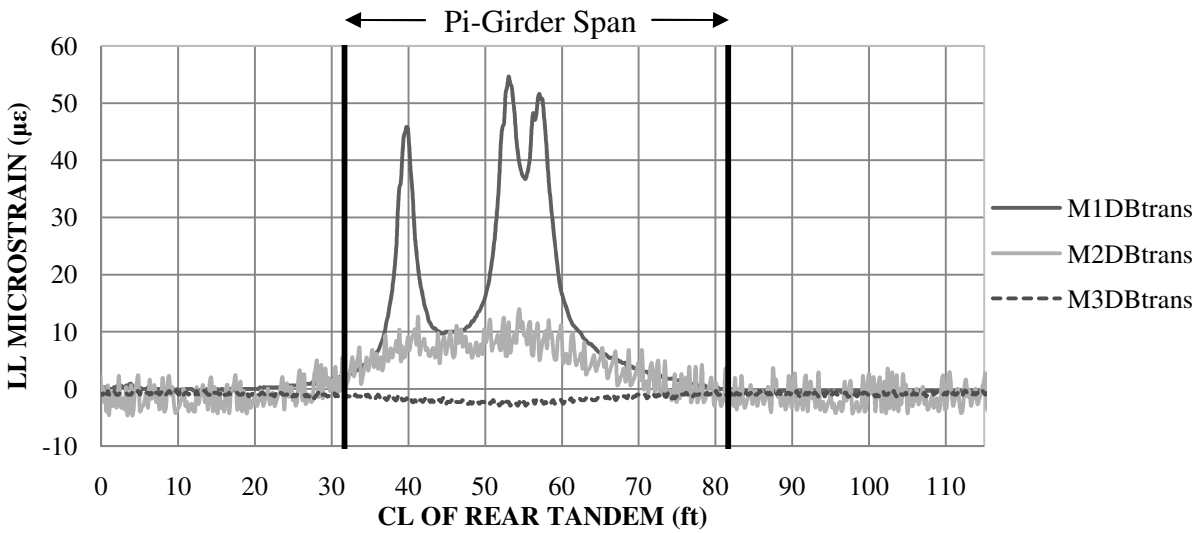

Figure 5.14-Representative Sample of LL Transverse Bottom Deck Strain along Path 2

5.3.8 Live Load Transverse Bottom Deck Strain Predicted by FEM

The FEM was able to reasonably predict the transverse strains observed on the bottom of the deck at midspan. The measured strains at these locations were not always bounded by the simply supported and partially restrained FEM predictions because these strains are much less sensitive to support conditions than the longitudinal strains. On average, the field test results varied from the FEM predictions by approximately 5 με. At worst, the measured field

test strain lay outside of the bounded predictions by 12 με at M2DBtrans along path 5. Figure 5.15a-d shows the predictions from the FEM when compared to the field test data. Paths 5, 6 and 7 are not shown because of their similarities to the data in paths 1, 2, and 3.

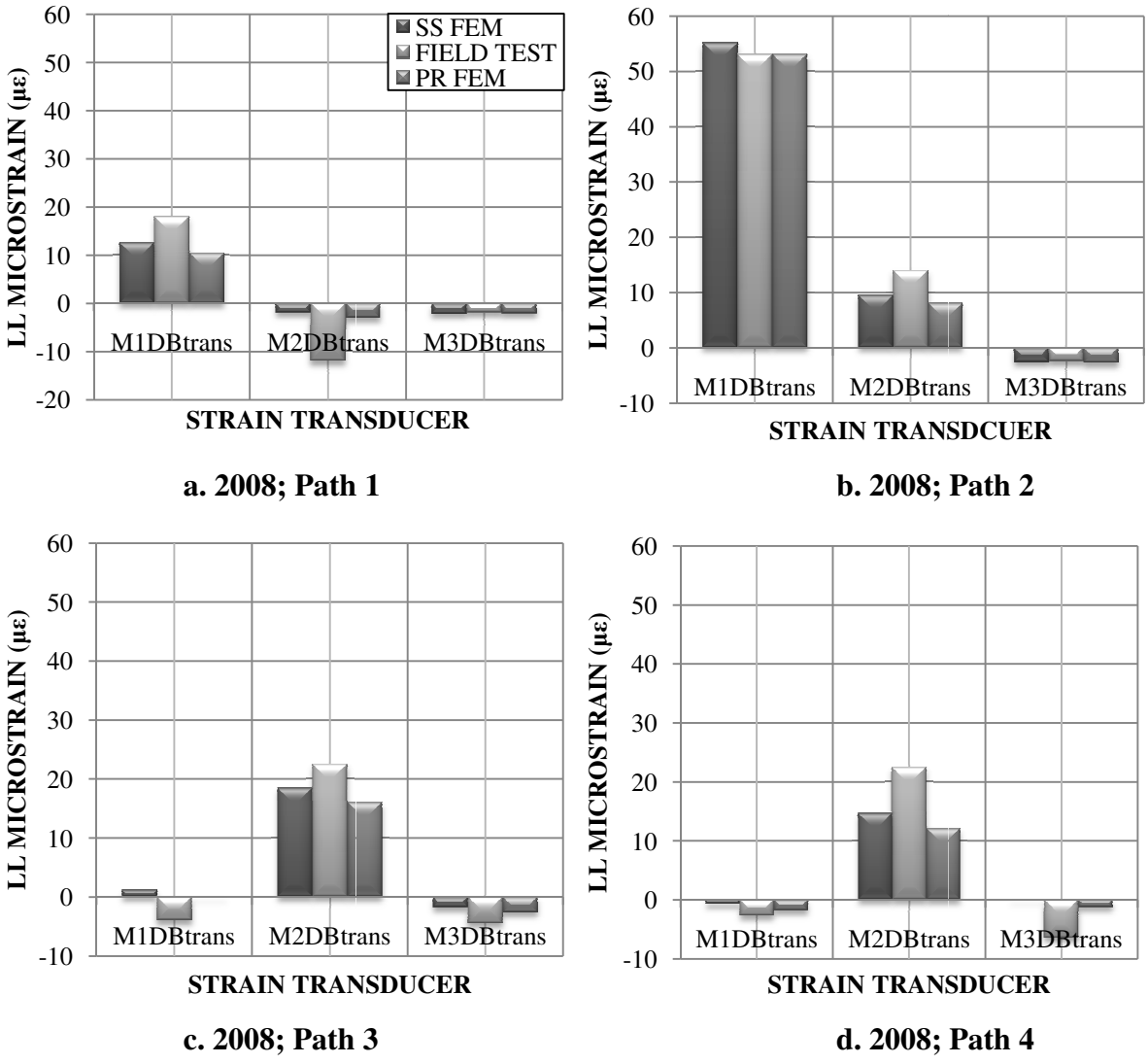

Figure 5.15-FEM LL Transverse Bottom Deck Strain at Midspan Paths 1-4

5.3.9 Live Load Transverse Top Deck Strain Predicted by FEM

As previously mentioned, four transverse strain transducers were placed on the top of the deck at midspan. The four transverse transducers located on the top of the deck became dislodged as the truck made its passes, inhibiting retrieval of valid data from these

transducers. Nevertheless, the transverse strains on the top of the deck were of significance because the bridge deck was designed so that all strains would be limited to below cracking. From the FEM it was possible to obtain estimates of the transverse top deck strains for both live load and total load. The transverse top deck strains were predicted at midspan for both a simply supported and partially restrained end condition. A maximum tensile live load strain of 38 με was predicted where the radius connecting the web meets the deck along paths 2 and 6 for a pinned end condition. The strains predicted by the FEM tended to be the highest where the radii of the webs met the deck. The maximum total tensile strain was predicted to be roughly 57 με in the same location as the maximum live load strain along paths 2 and 6. The maximum value of 57 με is less than half of the estimated cracking strain of UHPC (150-160 με). Therefore, cracking in the transverse direction on the top of the deck is unlikely to present a problem under service level loads.

5.3.10 Live Load Vertical Web Strain Measured at Midspan

Web spreading at midspan was monitored using eight strain transducers oriented vertically on the webs of the south and middle girder. The greatest live load tensile strains occurred along load paths 3 and 7. The maximum strains were recorded when the truck's rear axle position was approximately at midspan of the pi-girders. A maximum vertical live load strain of 45 με occurred when the truck was located on path 3. The maximum vertical tensile strains recorded are shown in Table 5.6. A representative sample of the data can be seen in Figure 5.16. Using the FEM, a maximum total strain of 70 με due to both dead and live load was estimated, ignoring residual construction strain.

Table 5.6-Maximum LL Vertical Tensile Web Strain at Midspan

	Path Number						
	1	2	3	4	5	6	7
Strain (με)	26	30	45	31	20	18	40
Location	M2WSIvert	M1WSEvert	M1WNIvert	M1WNIvert	M2WNIvert	M2WNIvert	M2WNIvert

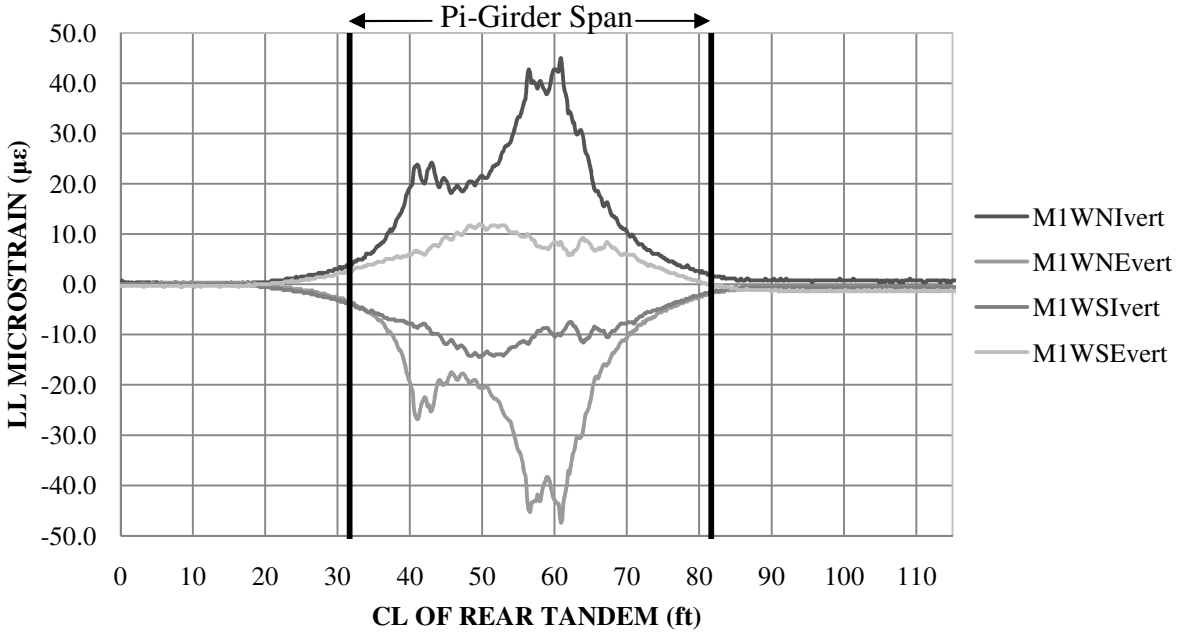

Figure 5.16-Representative Sample of LL Vertical Web Strain along Path 3

Total vertical web strains were also calculated using dead load strains predicted by the FEM, live load strains from static load tests, and the measured residual construction strains (see section 3). The maximum estimated total strain, including residual construction strain, was 115 με observed along path 3 at M1WNIvert. 115 με is 23% less than the predicted cracking strain of UHPC. Therefore, longitudinal cracking of the webs is unlikely under service level loads. Figure 5.17a-g displays the estimated total strains including residual construction strains for paths 1-7.

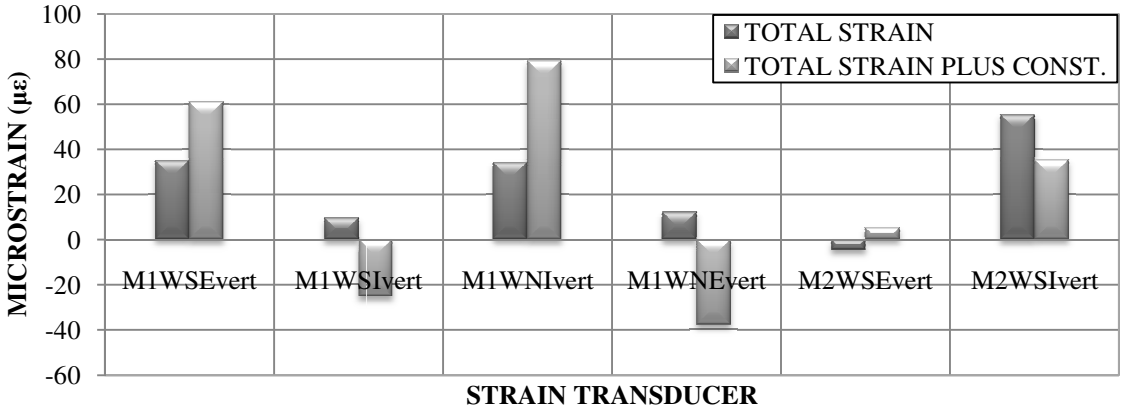

a. 2008; Path 1

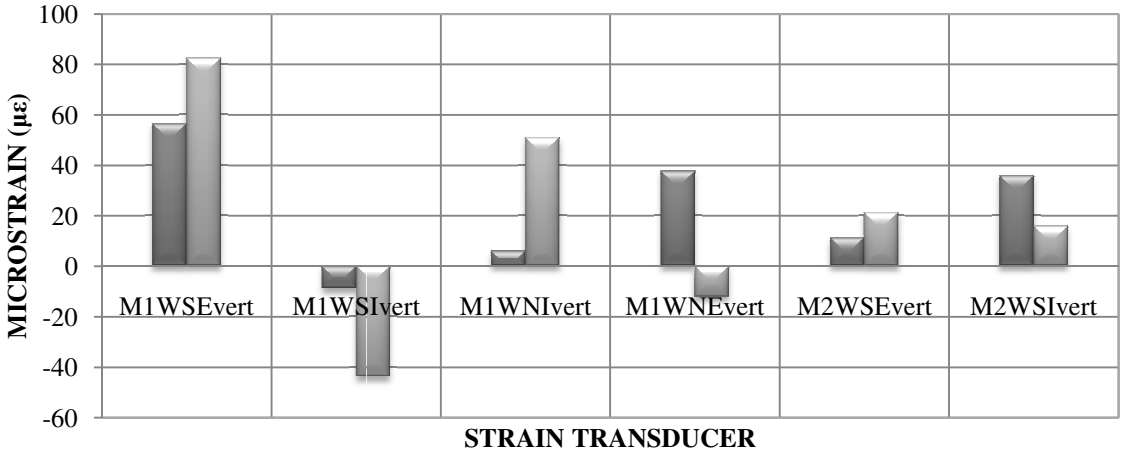

b. 2008; Path 2

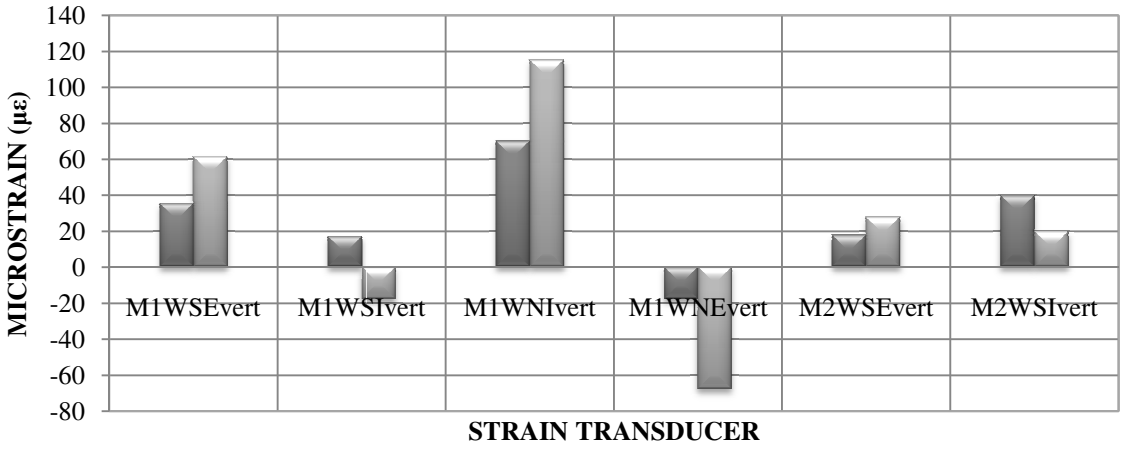

c. 2008; Path 3

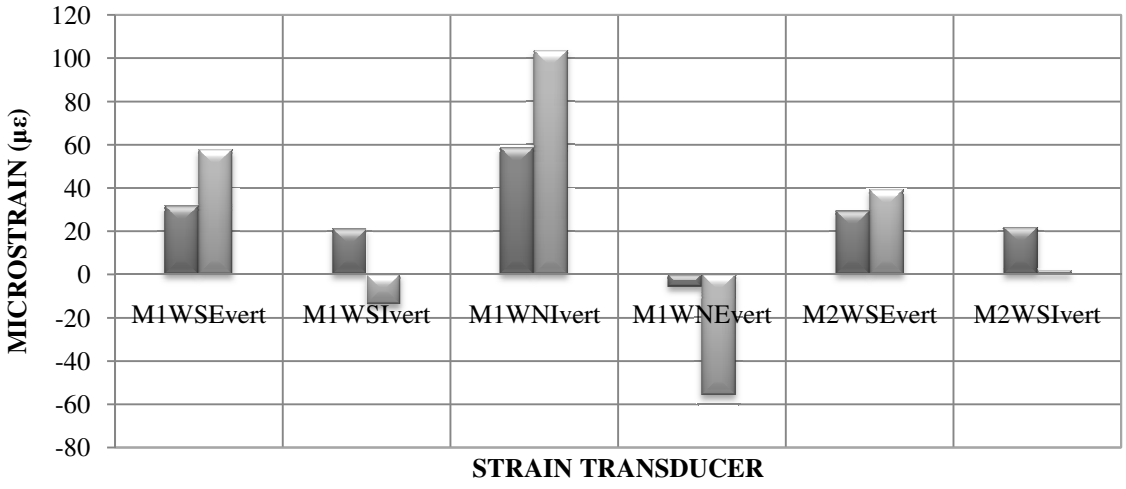

d. 2008; Path 4

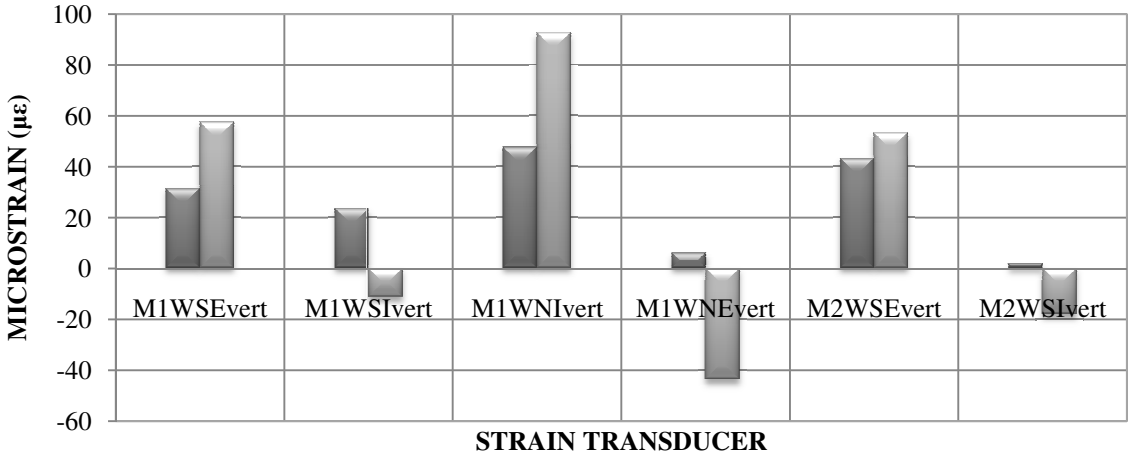

e. 2008; Path 5

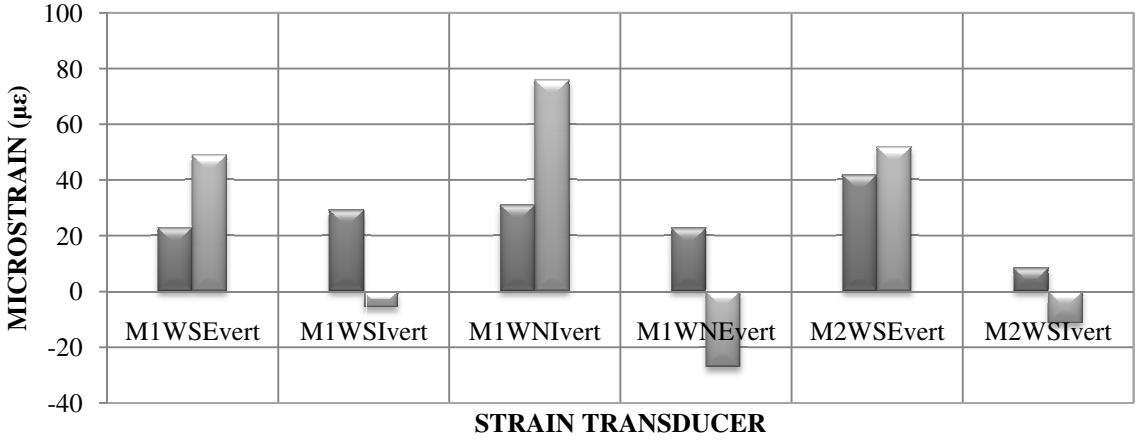

f. 2008; Path 6

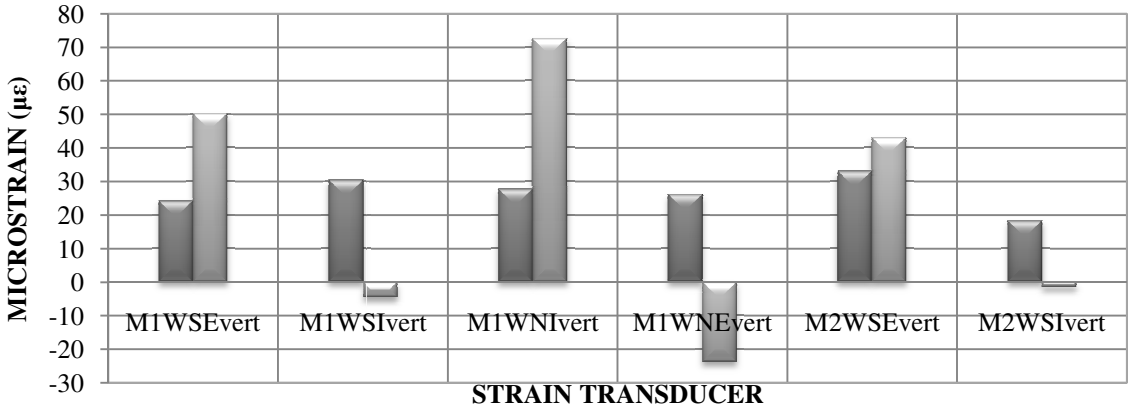

g. 2008; Path 7

Figure 5.17-Estimated Total Vertical Web Strain (includes residual construction strain) at Midspan

5.3.11 Live Load Vertical Web Strain Predicted by FEM

The FEM was only slightly less effective in predicting the vertical strains in the girder webs at midspan. On average, the field test results varied from the FEM predictions by approximately 12 με. At worst, the model varies by 35 με from the field results along paths 4 and 5 at M2WNIvert and M2WNEvert. Figure 5.18a-d shows the FEM predictions for path 1 through 4. Paths 5-7 are not shown but are very similar to trends for paths 1-3. Since the shear forces between girders strongly affect the web strain, the modeling of the connection between girders in the FEM is a likely source of the discrepancies. As previously discussed, adapting the model to incorporate elastic springs at the shear keys might better reflect the behavior observed in the field.

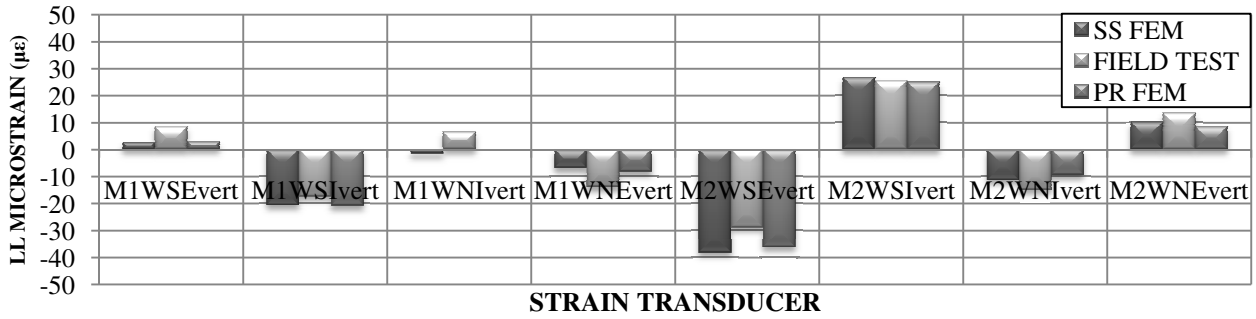

a. 2008; Path 1

b. 2008; Path 2

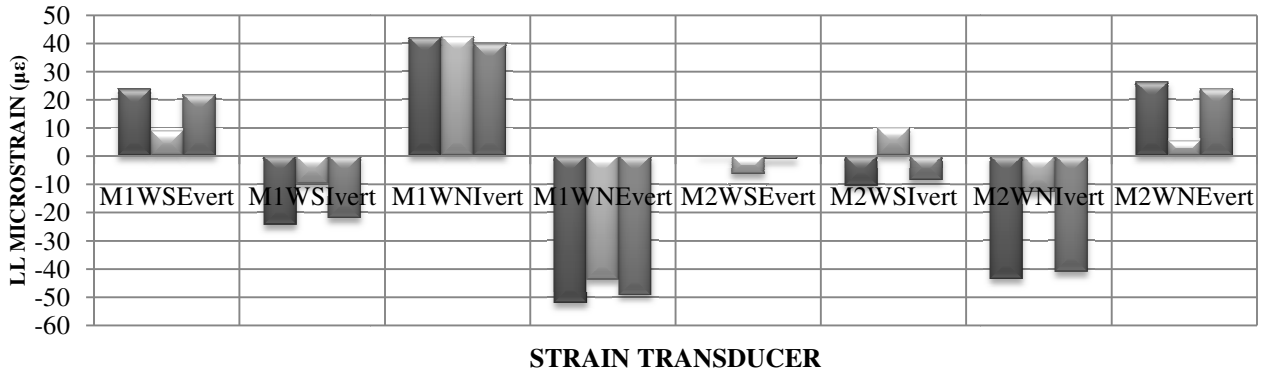

c. 2008; Path 3

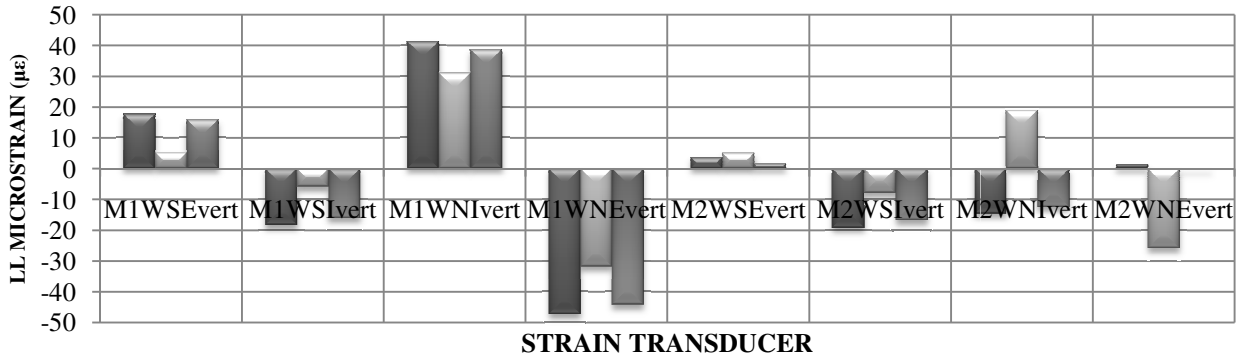

d. 2008; Path 4

Figure 5.18-FEM LL Vertical Web Strain at Midspan Paths 1-4

5.3.12 Longitudinal Live load Strains Measured near the Eastern Pier

Longitudinal strain transducers were placed near the eastern pier on the bottom of the two southernmost bulbs and on the deck above the northern bulb of the southernmost girder to attempt to quantify the amount of rotational restraint provided by the pier. In general, the maximum longitudinal live load tensile strain was recorded when the truck's rear axle position was near midspan of the pi-girder portion of the bridge or 50 ft. from the beginning of the first end span. 8 με was the largest tensile strain recorded by the longitudinal transducers near the eastern pier on the bottom of the bulbs, and occurred at the southernmost bulb when loaded along paths 6 and 7. 15 με was the largest tensile strain recorded by the longitudinal transducer near the eastern pier on the top of the deck and occurred when loaded along path 1. A representative sample of the data can be seen in Figure 5.19.

As the truck travelled along path 3 transducer P1BSlong began to record tensile strains at roughly 30 ft. The strain data for path 3 is provided in Figure 5.20. In addition, this strain reversal occurred on paths 4 through 7 as well, eventually including transducer P1BNlong. It should be noted that these strains are small often with a magnitude of 10 με or less.

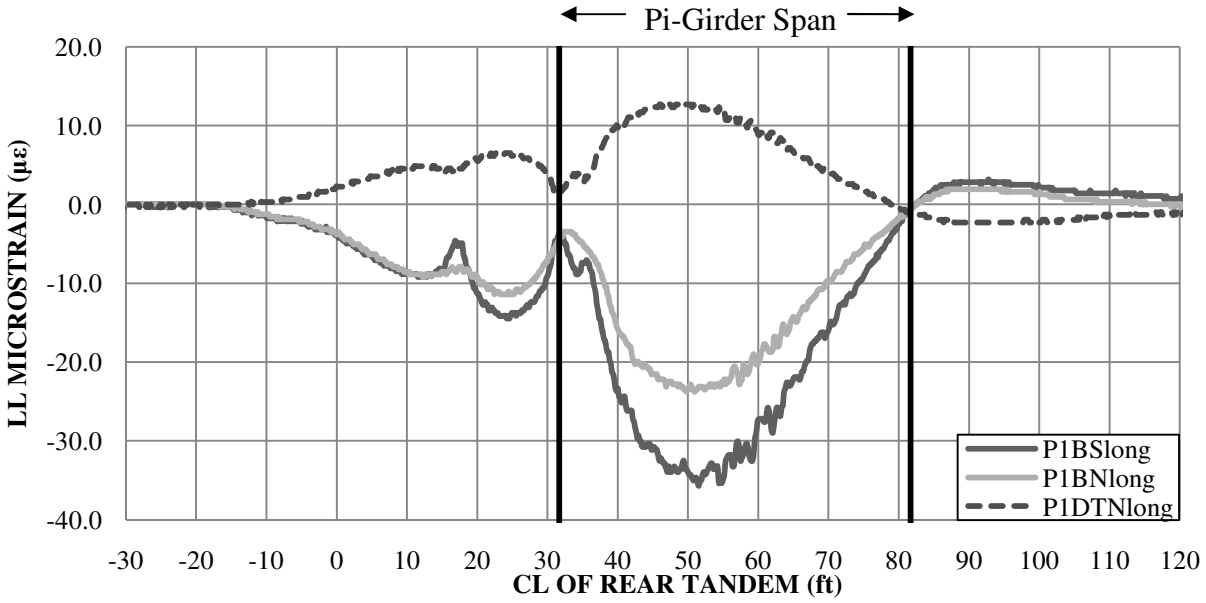

Figure 5.19-Representative Sample of LL Longitudinal Strain near the East Pier along Path 1

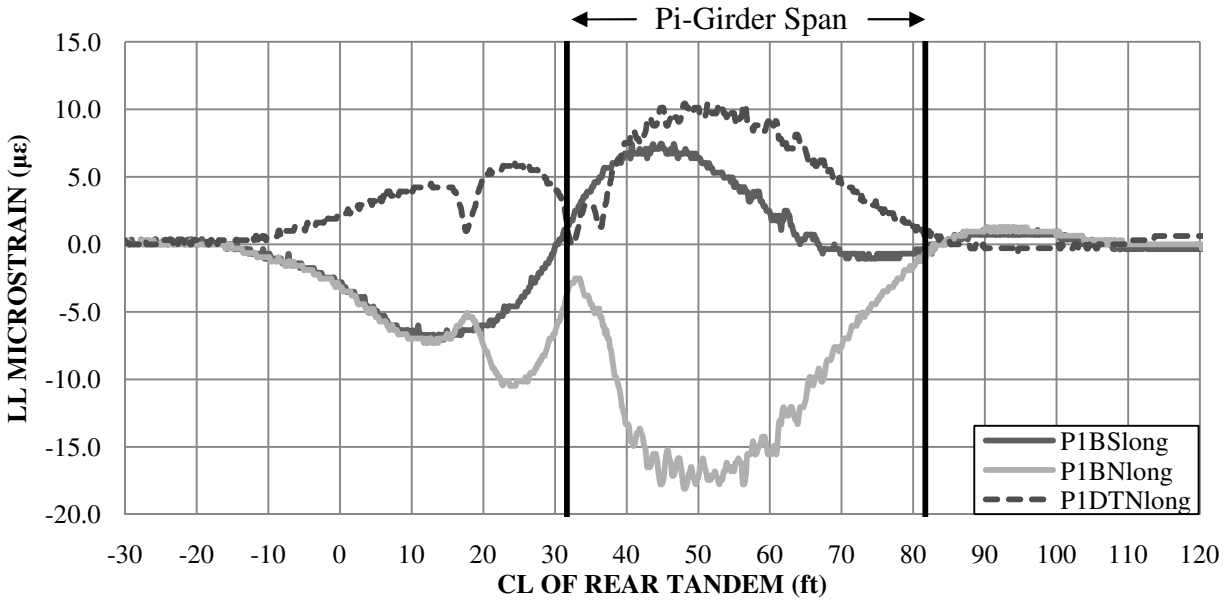

Figure 5.20-Representative Sample of Reversal of LL Longitudinal Strain near the East Pier along Path 3

5.3.13 Longitudinal Live Load Strains near the Eastern Pier Predicted by FEM

The FEM tended to under predict the live load strains for paths 1, 2, 6, and 7 while the strains for paths 3, 4, and 5 tend to be very similar to the FEM simply supported condition results. It was observed that the FEM did predict a reversal of readings similar to the LL strains measured during testing. From a review of the displacement readings at midspan it was observed that when the truck was along path 7 and the centerline of the rear tandem was at midspan the displacement of M1BSdisp was upward which would cause a reversal of strains at the support. The reversal of displacement readings at midspan corroborate the reversal of strains shown near the eastern pier. Figure 5.21a-g provide the field test results along with the FEM predictions for both a simply supported and partially restrained condition.

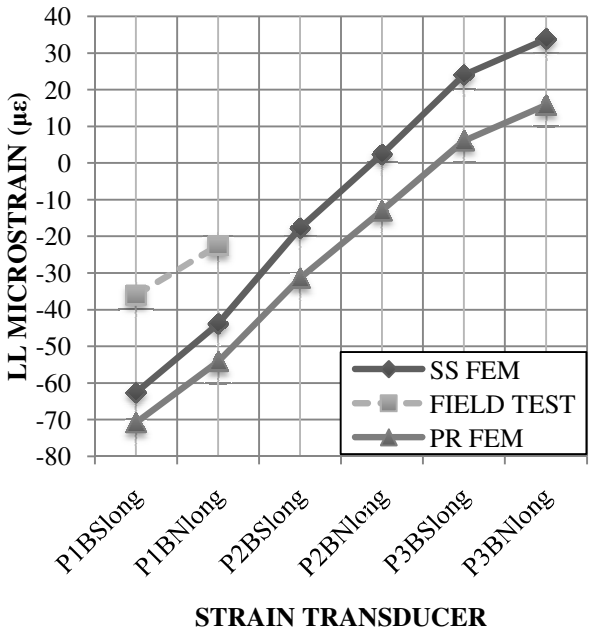

a. 2008; Path 1

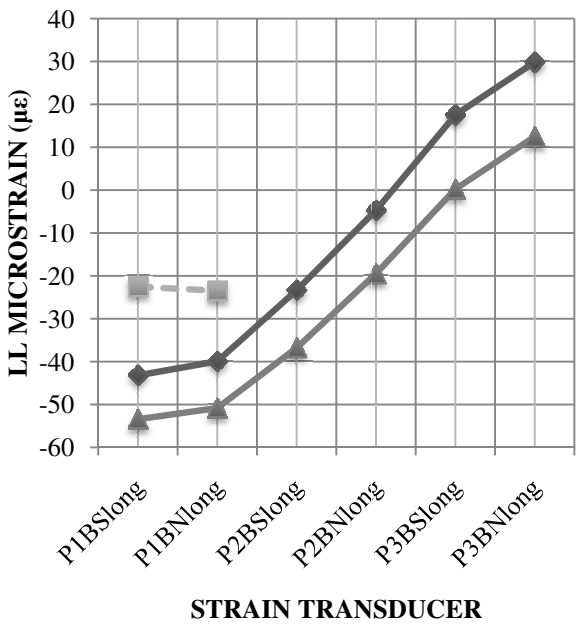

b. 2008; Path 2

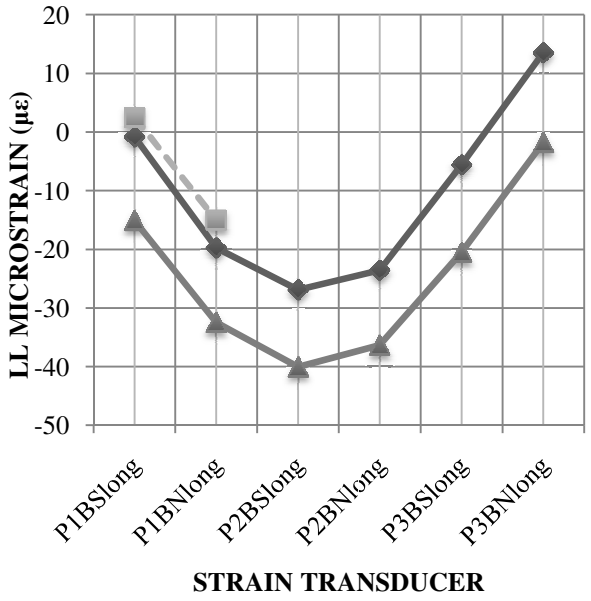

c. 2008; Path 3

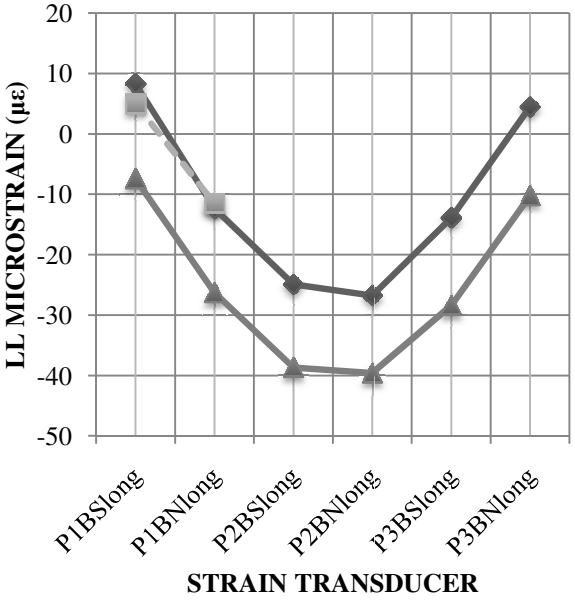

d. 2008; Path 4

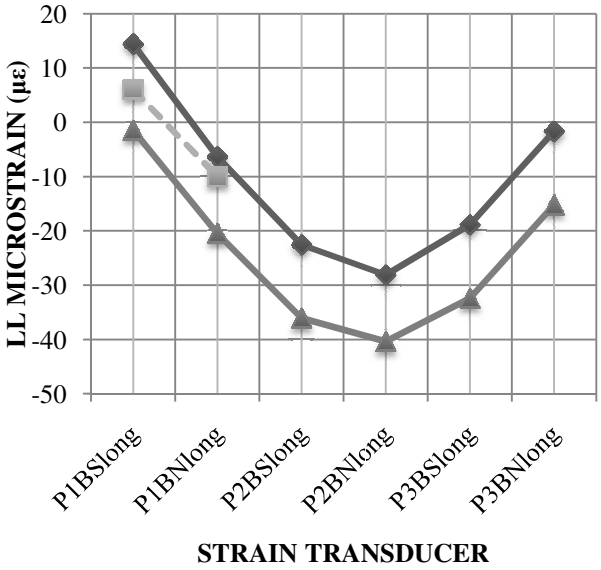

e. 2008; Path 5

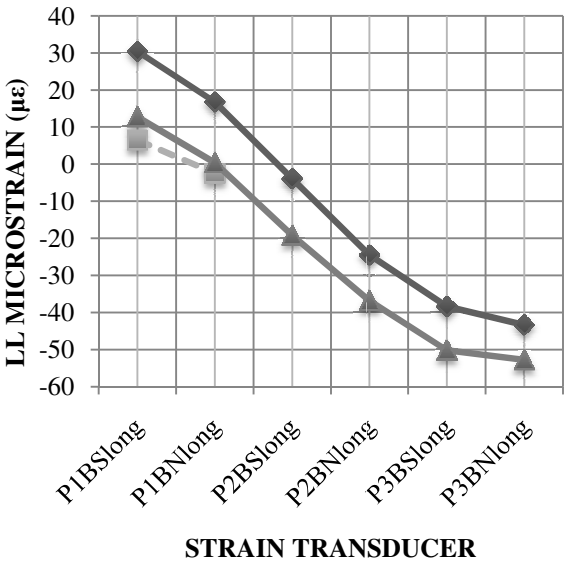

f. 2008; Path 6

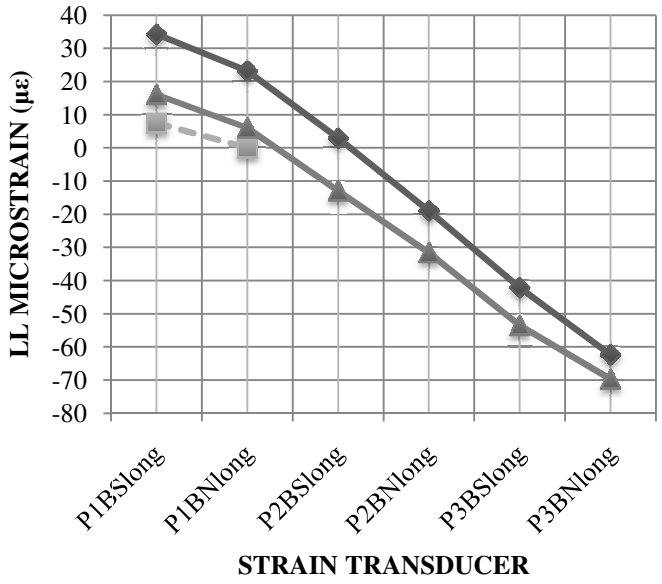

g. 2008; Path 7

Figure 5.21-FEM LL Longitudinal Strain near the East Pier Paths 1-7

5.3.14 Live load Axial Strain on the Diaphragm Measured at Midspan

Axial strain transducers were placed on the three southernmost HSS members at the midspan diaphragm to quantify the response of the diaphragm at midspan. The maximum axial live load strain was recorded when the truck's rear axle position was roughly at the midspan of the pi-girder portion of the bridge or 56 ft from the beginning of the first end span. 74 με was the largest strain recorded by the transducers located on the diaphragm at midspan, and occurred at MD2 when loaded along path 3. A tensile strain of 74 με corresponds to a tensile force of 9.22 kips and a tensile stress of 2.15 ksi in MD2. Table 5.7 provides the maximum values for live load strains measured in the diaphragm members. A representative sample of the data can be seen in Figure 5.22.

Table 5.7-Maximum LL Axial Diaphragm Strain at Midspan

	Path Number						
	1	2	3	4	5	6	7
Strain (με)	42	54	74	49	44	15	-14
Location	MD2	MD1	MD2	MD2	MD3	MD3	MD3

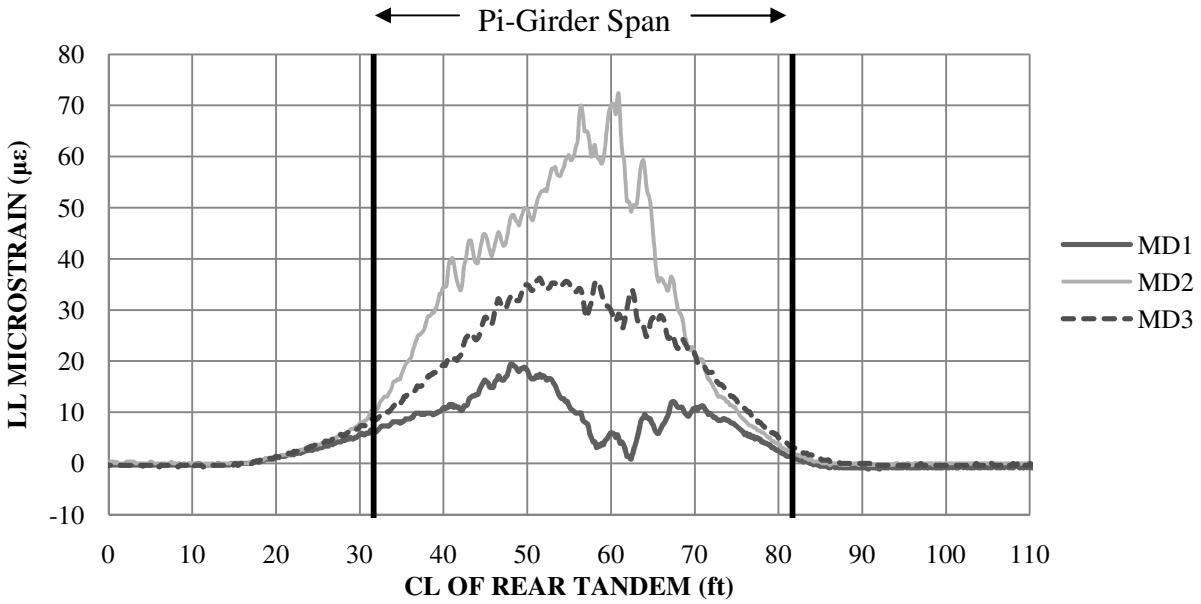

Figure 5.22- Representative Sample of LL Axial Diaphragm Strain at Midspan along Path 3

5.3.15 Axial Live load Strain on the Diaphragm at Midspan Predicted by FEM

The FEM was able to replicate some the trends seen in the field for the axial diaphragm strains. At worst, the model varies by roughly 30 με from the field results along path 2. A possible explanation of the deviation of analytical results from field measurements could be the imprecise fit of diaphragm members between webs, as discussed in Section 3. Figure 5.23a-g show the FEM predictions for path 1 through 7.

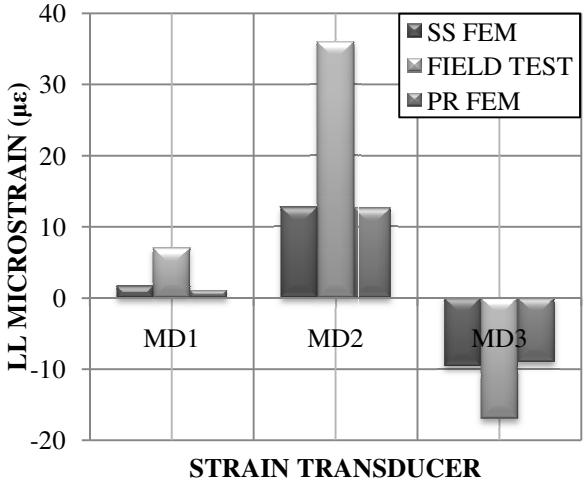

a. 2008; Path 1

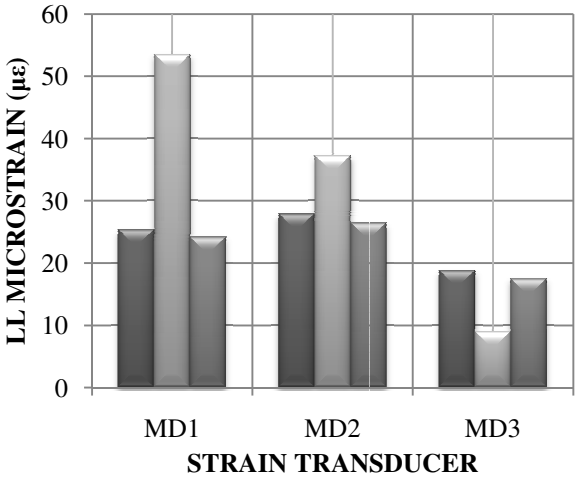

b. 2008; Path 2

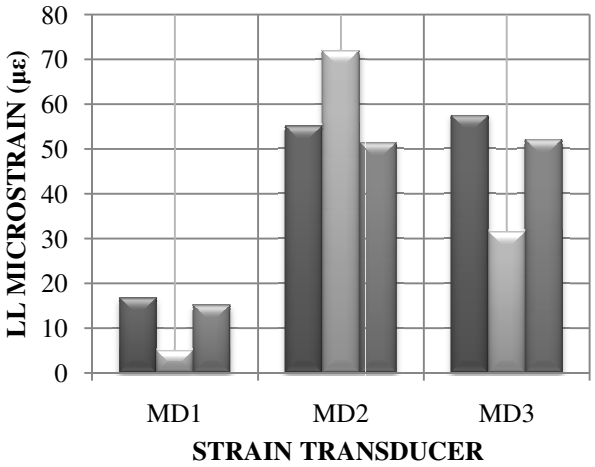

c. 2008; Path 3

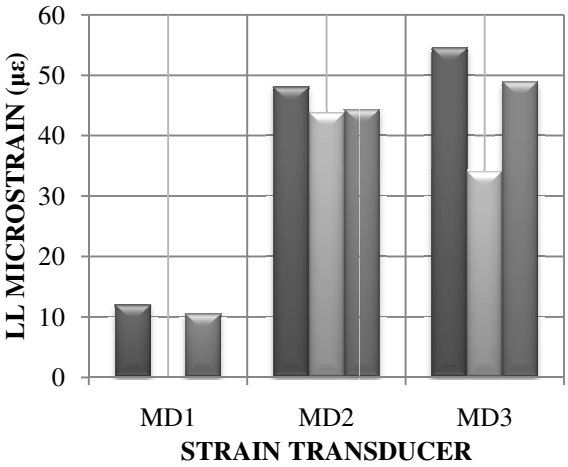

d. 2008; Path 4

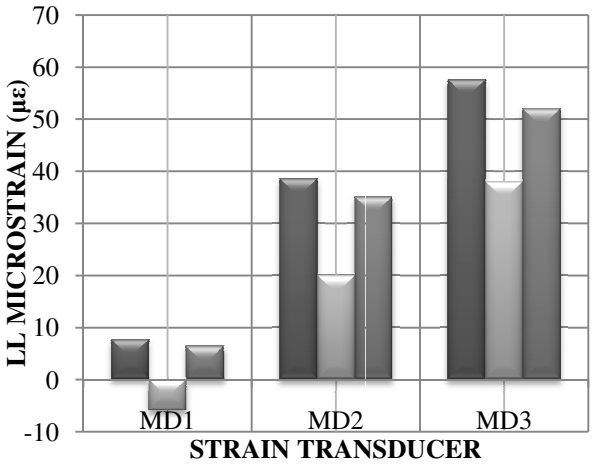

e. 2008; Path 5

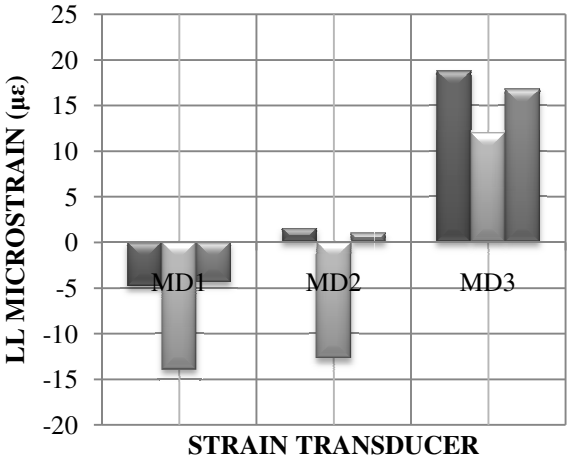

f. 2008; Path 6

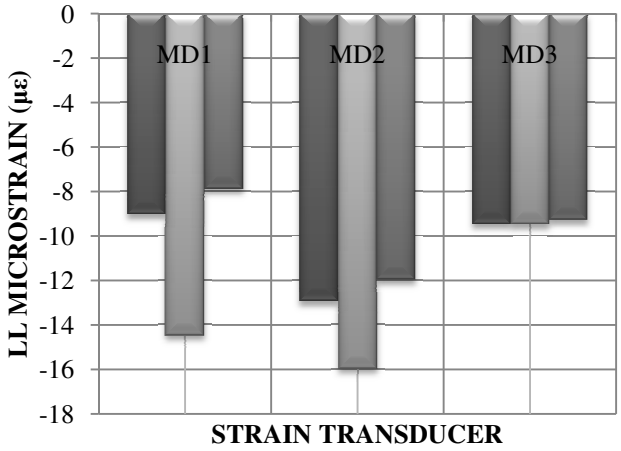

g. 2008; Path 7

Figure 5.23-FEM LL Axial Diaphragm Strain at Midspan Paths 1-7

5.4 2008 Static Live Load Test with Midspan Diaphragm Loose

As mentioned in section 5.3, the loosening of the nuts at the midspan diaphragm was performed to examine the bridge behavior had the midspan steel HSS members not been incorporated into the design. From this test, the BEC hoped to gain insight on diaphragm performance and spacing requirements. After the test data was analyzed, it was determined that two of the transducers placed on the diaphragm members still recorded strains while the bolts were loose. This indicates that the diaphragm was transmitting forces during the load test. This transmission of forces was most likely due to the tight fit of diaphragm members from construction placement. The presence of forces in the diaphragm showed that the diaphragm was still partially effective during this test. The following sections will examine the effects of the diaphragm on longitudinal, transverse deck, and vertical web strains at midspan.

5.4.1 Longitudinal Live Load Bulb Strains at Midspan with Midspan Diaphragm Loose

When the diaphragm was partially inactive the bulbs located closest to the load experienced higher strains without the diaphragm, but farther away from the load the strains without the

diaphragm are similar if not less than the strains recorded when the diaphragm was present. This increase in strain can be attributed to a partial reduction in the lateral live load distribution factors, discussed in Section 6.4. The overall average increase in strain was 4 με. The strains recorded for paths 1 through 4 with the diaphragm nuts tight and loose are shown in Figure 5.24a-d.

Table 5.8-Comparison of Maximum LL Longitudinal Bulb Strain at Midspan

	Path Number						
	1	2	3	4	5	6	7
Nuts Tight (με)	107	80	69	71	71	74	101
Nuts Loose (με)	110	81	79	80	76	78	109
Location	M1BSlong	M1BSlong	M2BSlong	M2BSlong	M2BSlong	M3BNlong	M3BNlong

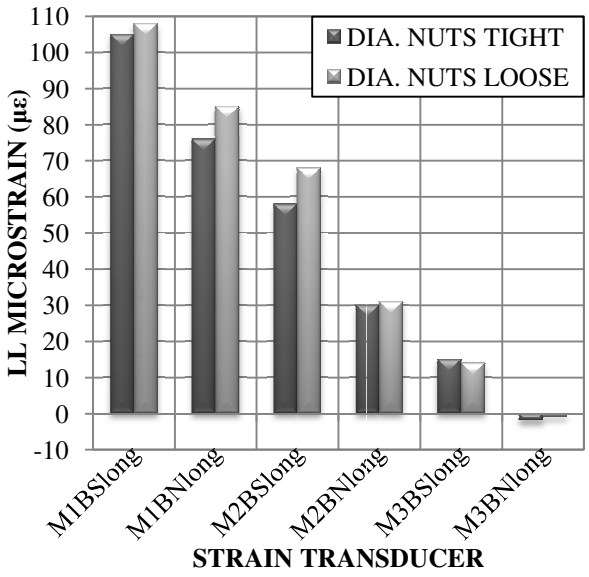

a. 2008; Path 1

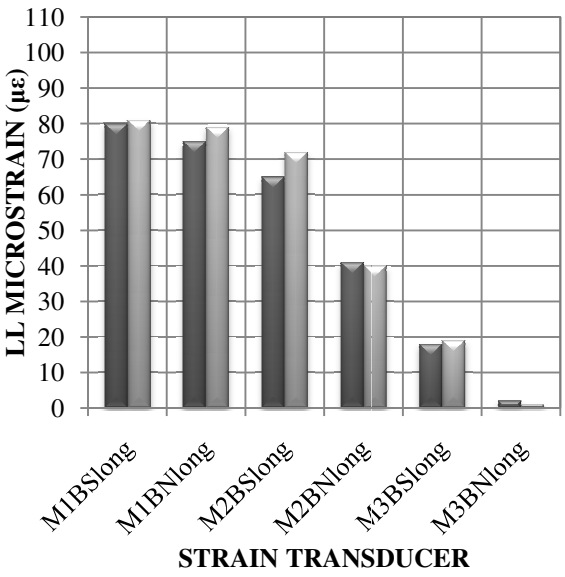

b. 2008; Path 2

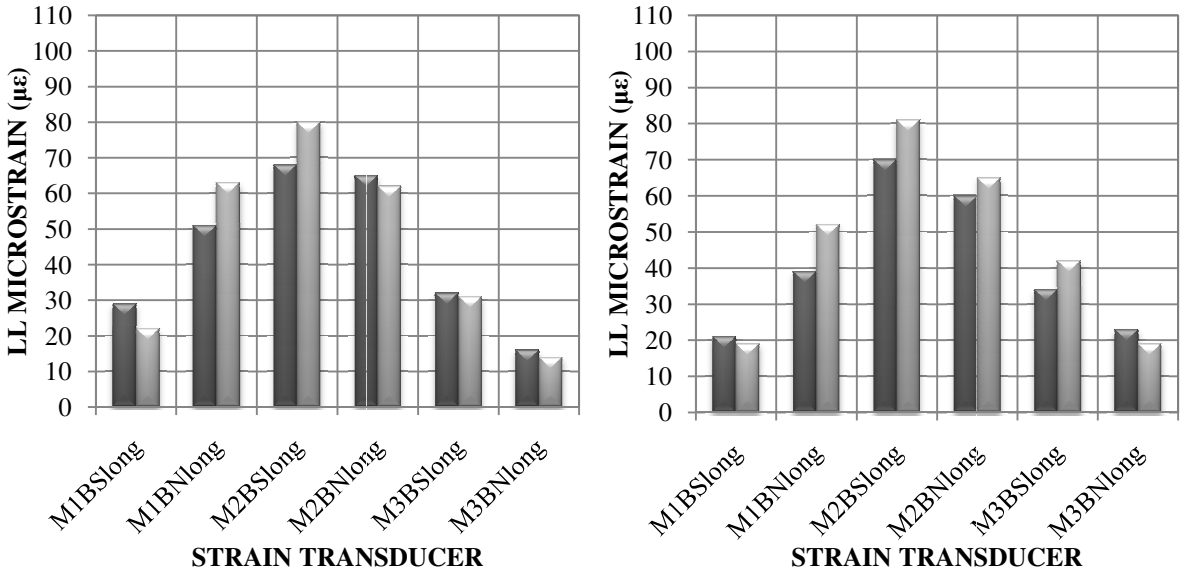

c. 2008; Path 3 **d. 2008; Path 4**

Figure 5.24-Longitudinal LL Bulb Strain at Midspan with Midspan Diaphragm Loosened

5.4.2 Live Load Transverse Bottom Deck Strains at Midspan with Mid. Diaphragm Loose

The loosening of the nuts on the diaphragm appeared to have little if any effect on the transverse strains recorded on the bottom of the deck. The magnitude of the strain readings had minimal variance between the data recorded when the diaphragm nuts were tight and when the nuts were loose. Table 5.9 shows the maximum transverse deck strains recorded for both sets of data. A maximum difference of 6 με was observed along path 1 as shown in Table 5.9. The locations of maximum strain also remained the same for both rounds of tests with nuts tight and nuts loose, again indicating that the bottom deck strains were minimally affected by the loosening of the diaphragm nuts.

Table 5.9-Comparison of Maximum LL Transverse Tensile Deck Strain at Midspan

	Path Number						
	1	2	3	4	5	6	7
Nuts Tight (με)	21	55	23	23	30	43	9
Nuts Loose (με)	15	56	24	24	30	47	5
Location	M1DBtrans	M1DBtrans	M2DBtrans	M2DBtrans	M2DBtrans	M3DBtrans	M3DBtrans

5.4.3 Live Load Vertical Web Strains with Midspan Diaphragm Loose

The loosening of the diaphragm caused a decrease in a majority of the vertical strain readings on the webs at midspan. The maximum web tensile strain data for all passes is presented in Table 5.10.

Table 5.10-Comparison of Maximum LL Vertical Tensile Web Strain at Midspan

	Path Number						
	1	2	3	4	5	6	7
Tight (με)	28	31	45	35	26	21	40
Loose (με)	14	22	18	18	28	28	39
Location	M2WSIvert	M1WSEvert	M1WNIvert	M1WNIvert	M2WNvert	M2WNIvert	M2WNIvert

The FEM model predicted the decreased web strains when the midspan diaphragm was removed. Figure 5.25a-d displays the finite element prediction for paths 1 through 4 for web strains with the diaphragm nuts tight and loose. Similar to the field tests, the FEM predicted that the majority of the web strains would be larger when the diaphragm is present. The similarity of the FEM results to the field test results provides confidence that the vertical strains in the web will not be decreased due to the presence of the diaphragm.

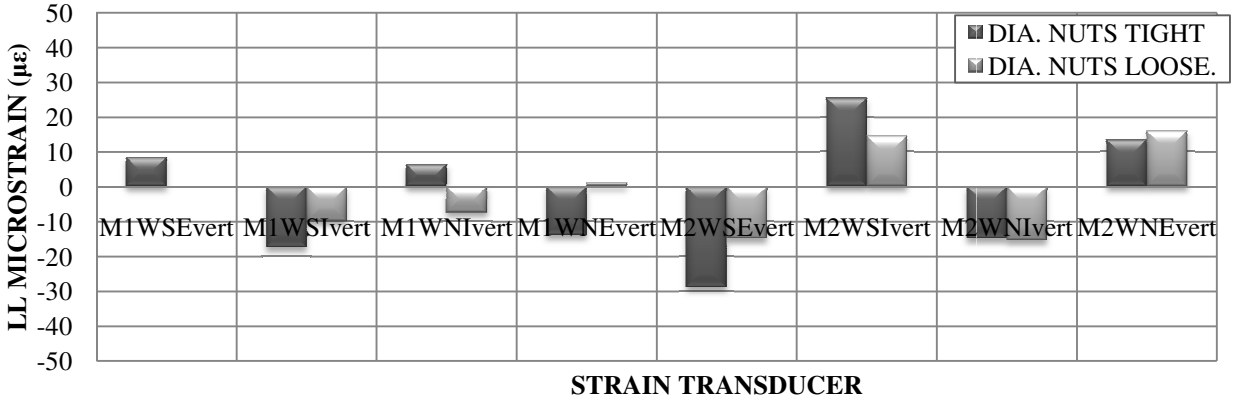

a. 2008; Path 1

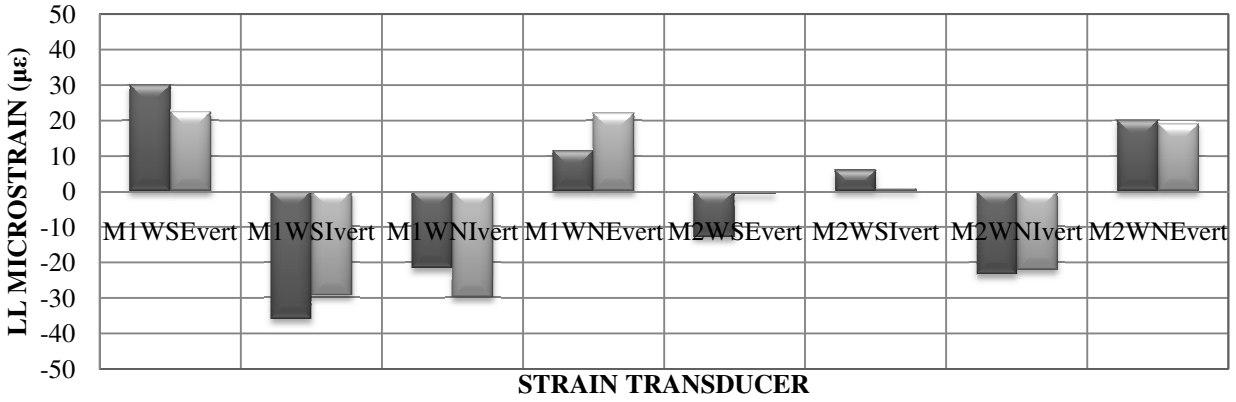

b. 2008; Path 2

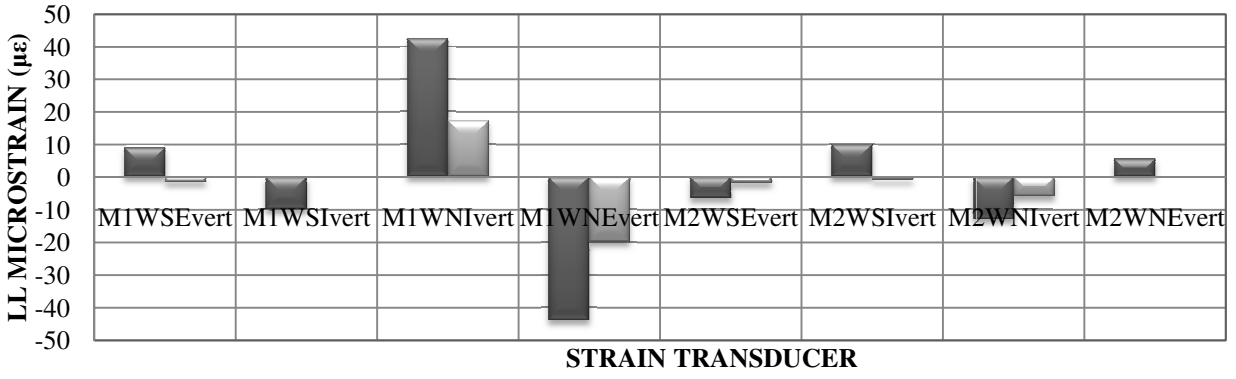

c. 2008; Path 3

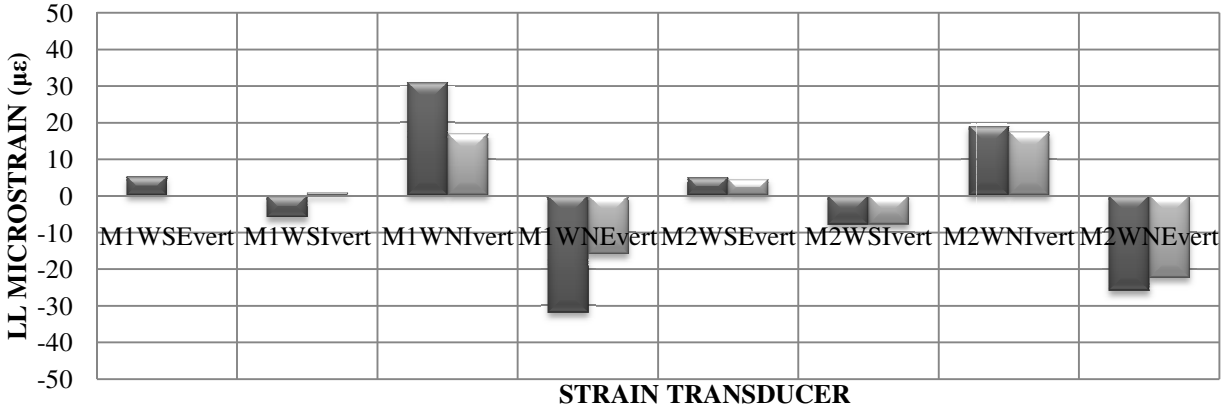

d. 2008; Path 4

Figure 5.25-FEM LL Vertical Web Strain Paths 1-4 with Midspan Diaphragm Loosened

Because some of the diaphragm members were still transmitting forces to the pi-girders, it is difficult to draw conclusions regarding the effectiveness and spacing of the diaphragms. However, the overall behavior of the bridge was affected little by loosening the nuts on the center diaphragm.

5.5 Comparison of 2008 to 2009 Static Live Load Tests

5.5.1 Longitudinal Live Load Strains Measured at Midspan

The results of the second static load field test exhibited a general increase in the strains recorded by the longitudinal transducers on the bottom of the bulbs at midspan. On average, an increase of 10 με was observed for all paths and all transducers. The largest increase of 11 με was recorded at M1BS, M2BS, and M3BN along paths 2, 3, and 6 respectively. The neutral axis location, as determined from testing, for the 2009 test was found to be 11.8 in. from the top of the girder compared to 11.6 in. from the 2008 test. It should be noted that the calculation of the neutral axis from the 2009 test differed from the 2008 test, as the longitudinal deck gages were located on the bottom of the deck due to the presence of an asphalt wearing surface. As a minor change in the neutral axis location took place, the average 10 με increase in strain cannot be attributed to loss of section properties. The overall

increase appears to be attributable to a reduction of continuity between the end spans and pi-girder span. The removal of continuity between the spans could be attributable to the freeze thaw cycles occurring over the course of the winter; thus breaking down any bond remaining between the end span and pi-girder span. Breaking down of bond would cause the bridge to behave as a simply supported span, therefore increasing strains. Cracking of the concrete end diaphragms, reducing stiffness, could also cause a decrease in rotational restraint of the piers. Figure 5.26 displays strain results from both the first and second round of testing for path 2 (only the three transducers with the largest strain from each test are shown for clarity). From the aforementioned figure, it is possible to see the deviations of the 2009 test from the 2008 test especially between forty to sixty feet. A comparison of 2008 and 2009 bottom bulb longitudinal strains from paths 1-4 is also shown in Figure 5.27a-d. Table 5.11 provides the measured maximum live load longitudinal bottom bulb strains for the first and second round of tests.

Table 5.11-2008 & 2009 Maximum LL Longitudinal Bulb Strain at Midspan

	Path Number						
	1	2	3	4	5	6	7
2008 (με)	107	80	69	71	71	74	101
2009 (με)	115	91	80	81	80	85	105
Location	M1BSlong	M1BSlong	M2BSlong	M2BSlong	M2BSlong	M3BNlong	M3BNlong

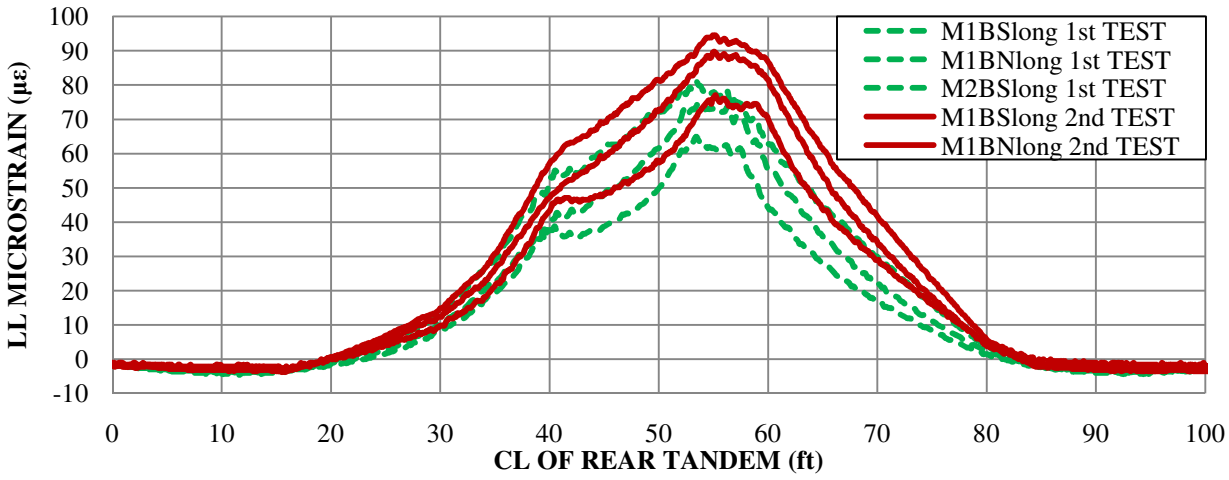

Figure 5.26-Comparison of 2008 & 2009 LL Longitudinal Strain at Midspan along Path 2

Using the finite element model to predict initial strains, the predicted maximum total strain for second round of testing for the longitudinal transducers on the bottom of the bulbs was -137 με. This value is still well below the estimated cracking strain of 150-160 με. Therefore, cracking of the bulbs in the longitudinal direction is unlikely under service level loads.

Due to loss of continuity between the end span and pi-girder span, the simply supported boundary condition finite element model should predict quite well the measured stains for the second test. Figure 5.27a-d provides comparisons between the first and second rounds of tests to the FEM predictions for a simply supported boundary condition for paths 1-4.

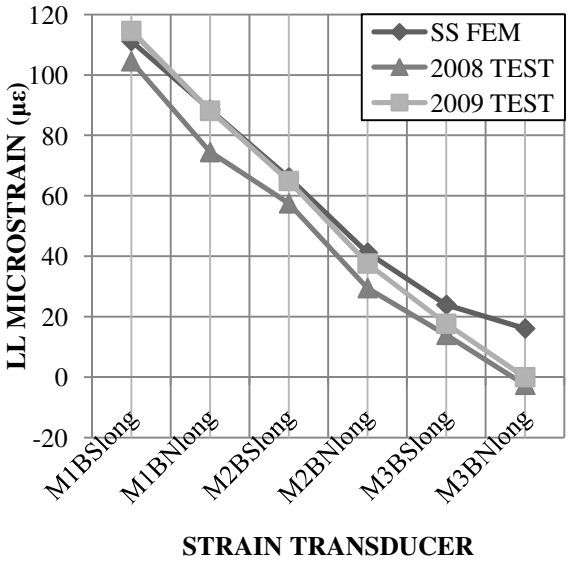

a. 2008 & 2009; Path 1

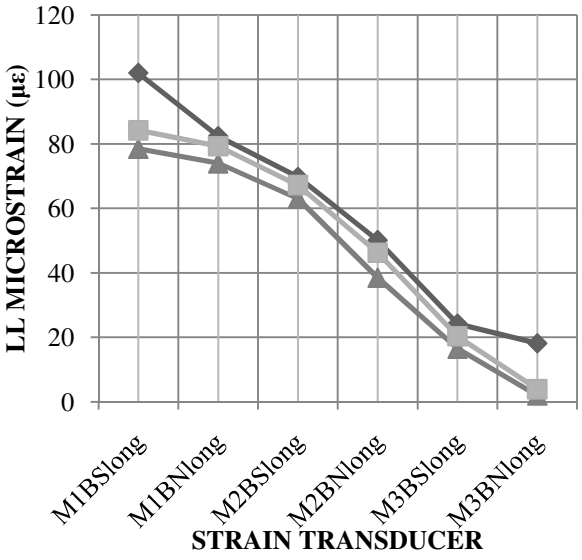

b. 2008 & 2009; Path 2

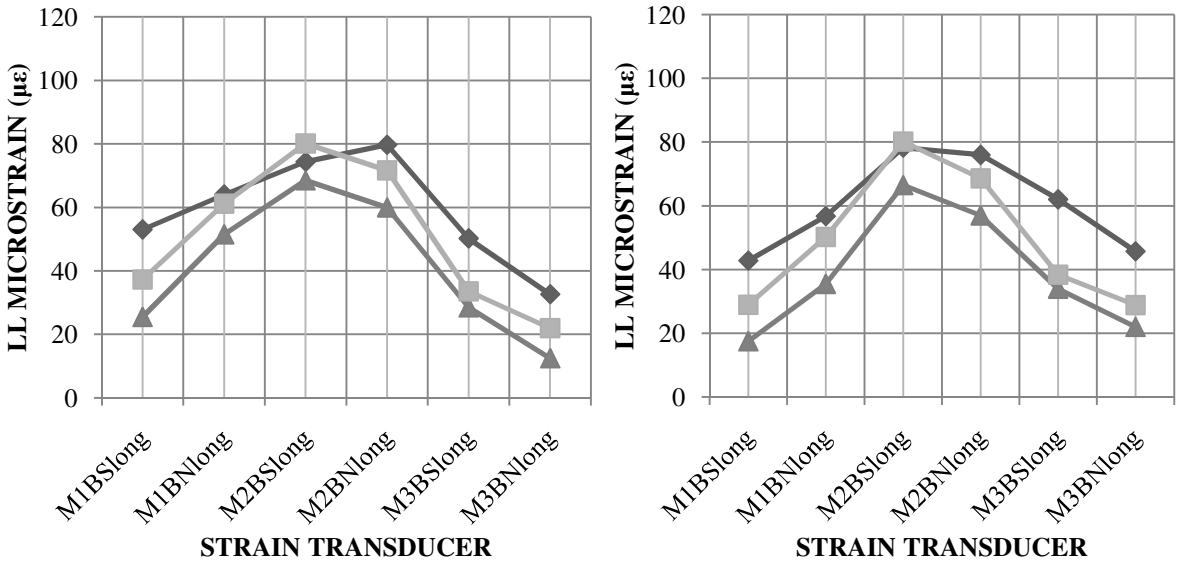

c. 2008 & 2009; Path 3 **d. 2008 & 2009; Path 4**

Figure 5.27-Comparison of 2008 & 2009 LL Longitudinal Strain to FEM at Midspan

The predictions for all paths are very close, often within several microstrain, to the pinned end condition predictions from the FEM. This provides evidence that the bridge has transitioned from a partially restrained condition to a less restrained connection.

A comparison of the distribution factors from longitudinal strain from the 2008 and 2009 tests will be presented in Section 6.3.

5.5.2 Longitudinal Live Load Bulb Strain Measured at Quarterspan

The results of the second static load field test showed an overall increase in the strains recorded by the longitudinal transducers at quarterspan on the bottom of the bulbs. The comparison of the results at quarterspan is similar to the comparison at midspan. On average, an increase of 11 με was observed for all paths and all transducers. This overall increase can be attributed to the removal of the continuity between the end span and pi-girder span. The largest increase of 20 με was recorded at Q1BS along path 1. Table 5.12 provides the measured maximum tensile values for the first and second round of tests. Figure 5.28a-d displays the comparison of the 2008 and 2009 test results.

Table 5.12-2008 & 2009 Maximum LL Longitudinal Bulb Strain at Quarterspan

	Path Number						
	1	2	3	4	5	6	7
2008 (με)	75	56	49	49	48	24	18
2009 (με)	95	71	62	63	60	33	26
Location	Q1BSlong	Q1BSlong	Q2BSlong	Q2BSlong	Q2BSlong	Q2BSlong	Q2BSlong

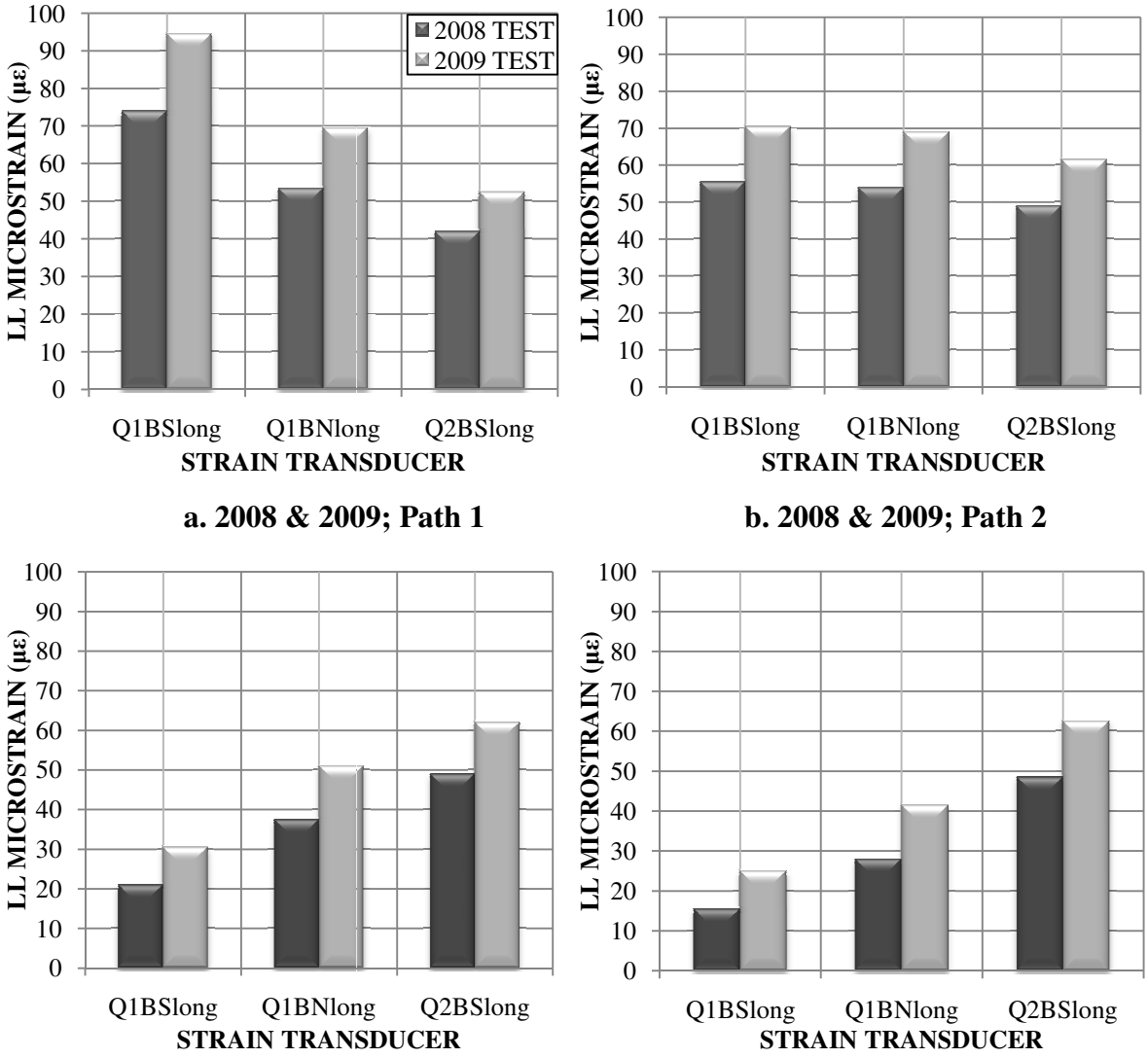

a. 2008 & 2009; Path 1

b. 2008 & 2009; Path 2

c. 2008 & 2009; Path 1

d. 2008 & 2009; Path 2

Figure 5.28-Comparison of 2008 & 2009 LL Longitudinal Strain at Quarterspan

5.5.3 Transverse Live Load Bottom Deck Strains Measured at Midspan

The results of the 2009 static load field test showed an overall marginal decrease in the strains recorded by the transverse bottom deck transducers. As expected, the decrease in continuity between the spans did not have a pronounced effect on the transverse bottom deck strains. Similar to the 2008 test, the maximum values occurred when truck was on paths 2 and 6 when one of the wheel loads was near the centerline of a girder. Table 5.13 provides the measured maximum tensile values for the first and second round of tests. Overall, no significant changes took place in the readings between the 2008 and 2009 tests. Figure 5.29 provides a graphical representation of the maximum strains measured at midspan for paths 1-4, paths 5-7 are not shown due to their similarity to paths 1-3.

Table 5.13-2008 & 2009 Maximum LL Transverse Deck Strain at Midspan

	Path Number						
	1	2	3	4	5	6	7
2008 (με)	21	55	23	23	30	43	9
2009 (με)	13	56	27	25	29	44	13
Location	M1DBtrans	M1DBtrans	M2DBtrans	M2DBtrans	M2DBtrans	M3DBtrans	M3DBtrans

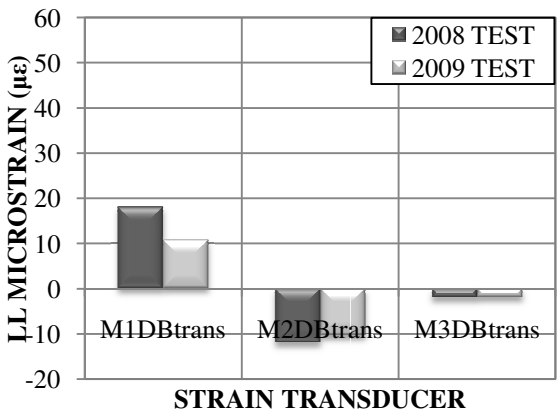

a. 2008 & 2009; Path 1

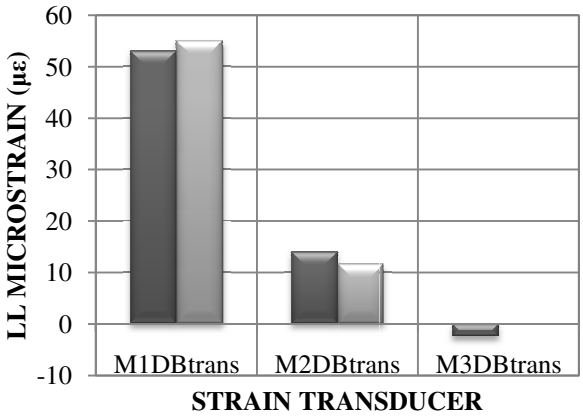

b. 2008 & 2009; Path 2

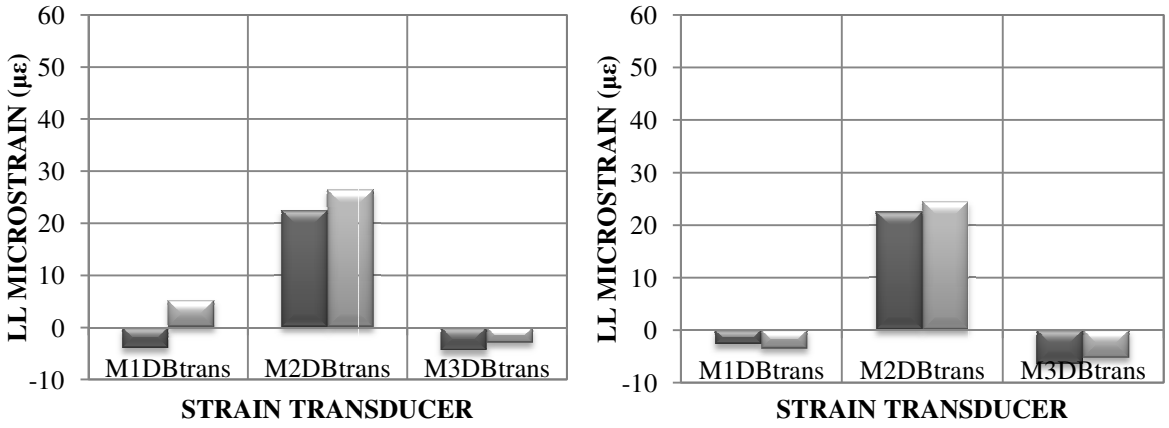

c. 2008 & 2009; Path 3 **d. 2008 & 2009; Path 4**

Figure 5.29-Comparison of 2008 & 2009 LL Transverse Deck Strains at Midspan

5.5.4 Live Load Vertical Web Strains Measured at Midspan

The results of the second static load field test displayed an average decrease of 3 με in the strains recorded by the vertical transducers located on the webs. Similar to the transverse deck strain, the decrease in continuity did not have a pronounced effect on the vertical web strains. However, some transducers did record increases of 10 με or more. The largest increase of 12με was recorded at M1WNIvert along path 4. Small localized variations in strain could be due to deviations of the test truck from path centerlines, or slight differences in gage locations between tests. Table 5.14 provides the measured maximum tensile values for the first and second round of tests. The initial strains predicted by the FEM coupled with the measured live load strains and residual construction strains predict a total strain of 120 με, roughly 30 με below cracking. Therefore cracking of the webs in the vertical direction is unlikely under service level loads. Figure 5.30a-d provides a graphical representation of the maximum strains measured at midspan for paths 1-4, paths 5-7 are not shown due to their similarity to paths 1-3.

Table 5.14-2008 & 2009 Maximum LL Vertical Tensile Web Strain at Midspan

	Path Number						
	1	2	3	4	5	6	7
2008 (με)	26	30	45	31	20	18	40
2009 (με)	32	32	45	43	28	23	40
Location	M2WSIvert	M1WSEvert	M1WNIvert	M1WNIvert	M2WNIvert	M2WNIvert	M2WNIvert

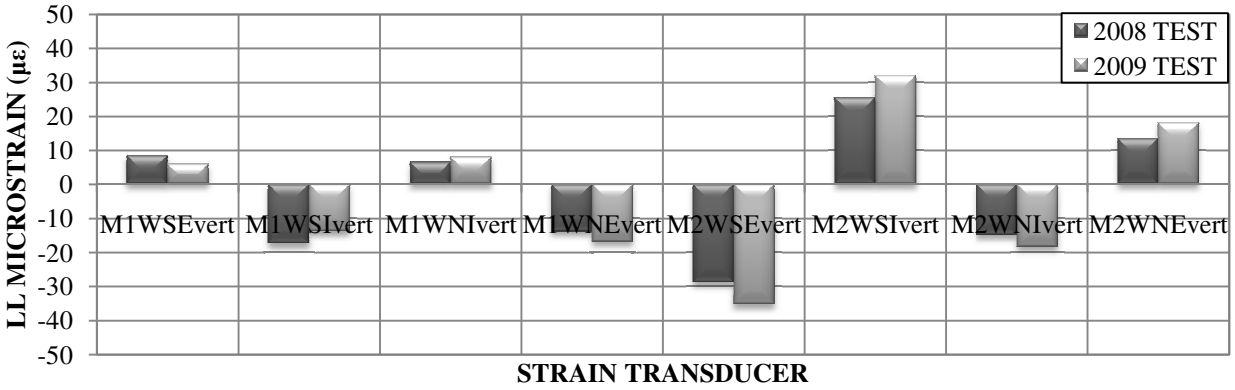

a. 2008 & 2009; Path 1

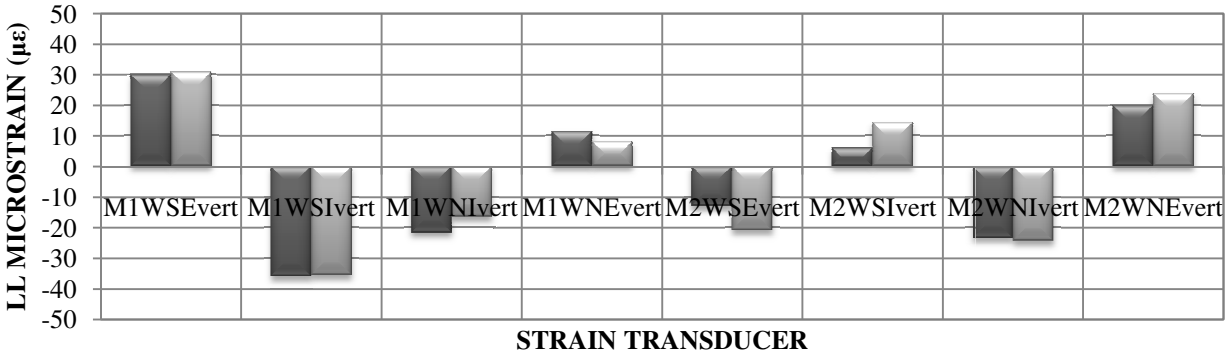

b. 2008 & 2009; Path 2

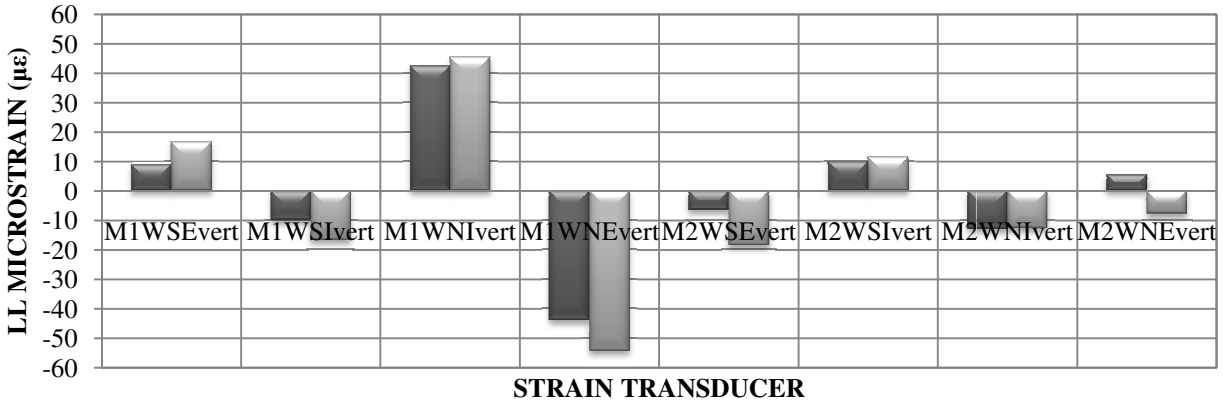

c. 2008 & 2009; Path 3

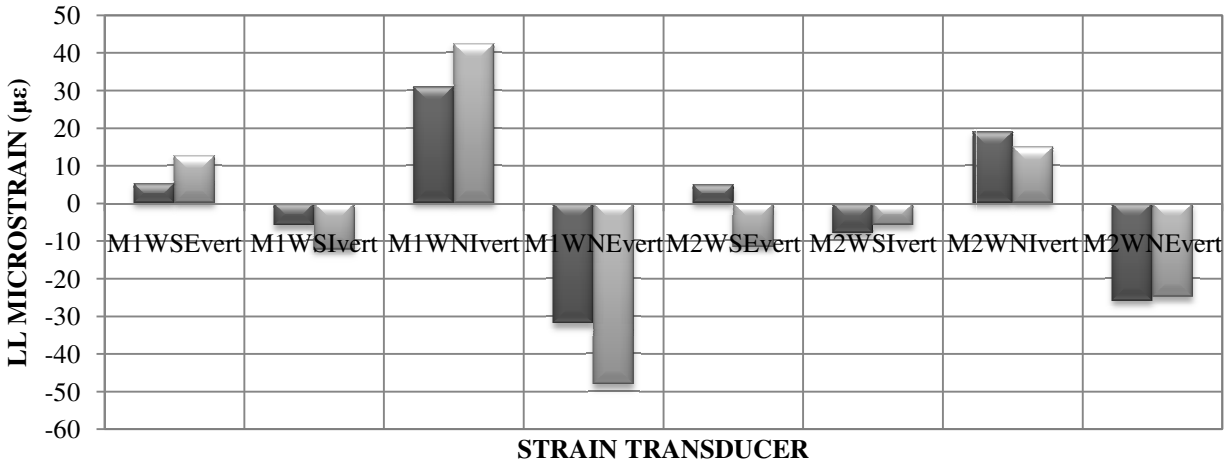

d. 2008 & 2009; Path 4

Figure 5.30-Comparison of 2008 & 2009 LL Vertical Web Strain at Midspan

5.5.5 Live Load Vertical Web Strains Measured at Three-Eighths Span

The vertical live load web strain at three-eighths span was only measured for the 2009 test. Four strain transducers located on the southernmost girder were orientated vertically near the web fillet juncture on the webs at three-eighths span. The maximum strains were recorded when the truck's rear axle position was approximately at three-eighths span of the pi-girders. The largest measured tensile strain was 25 με at E1WNIvert along path 3. This value occurred at the same web location as the maximum web strain at midspan (M1WNIvert, see Section 5.5.4), but is 20 με less. The maximum bulb live loads strains are shown in Table

5.15. The maximum estimated total strain was 50 με at E1WNIvert. This indicates that longitudinal cracking of the bulbs at three-eighths span is unlikely under service level loads.

Table 5.15-Maximum LL Vertical Web Strain at 3/8 span

	Path Number						
	1	2	3	4	5	6	7
Strain (με)	6.0	22	25	24	16	4	2
Location	E1WSEvert	E1WSEvert	E1WNIvert	E1WNIvert	E1WNIvert	E1WNIvert	E1WNEvert

Including residual construction strains the maximum estimated total strain was 100 με observed along path 2 at E1WSEIvert. 100 με is roughly 35% less than the predicted cracking strain of UHPC therefore cracking of the bulbs is unlikely under service level loads. Figure 5.31a-g displays the estimated total strains for paths 1-7.

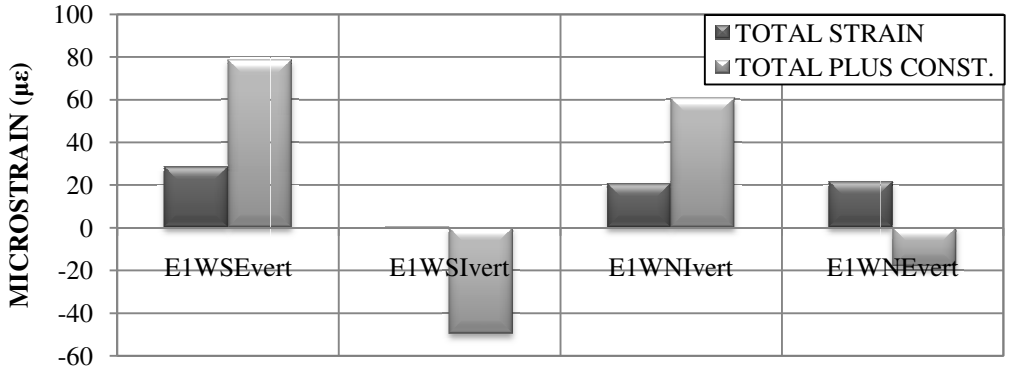

a. 2009; Path 1

b. 2009; Path 2

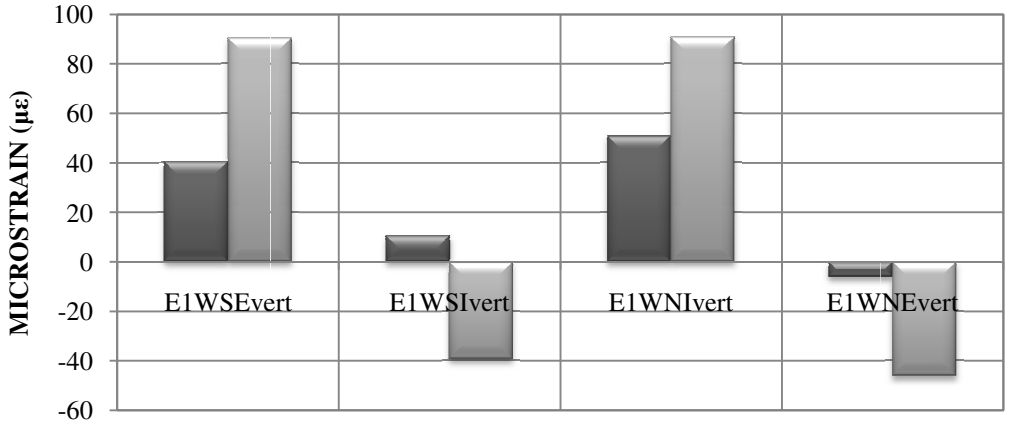

c. 2009; Path 3

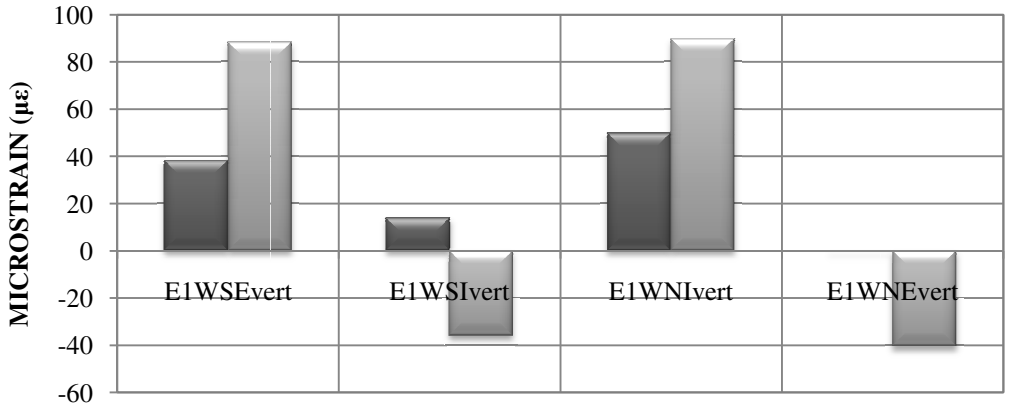

d. 2009; Path 4

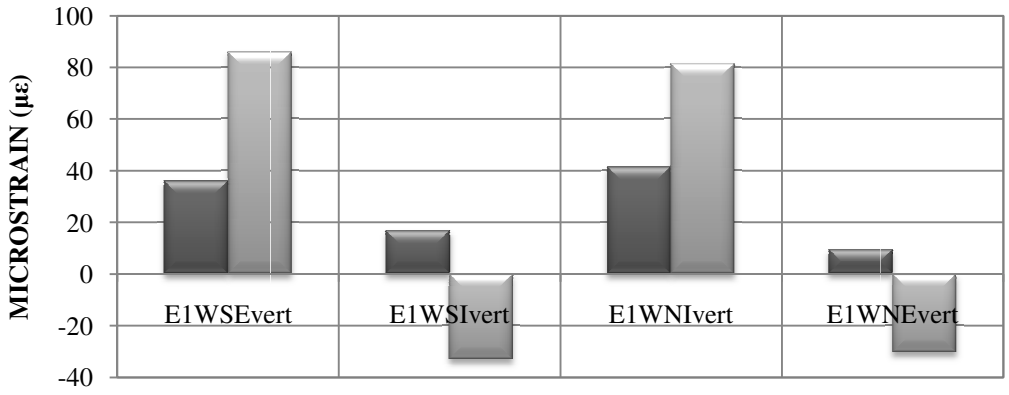

e. 2009; Path 5

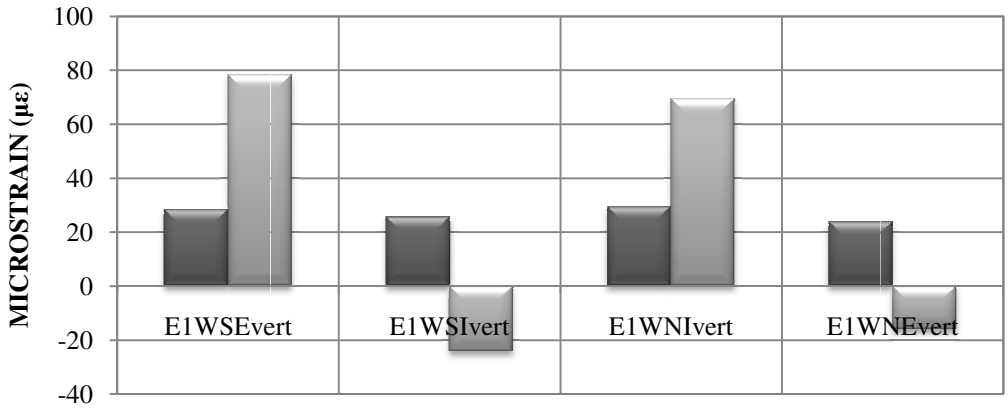

f. 2009; Path 6

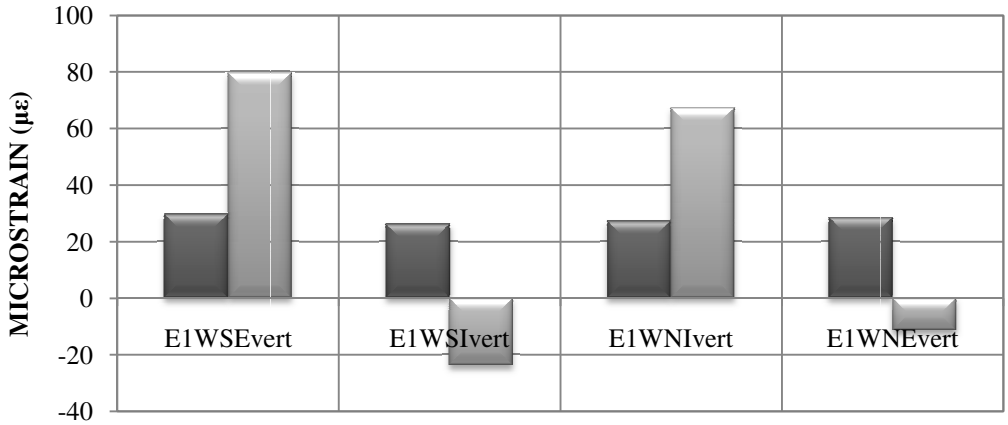

g. 2009; Path 7

Figure 5.31-Estimated Total Vertical Web Strain (includes residual construction strain) at 3/8 Span

The majority of the vertical web strain readings at midspan were larger than the readings at three-eighths span. A comparison of the vertical web strains at three-eighths span and midspan are presented in Figure 5.32a-d. Paths 5-7 are not shown as the results are similar to those from paths 1-4. The increased vertical web strain at midspan could be due to the presence of the diaphragms at midspan, or due to the increased moment on the section at midspan.

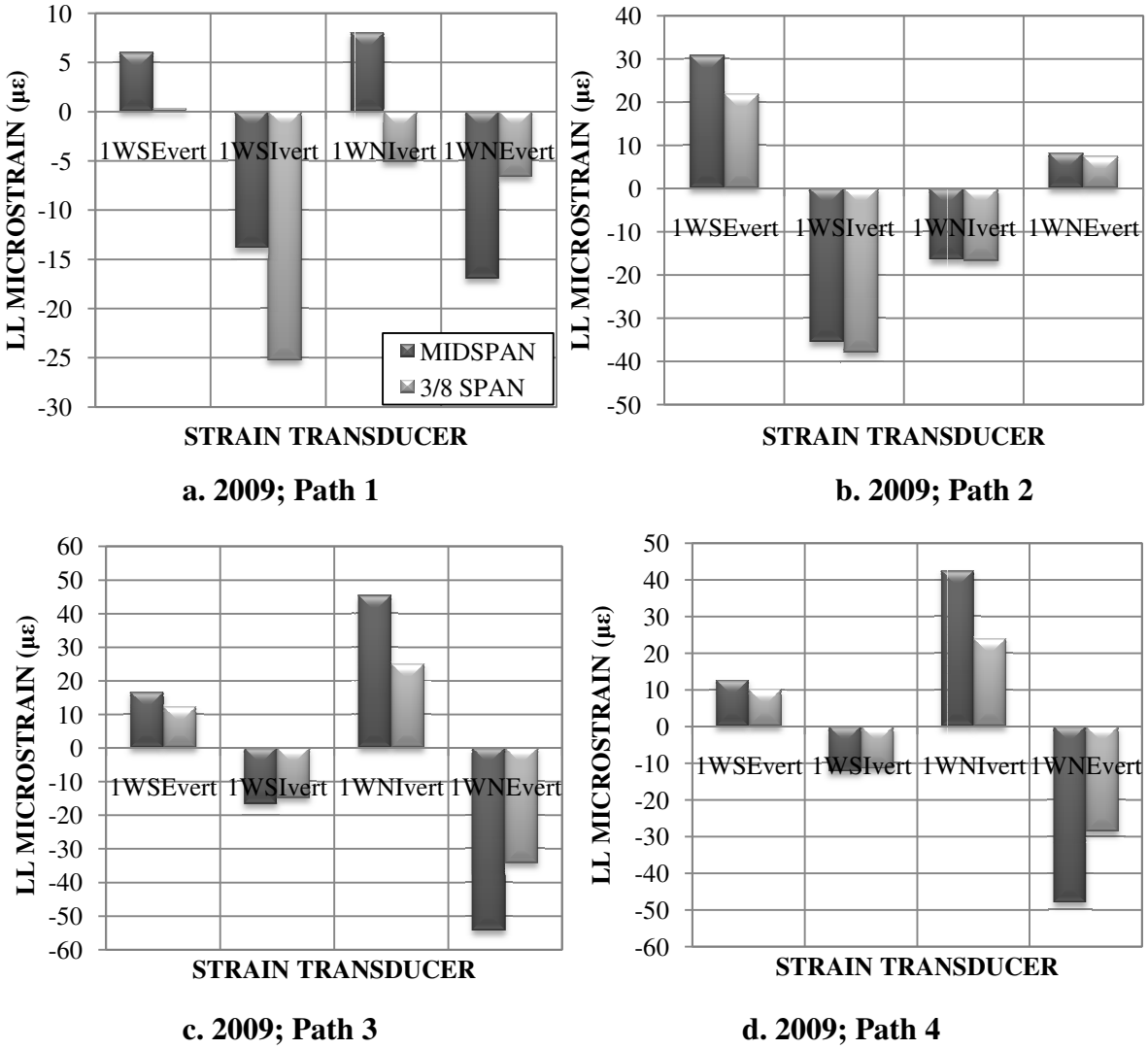

Figure 5.32-Comparison of 2009 Midspan and 3/8 Span Live Load Vertical Web Strain

The FEM predicted lower strains for the majority of the web strains at three-eighths span when compared to midspan. The finite element comparisons are provided in Figure 5.33a-d.

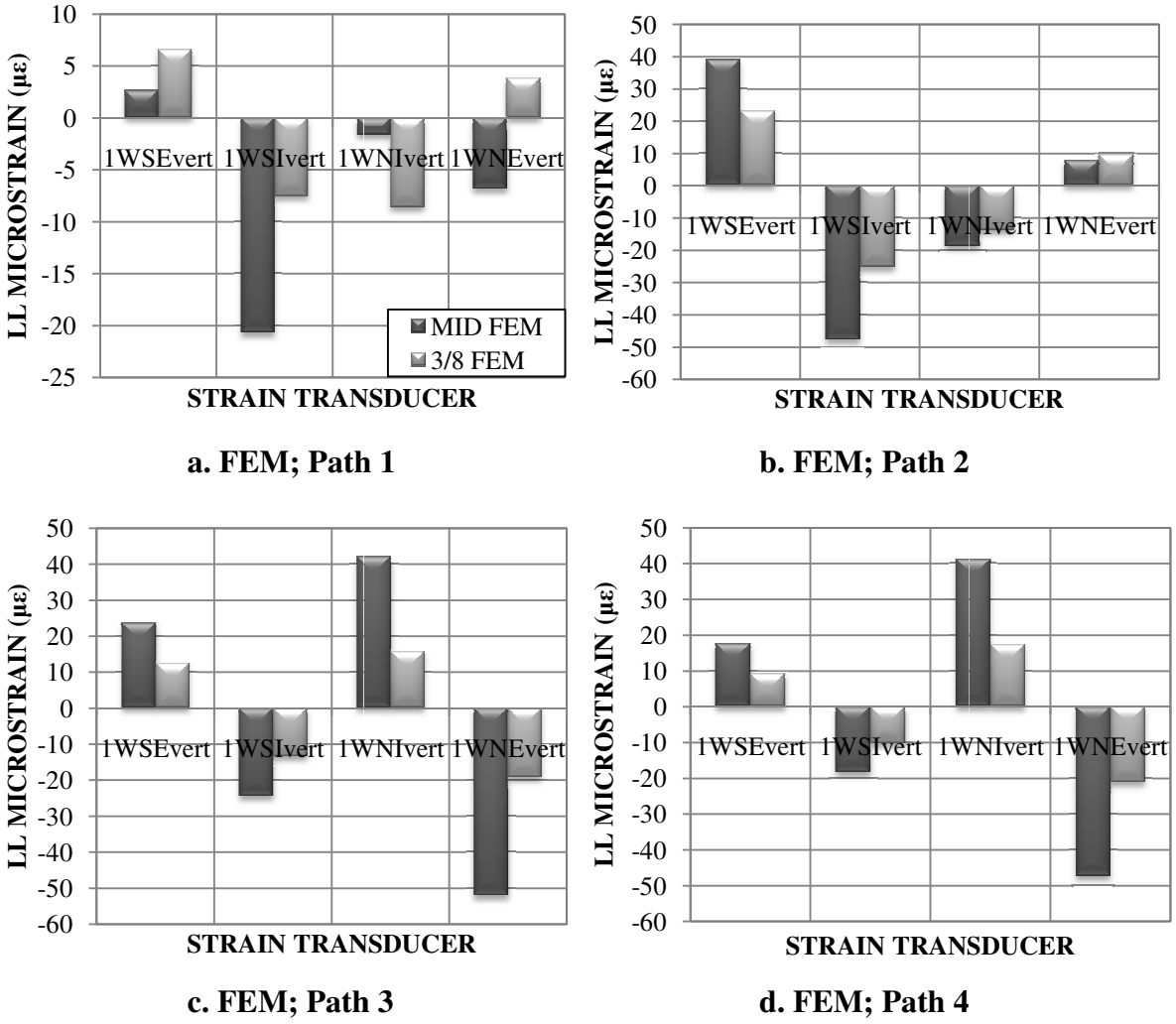

Figure 5.33-Comparison of FEM Midspan and 3/8 Span Live Load Vertical Web Strain

5.5.6 Longitudinal Live Load Strains Measured Near the Eastern Pier

The results of the 2009 static load field test showed that the strains measured near the eastern pier on the bottom of the bulbs tended to be closer to tension readings (i.e. less negative) than those from the first test. This corroborates that a loss of continuity at the pier has occurred. Figure 5.34 provides a graphical representation of the maximum strains measured near the pier for paths 1-7. From Figure 5.34 a-f every 2009 reading is larger (i.e. less negative) than the corresponding reading from 2008. Figure 5.20 a-g shows that the strains predicted by the FEM were always larger (more positive) for a simply supported condition when compared to

a partially restrained condition. Therefore, the transition from 2008 to 2009 readings provides evidence that the bridge is transitioning from a partially restrained condition to a simply supported condition.

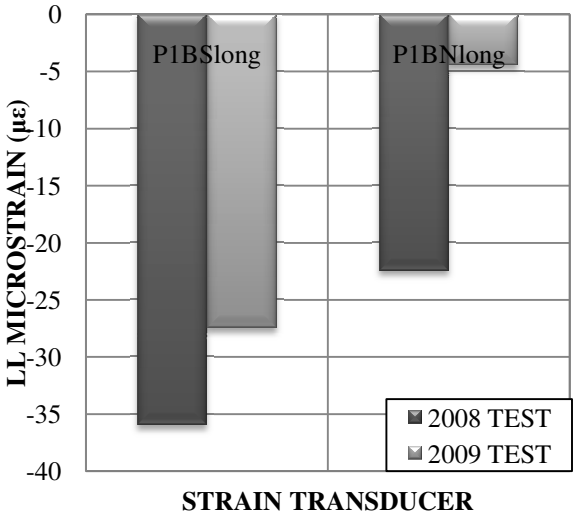

a. 2008 & 2009; Path 1

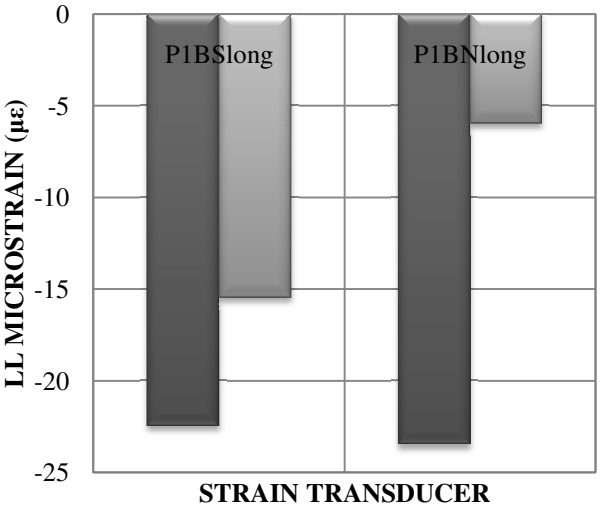

b. 2008 & 2009; Path 2

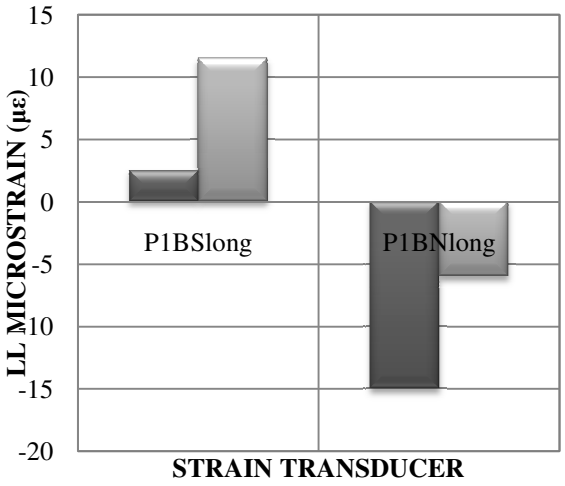

c. 2008 & 2009; Path 3

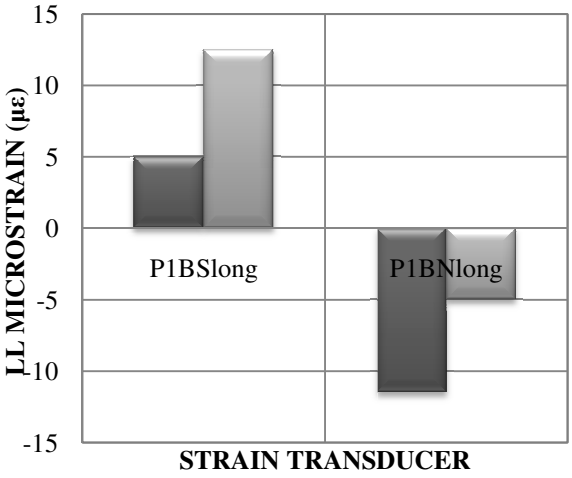

d. 2008 & 2009; Path 4

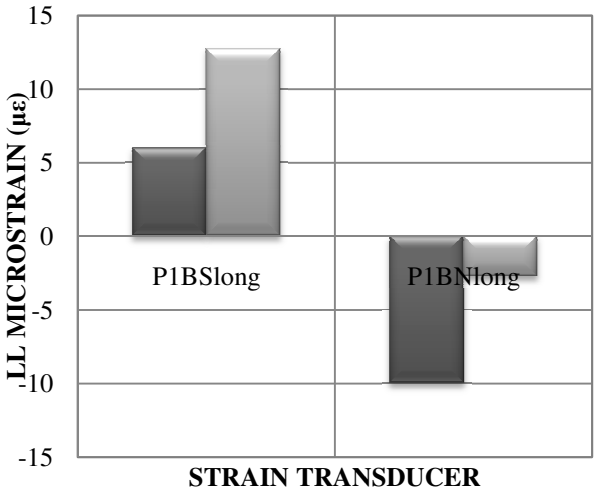

e. 2008 & 2009; Path 5

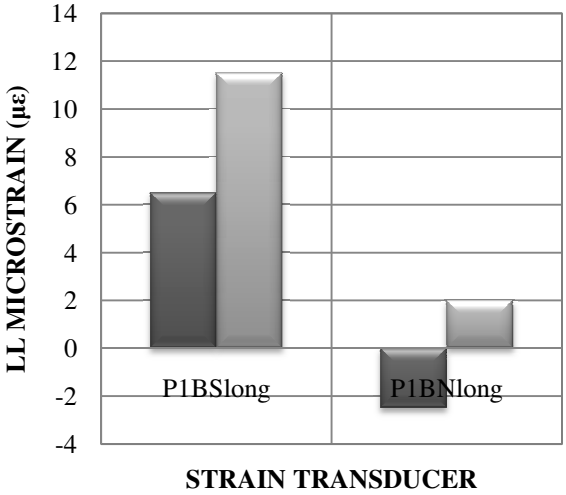

f. 2008 & 2009; Path 6

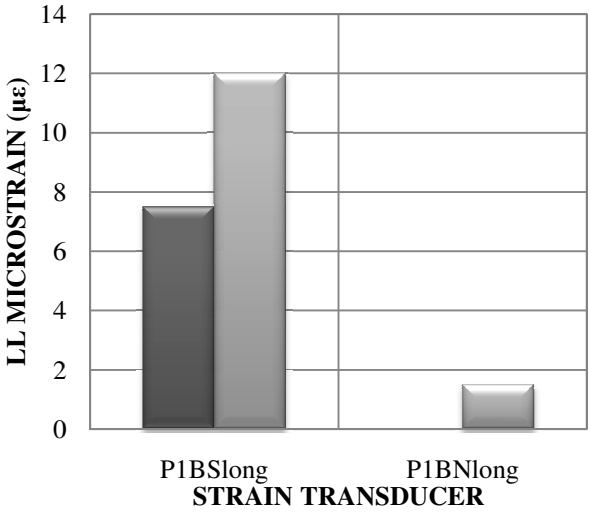

g. 2008 & 2009; Path 7

Figure 5.34-Comparison of 2008 & 2009 LL Longitudinal Strain near the Eastern Pier

5.5.7 Midspan Live Load Diaphragm Strains Measured at Midspan

The results of the second static load field test showed an average increase of 3 με in the strains recorded by the diaphragm transducers. As expected, the largest increase in diaphragm strain was along path 4 where the largest increase in vertical web strain was recorded (section 5.5.4). Table 5.16 provides the measured maximum values for the first and

second round of tests. Figure 5.36a-d provides a graphical representation of the maximum strains measured at midspan for paths 1-4, paths 5-7 are not shown due to their similarity to paths 1-3. In general, the changes between the 2008 and 2009 midspan diaphragm strains were minor.

Table 5.16-2008 & 2009 Maximum LL Axial Diaphragm Strain at Midspan

	Path Number						
	1	2	3	4	5	6	7
2008 Strain (με)	42	54	74	49	44	15	-14
2009 Strain (με)	39	52	73	61	49	22	-10
Location	MD2	MD1	MD2	MD2	MD3	MD3	MD3

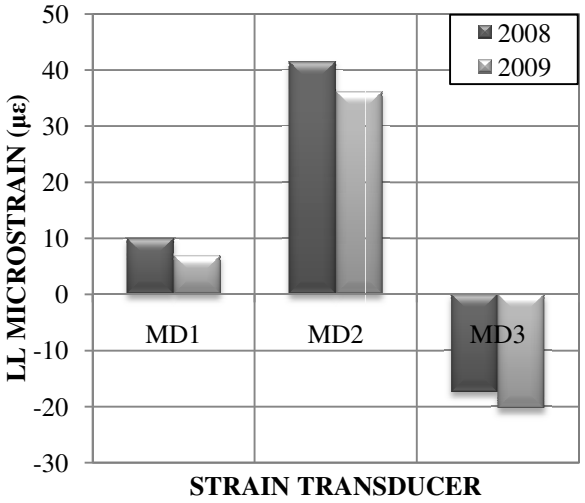

a. 2008 & 2009; Path 1

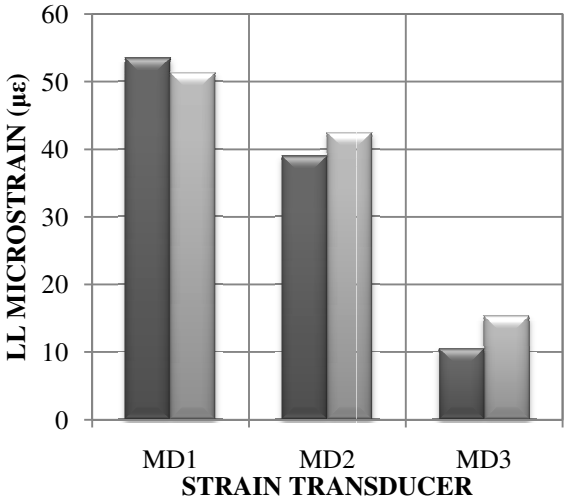

b. 2008 & 2009; Path 2

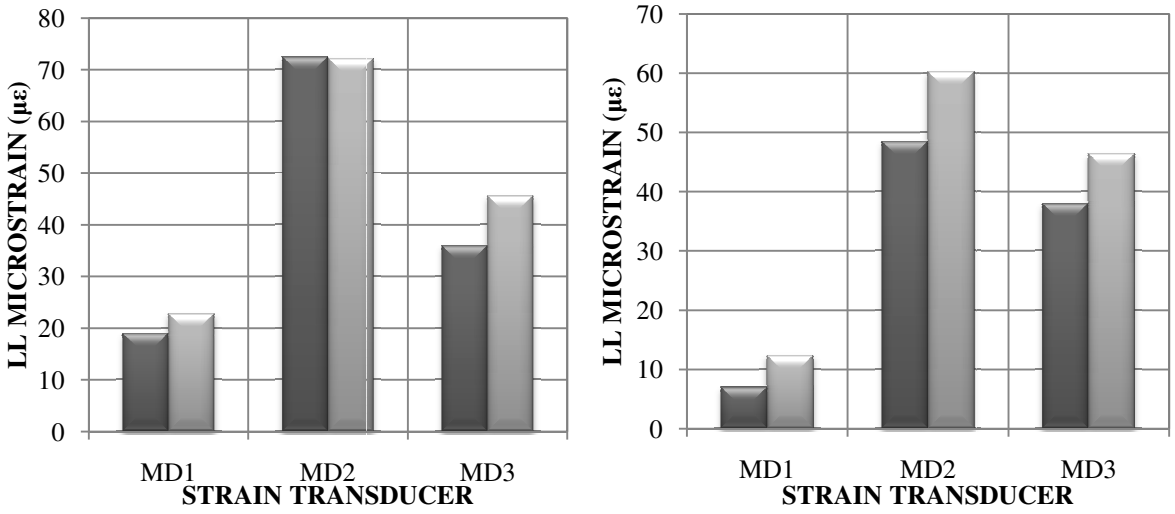

c. 2008 & 2009; Path 3 **d. 2008 & 2009; Path 4**

Figure 5.35-Comparison of 2008 to 2009 LL Axial Diaphragm Strain at Midspan

5.6 2009 Dynamic Live Load Test

Load paths 2 and 4 were used for dynamic load testing. During the static load test, the truck was driven over the bridge at a crawl speed to determine the baseline strain and deflection. For dynamic testing the truck was driven over the bridge at 15mph and 25mph to quantify dynamic amplification. Due to limitations on approach conditions, passes with speeds faster than 25 mph were not practical, or safe.

5.6.1 Dynamic Amplification Factor

To verify the effects of dynamic loading, five high-speed passes were made along two paths to determine a dynamic amplification factor. The dynamic load allowance, which is also known as dynamic amplification (DA), accounts for hammering effects due to irregularities in the bridge deck, and resonant excitation as a result of similar frequencies of vibration between bridge and roadway (Interim AASHTO 2008). The 2008 Interim AASHTO LRFD DAF design value is 1.33. The experimentally obtained dynamic amplification (DA) is the ratio defined as:

$$DA = \frac{\varepsilon_{dyn} - \varepsilon_{stat}}{\varepsilon_{stat}} \tag{5.1}$$

Where ε_{dyn} = the maximum strain caused by the vehicle traveling at normal speed (at a given location) and ε_{stat} = the maximum strain caused by the vehicle traveling at crawl speeds (at corresponding location).

The amplification factor (DAF) is then given by:

$$DAF = 1 + DA \tag{5.2}$$

The dynamic response of the longitudinal strain transducers at midspan on the bottom of the bulbs for load paths 2 and 4 were the focus for determining the DAF. A representative sample of the data obtained from the longitudinal transducers located on the bottom of the bulbs can be seen in Figure 5.36.

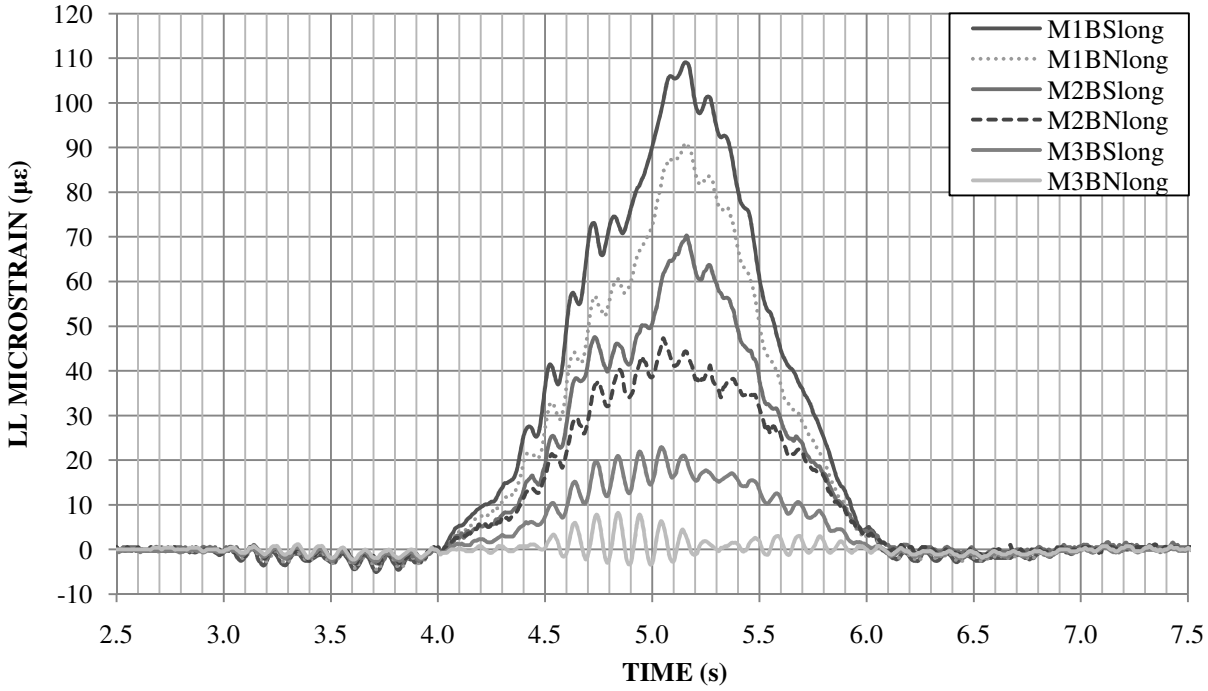

Figure 5.36-Representative Sample of Dynamic LL Longitudinal Strain at Midspan along Path 2

The largest DAF was found to be 1.15 from transducer M1BSlong along path 2. This DAF is 13.5% less than the factor used for design. Table 5.17 provides the various DAF's for load paths 2 and 4. Figure 5.37a-d provides strain comparisons for both dynamic and static loading for paths 1-4. Load paths 5-7 are not shown due to their similarity to paths 1-3.

Table 5.17-Dynamic Amplification Factors

PATH	TRANSDUCER	15 mph	25 mph
Path 2	M1BSlong	0.99	1.15
Path 2	M1BNlong	0.97	1.01
Path 4	M2BSlong	0.98	0.96
Path 4	M2BNlong	0.98	0.94

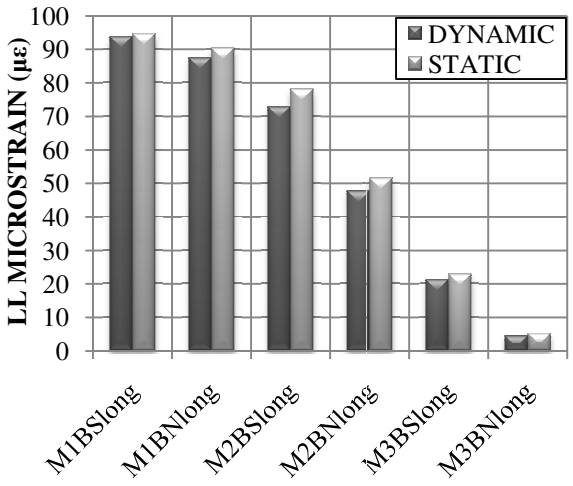

a. 2009; Path 2-15 mph

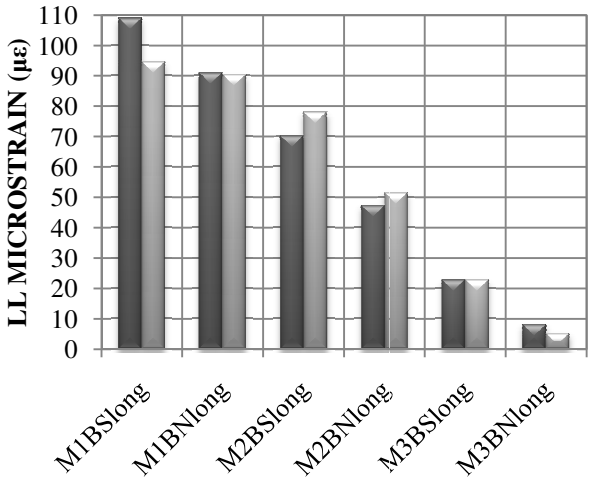

b. 2009; Path 2-25 mph

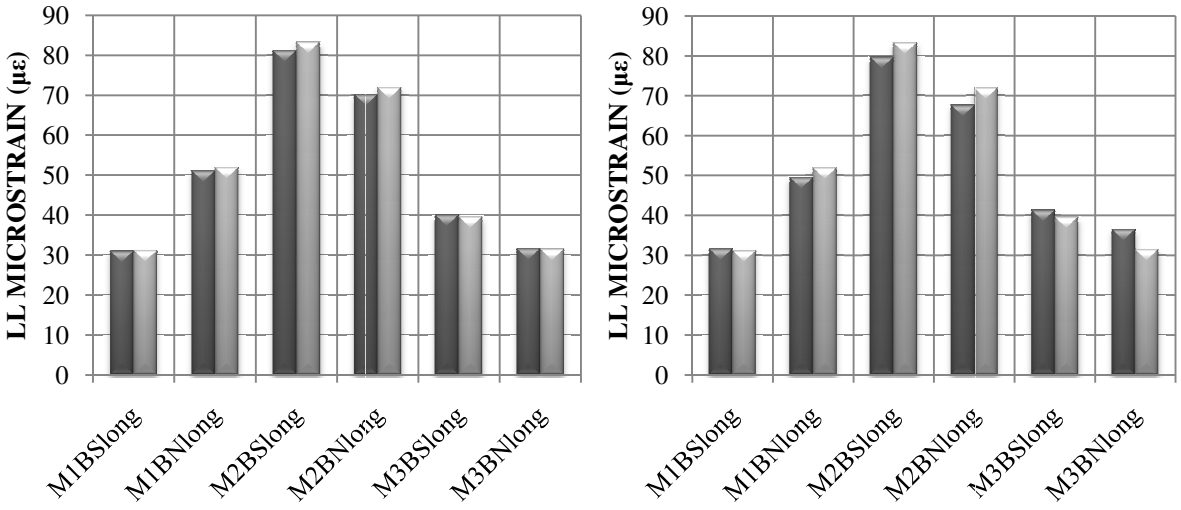

c. 2009; Path 4-15 mph **d. 2009; Path 4-25 mph**

Figure 5.37-Comparison of LL Longitudinal Bulb Strain for Static and Dynamic Loading

6 GIRDER LOAD FRACTION AND LOAD DISTRIBUTION

6.1 Introduction

Load fraction is the fraction of the total load supported by each individual girder for a given load placement. Load fraction was calculated for each load path based on the assumption that the girders are of equal stiffness. The path load fraction for each girder can be calculated by either the following equations:

$$LF_i = \frac{\varepsilon_i}{\sum_{i=1}^{n} \varepsilon_i} \qquad \text{(6.1)-Load Fraction based on Strain}$$

Where LF_i = load fraction of the ith girder, ε_i = strain ith girder, $\Sigma\varepsilon_i$ = sum of all girder strains, and n = number of girders

$$LF_i = \frac{d_i}{\sum_{i=1}^{n} d_i} \qquad \text{(6.2)-Load Fraction based on Deflection}$$

Where LF_i = load fraction of the ith girder, d_i= deflection of the ith girder, Σd_i= sum of all girder deflections, and n = number of girders.

A distribution factor (DF) is the fraction of the total load a girder must be designed to support when all lanes are loaded to produce the maximum effects on the girder. From the load fractions based on strain or displacement the distribution factors were calculated experimentally by adding the load fractions of two complementing load cases, Equation 6.3 shows this calculation. By summing load fractions measured from paths 2 and 6 (i.e. when the truck is at the center of each respective lane of the bridge) distribution factors for each girder were computed using Equation 6.3.

$$DF_i = LF_{2i} + LF_{6i} \qquad \text{(6.3)-Experimental Distribution Factor}$$

Where DF_i =distribution factor of the ith girder, LF_{2i} = load fraction from path 2 of the ith girder, LF_{6i} = load fraction from path 6 of the ith girder.

6.2 2008 Distribution Factors

As previously mentioned the distribution factors used in design were 1.0 for all girders. The calculated factors based on 2008 strain and deflection are shown in Table 6.1. From the experimental distribution factors calculated using Equations 6.3, the design distribution factor of 1.0 was clearly conservative.

It is possible to obtain an accurate prediction of the distribution factors using a simple, linear elastic finite element model. Such models are relatively simple to create, and can be used to evaluate complex geometry. From the longitudinal strains predicted by the FEM, distribution factors were calculated using Equation 6.1 and 6.3. These predicted distribution factors are shown in Table 6.1. The percent errors of the FEM distributions factors are less than 8% when compared to the measured distribution factors based on strain or displacement.

Table 6.1-2008 Distribution Factors and Predicted FEM Distribution Factors

Girder	DF Strain	DF Displacement	DF FEM Pinned	DF FEM Fixed
1	0.63	0.67	0.65	0.64
2	0.75	0.70	0.69	0.71
3	0.62	0.63	0.65	0.64

6.3 2009 Distribution Factors

The 2009 distribution factor results showed minimal change from the 2008 factors. The percentage change in distribution factors was less than 4% for the 2008 and 2009 live load tests. The 2009 results were calculated using strain as no displacement transducers were

placed on the bridge. A comparison of the 2008 to 2009 distribution factors are shown in Table 6.2.

Table 6.2-Comparison of 2008 & 2009 Distribution Factors

Girder	2008 DF	2009 DF	Percent Change (%)
1	0.63	0.63	0
2	0.75	0.76	1.33
3	0.62	0.60	-3.22

6.4 Effect of Midspan Diaphragm on Distribution Factors

The effect of loosening the nuts on the midspan diaphragm appeared to have a small effect on the bridge distribution factors. As discussed in Section 2, one of the main reasons for including the diaphragms was to improve live load distribution. Because some of the diaphragm members were still transmitting forces to the pi-girders, it is difficult to draw conclusions regarding the effect of the diaphragms on distribution factors. A comparison of distribution factors can be seen in Table 6.3.

Table 6.3-Comparison of Distribution Factors with Midspan Diaphragm Nuts Loose

Girder	DF Nuts Tight	DF Nuts Loose
1	0.63	0.60
2	0.75	0.73
3	0.62	0.67

6.5 AASHTO Distribution Factors

Using the Interim 2008 AASHTO LRFD Bridge Design Specification, the AASHTO LRFD distribution factors for the interior and exterior girders were calculated. Case (i) from Table 4.6.2.2.1-1, a Precast Concrete Double Tee Section without Transverse Post-Tensioning, might be the most similar to the Jakway Park Bridge system. The interior beam distribution factors were estimated using Table 4.6.2.2b-1, while the lever method was used for calculating the exterior beam distribution factors treating each web as a beam. The

AASHTO equations used are shown in Equation 6.4 through 6.8. Due to the non-uniform web spacing, both maximum and average web spacing were used for computation of the distribution factors. Comparing the AASHTO distribution factors to the experimental factors, the maximum percent difference is approximately 27% for maximum spacing and 13% for average spacing. The calculated factors can be seen in

Table 6.4.

$$DF_i = \frac{S}{D}$$ (6.4)-AASHTO Distribution Factor

Where DF_i=Interior beam distribution factor, S=Spacing of Beams or webs (ft), D=Width of distribution per lane (ft).

$$C = K(W/L) \leq K$$ (6.5)-Stiffness Parameter

Where C=Stiffness Parameter, W=Edge-to-Edge width of bridge, L=Span of beam, K=Constant for different types of construction.

$$D = 11.5 - N_L + 1.4N_L(1-0.2C)^2$$ (6.6)-Width of Distribution per Lane

Where D=Width of distribution per lane (ft), N_L=Number of design lanes, C=Stiffness Parameter.

$$K = \sqrt{\frac{(1+\mu)I_p}{J}}$$ (6.7)-Constant for Different Types of Construction

Where K=Constant for different types of construction, μ=Poisson's Ratio, I_p=Polar Moment of Inertia, J=St. Venant Torsional Inertia.

$$J = \frac{A}{40I_p} \qquad \text{(6.8)-St. Venant Tosional Inertia}$$

Where J=St. Venant Torsional Inertia, I_p=Polar Moment of Inertia, A=Area of Beam or Girder.

Table 6.4-AASHTO Distribution Factors

Girder	AASHTO DF Maximum Spacing	AASHTO DF Average Spacing	DF (based on strain)	DF (based on displacement)
1	0.81	0.71	0.63	0.67
2	0.95	0.76	0.75	0.70
3	0.81	0.71	0.62	0.63

7 CONCLUSIONS AND RECOMMENDATIONS

The unique UHPC pi-girders used in the construction of the Jakway Park Bridge provide a new and effective option for bridge superstructures especially for projects with accelerated construction schedules. This bridge appears to be performing well and within the general design parameters. Additionally, testing revealed that over the first year of service the bridge experienced no significant changes in structural behavior.

The design approach for the bridge was appropriately conservative in consideration of the relatively new geometry and materials. Future applications of this technology may be less conservative. In particular, future designs could utilize longer spans, lower live load distribution factors, and most likely dispense with transverse mild steel reinforcement in the deck of the girders. From the recommendations provided in this thesis, and the continued decrease in cost of UHPC and fiber reinforcement in North America, $\$2000/yd^3$ as of 2007 (Vande Voort, Suleiman and Sritharan 2008), UHPC pi-girder bridges will become a more cost effect option.

If cracking of the UHPC is used as a criterion to limit stresses for durability considerations, relatively simple, linear-elastic finite element models can provide a highly useful tool in predicting behavior of the UHPC pi-girders. Such models can be developed cost-effectively and provide a useful tool for designers in predicting behavior, anticipating locations of concern, evaluating details, and identifying global changes in bridge performance through subsequent load tests. The verification of these models is of particular significance for future designs employing the distinctive UHPC pi-girder.

The laboratory and live load testing as well as analytical work regarding finite element model verification resulted in the formulation of the following conclusions:

Design Assumptions and Future Design Guidance

- The pi-girders have lateral distribution factors ranging from 0.62 for exterior girders and 0.75 for interior girders. The design value of 1.0 was, therefore, conservative.

- The bridge did not behave as if perfectly simply supported as assumed in design. The concrete diaphragms at the piers appear to have provided some degree of continuity between the end spans and pi-girder span. However, the 2009 test showed that the UHPC centerspan appeared to have lost some degree of rotational restraint.

- The Interim 2008 AASHTO case (i), Precast Double T Beam equations for distribution factors, predicted reasonable and somewhat conservative estimates of distribution factors for this UHPC pi-girder bridge.

- Based on the measured live load strains and allowing for a 5 cm (2 in.) asphalt overlay and an impact factor of 1.33, the girder length could be increased to roughly 20 meters (65ft) without cracking for Interim 2008 AASHTO specified loads.

- Construction strains induced by tightening of the HSS members are significant in the webs often on the magnitude of the strains recorded during live load tests. Possible use of shims or tighter Fabrication tolerances for diaphragms members should be specified.

- The maximum measured dynamic amplification factor was 1.15 for speeds up to 25 mph. The specified AASHTO dynamic amplification factor of 1.33 is conservative for this bridge.

- The steel diaphragms are not overly effective in improving the live load distribution between pi-girders for service level loads. However, when the midspan diaphragm was active the maximum live load strains on the bulbs were reduced by roughly 6%.

- The steel diaphragm at midspan is not effective in decreasing the vertical web strain.

- The use of ready-mix trucks in UHPC batching can provide compressive material strengths of 28 ksi.

Finite Element Model

- The simplified, linear-elastic FEM provided accurate means of predicting values of live load strains and deflections, and thus distribution factors for this UHPC pi-girder bridge.

- The distribution factors predicted by the FEM model matched to within 8%, of the actual distribution factors measured in the field.

- The simplified method of modeling prestressing strands as pressures distributed over the bulbs of the pi-girder provided accurate estimates for both strain and deflection.

- Some improvement in predictions with relatively little additional cost might be achieved by employing elastic rather than coupled connections between individual girders.

Maximum Bridge Strains

- The estimated total longitudinal strains for the bottom of the bulbs at midspan were always compressive during testing and approximately 265 με below the cracking threshold, indicating that transverse cracking is unlikely at service level loads.

- The estimated total longitudinal strains for the bottom of the bulbs at quarterspan were always compressive during testing and approximately 325 με below the cracking threshold, indicating that transverse cracking is unlikely at service level loads.

- The estimated total transverse strains on the bottom of deck were roughly 80 με below the cracking threshold, indicating that longitudinal cracking on the bottom of the deck is unlikely at service level loads.

- The estimated total longitudinal strains for the top deck transducers were roughly 155 με below the cracking threshold, indicating that transverse cracking is unlikely at service level loads.

- The estimated total vertical strains for the webs at midspan including residual strains from diaphragm installation were 30 με below the cracking threshold, indicating that horizontal cracking of the webs is unlikely at service level loads.

- The estimated total vertical strains for the webs at three-eighths span including residual strains from diaphragm installation were 50 με below the cracking threshold, indicating that horizontal cracking of the webs is unlikely at service level loads.

Comparison of 2008 and 2009 Static Live Load Tests

- In general, the changes in strain observed for the comparison of the 2008 to 2009 static live load tests were marginal.

- No significant change in the neutral axis location was observed. The 2008 neutral axis was 11.6 in. and the 2009 the neutral axis was measured to be 11.8 in. from the top from the section.

- The largest increase in strain was observed on longitudinal gages, where a loss of rotational restraint at the pier appeared to have caused an increase in strain.

Future Research

Additional research could include the following topics:

- Use of partial prestressing in UHPC pi-girder design, i.e. cracking of UHPC on the bottom of the bulbs is allowed under maximum service level loads. The unhydrated cement content of UHPC would provide for second hydration thus providing crack-sealing capabilities.

- Investigation of the torsional properties of the 2nd generation pi-section, and the section's ability to resist eccentric loading.

- Use of the verified finite element model to further reduce section dimensions.

- Economic analysis of pi-girder compared to traditional prestressed concrete.

WORKS CITED

AASHTO. *AASHTO LRFD. 2008. LRFD Bridge Design Specifications, 4th Edition, Interim Revisions.* Washington, DC: American Association of State Highway and Transportation Officials, 2008.

Aitcin, P. C., S. L. Sarkar, R. Ranc, and C. Levy. "A High-Silica-Modulus Cement for high Performance Concrete." *Ceramic Transactions:Advances in Cememtitious Materials* 16 (1991): 103-20.

Carpinteri, Alberto, and Bernardino Chiaia. "Embrittlement and Decrease of Apparent Strength in Large-Sized Concrete Structures." *Sadhana* (India Academy of Sciences) 27, no. 4 (2002): 425-448.

Chanvillard, Gilles, and Stephane Rigaud. "Complete Characterisation of Tensile Properties of DUCTAL UHPFRC According to the French Recommendations." *Proceedings of the 4th International RILEM Workshop on High Performance Fiber Reinforced Cement Composites (HPFRCC4.* Ann Arbor, 2003. 14pp.

de Larrard, F., and T. Sedran. "Optimization of Ultra-High-Performance Concrete by the Use of a Packing Model." *Cement and Concrete Research* 24, no. 6 (1994): 997-1009.

Gowripalan, N, and R I Gilberg. *Design Guidelines for RPC Prestressed Concrete Beams.* The University of New South Wales, 2000.

Graybeal, Benjamin. *Material Property Characterization of Ultra-High Performance Concrete FHWA-HRT-06-103.* Washington, DC: Federal Highway Administration, 2006a.

Graybeal, Benjamin. *Structural Behavior of a 2nd Generation UHPC Pi-Girder, NTIS Report PB2009-115496.* Springfield, VA: National Technical Information Service, 2009b.

Graybeal, Benjamin. *Structural Behavior of a Protorype Ultra-High Performance Concrete Pi-Grider, NTIS Report PB2009-115495.* Springfield, VA: National Technical Information Service, 2009a.

Graybeal, Benjamin. *Structural Behavior of a Protorype Ultra-High Performance Concrete Pi-Grider, NTIS Report PB2009-115495.* Springfield, VA: National Technical Information Service, 2009a.

Graybeal, Benjamin. *Structural Behavior of Ultra-High Performance Concrete Prestressed I-Girders FHWA-HRT-06-115.* Washington, DC: Federal Highway Administration, 2006b.

Japan Society of Civil Engineers. *Recommendations for Design and Construction of Ultra High Strength Fiber Reinforced Concrete Structures (Draft).* Tokyo: Subcommittee on Research of Ultra High Strength Fiber Reinforced Concrete, 2006.

Keierleber, Brian, Dean Bierwagen, Terry Wipf, and Ahmad Abu-Hawash. "Design of Buchanan County, Iowa, Bridge Using Ultra High Performance Concrete and PI Girders." *PCI National Bridge Conference.* Ames, 2008.

Ma, J, and H Schneider. "Properties of Ultra-High Performance Concrete." *Leipzig Annual*

Civil Engineering Report (LACER), no. 7 (2002): 25-32.

Park, Hesson. "Model-Based Optimization of Ultra-High Performance Concrete Highway Bridges." Master Thesis, Massachusetts Institute of Technology, 2003, 139.

Richard, Pierre, and Marcel Cheyrezy. "Composition of Reactive Powder Concretes." *Cement and Concrete Research* 25, no. 7 (1995): 1501-1511.

Soh, Melvin. "Model-Based Design of a Ultra High Performance Concrete Prototype Highway Bridge Girder." Master Thesis, Massachusetts Institute of Technology, 2002, 64.

Ulm, Franz Josef. "Bond and Shear Design of Iowa DOT Sampler Bridge." Massachusetts Institue of Technology, Cambridge, MA, 2004.

Vande Voort, T., M. Suleiman, and S. Sritharan. "Design and Performance Verification of Ultra-High Performance Concrete Piles for Deep Foundations." Iowa , Center for Transportation Research and Education, 2008.

Vernet, Christian P. "Ultra-Durable Concretes:Structure at the Micro-and Nanoscale." Materials Research Society, May 2004. 324-327.